

In silico and empirical analyses of the evolution and activity of diverse AB₅ toxins found within
the *Salmonella* genus

by

Adaobi Ojiakor

A thesis submitted in partial fulfillment of the requirements for the degree of

Master of Science

Department of Biological Sciences

University of Alberta

© Adaobi Ojiakor, 2023

Abstract

Bacterial AB₅ toxins are secreted protein complexes composed of an enzymatic A subunit that disrupts host cell functions and a pentameric B subunit that facilitates cellular entry of the toxin by binding to specific cell surface receptors. AB₅ toxins are widely recognized for their roles in the pathogenesis of several bacterial pathogens frequently associated with human disease. In *Salmonella*, two distinct AB₅ toxins, ArtAB and typhoid toxin appear to contribute to the virulence and disease properties of highly pathogenic strains and serovars like *Salmonella enterica* serovar Typhimurium definitive phage type (DT)104 and *Salmonella enterica* serovar Typhi, both of which cause severe infections in humans. However, the distribution and potential roles of AB₅ toxins in other virulent *Salmonella* serovars that are often implicated in human disease is not well understood.

Using an array of *in silico* methods and molecular and cell biology techniques, this thesis explores the broader arsenal of AB₅ toxins found within the *Salmonella* genus. We provide evidence that many *Salmonella* serovars harbour genes encoding the ArtAB and typhoid toxins and that there is substantial variation among these toxins. The B subunit sequences of these toxins are particularly variable, which is likely indicative of different glycan binding preferences, indicating that the toxins produced by different lineages likely exhibit differences in the nature of the cell type(s) they target. We also identify two novel “hybrid” AB₅ toxins, RIP-TT and RIP-HLT within the *Salmonella* genus that combine subunits from well-established and distinct toxin families. Phylogenetic and sequence analyses showed that the A subunit sequences of RIP-TT and RIP-HLT exhibit similarity to the A subunits of Shiga family toxins, but their B subunit sequences exhibit sequence similarity to the B subunits of the unrelated ArtAB (RIP-TT) and type II heat-labile toxins (RIP-HLT), respectively. Examination of the genomic loci where these toxins are

encoded revealed a likely role for prophages and transposases in the evolution of both toxins. For further analyses, we assessed and confirmed A-B interactions in both toxins using molecular cloning and protein purification systems and subsequently investigated the cellular effects of purified RIP-TT and RIP-HLT in HeLa cells using an MTT cytotoxicity assay. Here, we showed that both toxins induce significant levels of cytotoxicity in a dose dependent manner. Importantly, mutations to amino acid residues postulated to be essential for their enzymatic and binding activities abolish toxin activity, indicating that these toxins enter and intoxicate cells using the anticipated pathway. Interestingly, we observed that the Stx2a A subunit can form synthetic hybrid toxins with the B pentamers of RIP-TT and RIP-HLT, and that both of these synthetic toxins are capable of causing cytotoxicity in HeLa cells. Our collective findings reveal a remarkably diverse arsenal of AB₅ toxins is encoded by various *Salmonella* serovars and provide fundamental insights into the evolution of AB₅ toxins.

Acknowledgements

I am immensely grateful to all members of the Fowler lab for their continuous support during this work. I am especially appreciative of my supervisor, Dr. Casey Fowler who provided me with the opportunity to conduct this research, and for his continuous patience, encouragement, and willingness to teach and guide me through the last 2 plus years. He has been a great mentor and a key contributor to my academic and professional success. I would also like to thank Dr. Wael Elhanawy for providing relevant insights and project guidance during my committee meetings and to Dr. Lisa Stein for taking the time to go over this thesis and provide useful feedback and contributions.

I am very grateful to our collaborators, Dr. Zhe Chen and Dr. Xiang Gao at Shandong University, Qingdao, China for providing useful structural data on A-B interactions in several *Salmonella* AB₅ toxins relevant to this thesis. A special thank you to my graduate colleagues, Luke Barretto and Paris Brown for their unrelenting support and friendship both in and out of the lab. I am also grateful for the additional technical support provided by Paris, particularly in the set up and maintenance of cell culture equipment crucial to several of my experiments. A massive thank you to the University of Alberta molecular biology service unit (MBSU) for permitting the use of several equipment that were necessary to this project and to members of the Dennis and Raivio lab for providing me with experimental assistance on multiple occasions and for advising me when needed.

Finally, this work would not have been possible without the continuous support I received from family and friends and I very grateful for this.

Table of Contents

<i>Chapter 1: General Introduction</i>	1
1.1 The <i>Salmonella</i> genus and salmonellosis	1
1.1.1 Nontyphoidal <i>Salmonella</i>	1
1.1.2 Typhoidal <i>Salmonella</i>	3
1.2 <i>Salmonella</i> pathogenesis	4
1.3 AB₅ toxins: structure and function	6
1.4 The evolution and diversity of AB₅ toxins	9
1.4.1 AB ₅ toxins investigated in this thesis.....	9
1.4.2 Shiga family of toxins	10
1.4.2 The Cholera toxin family	13
1.4.3 Pertussis family toxins	17
1.4.4 <i>Salmonella</i> AB ₅ toxins: ArtAB and Typhoid toxin	18
1.5 Functional implications of AB₅ toxin evolution and flexibility	27
1.6 Thesis objectives	28
<i>Chapter 2: The evolutionary diversification of the <i>Salmonella artAB</i> toxin locus</i>	<i>30</i>
2.1 Introduction	32
2.2 Materials and methods	37
2.2.1 Identification and analysis of <i>artAB</i> genetic elements and ArtAB toxin subtypes.....	37
2.2.2 Identification and analysis of <i>pltC</i> genetic elements	38
2.2.3 Analyzing rates of non-synonymous and synonymous mutations (dN/dS).....	39
2.2.4 Identification and analysis of prophages encoding <i>artAB</i> and <i>pltC</i>	40

2.2.5 Structural analysis of B subunit interactions with A subunits and with glycans	41
2.3 Results	42
2.3.1 Multiple subtypes of the ArtAB toxin are encoded by diverse prophages within the <i>Salmonella</i> lineage	42
2.3.2 Evolutionary adaptations of the <i>pltC</i> locus	46
2.3.3 Widespread distribution of <i>pltC</i> elements indicates a pervasive role in expanding the functional versatility of typhoid toxins	51
2.3.4 Sequence diversity amongst ArtB/PltC glycan binding residues	56
2.4 Discussion.....	60
2.5 General conclusions and link to Chapter 3.....	65
Supplementary Data and Figures (Chapter 2).....	66
<i>Chapter 3: Identification and characterization of two novel putative AB₅ toxins identified in Salmonella.....</i>	<i>72</i>
3.1 Introduction.....	73
3.2 Materials and Methods.....	76
3.2.1 Identification and analysis of putative AB ₅ toxins in <i>Salmonella</i>	76
3.2.2 Bacterial strains, plasmids, and growth conditions.....	77
3.2.3 Plasmid design	79
3.2.4 Purification of His ₆ -tagged proteins	81
3.2.5 Sodium Dodecyl Sulphate-Polyacrylamide Gel Electrophoresis (SDS-PAGE) analysis of purified toxins	83
3.2.6 Cell viability assays	84

3.3 Results	86
3.3.1 The <i>rip-tt</i> genomic locus exhibits significant similarity to the <i>artAB</i> genomic locus	86
3.3.2 The RIP-TT toxin is widely distributed in the <i>Salmonella</i> genus.....	87
3.3.3 Identification, analysis, and distribution of the <i>rip-hlt</i> genomic locus	88
3.3.4 Phylogenetic and comparative sequence analyses of the RIP-TT and RIP-HLT toxins	90
.....	96
3.3.5 Molecular cloning of a collection of plasmids for heterologous overexpression and analysis of RIP-TT, RIP-HLT and related toxins	97
3.3.6 Purification of RIP-TT, RIP-HLT and related toxins indicates interactions between RIP-like A subunits and homologs of ArtB and LT-II B	99
3.3.7 Cytotoxicity of HeLa cells following intoxication with purified RIP-TT, RIP-HLT and related toxins	101
3.3.8 The Stx2a A subunit is able to form a functional toxin complex with the B subunits of both RIP-TT and RIP-HLT	104
3.4 Discussion.....	107
<i>Chapter 4: General discussion and relevance of both studies</i>	<i>117</i>
References	125
Appendices.....	165

List of Tables

Table S2.1. Percent query coverage matrix between the identified groups of <i>artAB</i> and <i>pltC</i> -encoding <i>Salmonella</i> phages.....	66
Table 3.2.2. List of bacterial strains, plasmids and mammalian cells used in this study.....	77
Table 3.2.3. List of reagents used in this study.....	78
Table 3.2.4. Primers used in this study.....	80
Table 3.2.5. Restriction enzymes used in cloning the collection of plasmids used in this study.	81
Table S3.1. Summary of <i>Salmonella</i> strains and serovars encoding the RIP-TT toxin, compiled in September 2021.	163

List of Figures

Figure 1.1. The Canonical AB ₅ toxin architecture.....	8
Figure 1.2. General AB ₅ intoxication pathway.....	8
Figure 1.3. Cellular activity and effects of the ribosome inactivating Stx A subunit.....	13
Figure 1.4. Schematic diagram depicting the unique architecture of the <i>Salmonella</i> typhoid toxin that resulted through a combination of homologous A and B subunits from two distinct AB-type toxins.....	24
Figure 1.5. <i>S. Typhi</i> produces two forms of typhoid toxin with identical enzymatic A subunits but different binding B subunits.....	25
Figure 1.6. Schematic diagram showing the sequence diversity found in the Shiga and Cholera family toxins.....	26
Figure 2.3.1. Several different ArtAB toxin subtypes are encoded by diverse prophages in <i>Salmonella</i>	44
Figure 2.3.2. Evolutionary divergence of the <i>pltC</i> and <i>artB</i> genetic elements.....	49
Figure 2.3.3. The <i>pltC</i> genetic element has been subject to significant diversification and horizontal transfer within the <i>Salmonella</i> lineage.....	54
Figure 2.3.4. Analysis of the diversity within the glycan binding pockets of different <i>Salmonella</i> ArtB subtypes and PltC groups.....	58
Figure S2.1. Amino acid sequence alignment of the subunits of different ArtAB toxin subtypes.....	67
Figure S2.2. Phylogenetic trees depicting the relationships between the amino acid sequences encoded by different <i>Salmonella artAB</i> -like genetic elements.....	68
Figure S2.3. DNA sequence alignment of the <i>S. Typhimurium</i> DT104 <i>artAB</i> locus and the <i>pltC</i> loci of <i>S. Typhi</i> TY2 and <i>S. Javiana</i> CFSAN001070.....	69

Figure S2.4. PltC and ArtB have similar central pores capable of accommodating the PltA C-terminal α -helix.	70
Figure S2.5. Phylogenetic trees depicting the relationships between the amino acid sequences of the various PltC groups identified in this study.	70
Figure S2.6. Phylogenetic trees depicting the relationships between the DNA sequences of the various <i>artAB</i> type 1 and <i>pltC</i> genetic elements identified in this study.	71
Figure S2.7. Conservation of glycan-binding residues amongst the different ArtB type 1 subtypes and PltC groups.	71
Figure 3.1. Schematic representation of the predicted architectures of two novel AB ₅ toxins identified in <i>Salmonella</i> and their relationships to other known AB ₅ toxins.....	75
Figure 3.3.1. Genomic loci encoding the putative RIP-TT and RIP-HLT hybrid toxins.	89
Figure 3.3.2. Sequence alignment and phylogenetic analysis of the amino acid sequences of RIP A subunits from different bacterial species.	93
Figure 3.3.3. Sequence alignment and phylogenetic analyses of the B subunit protein sequences of RIP-TT and RIP-HLT.....	97
Figure 3.3.4. Collection of designed plasmids used in the overexpression of RIP-TT, RIP-HLT and related toxins.	99
Figure 3.3.5. Analysis and verification of A-B interactions in the RIP-TT and RIP-HLT toxins.....	101
Figure 3.3.6. The RIP-TT and RIP-HLT toxins induce a dose-dependent cytotoxicity in HeLa cells using an RIP-like mechanism.	104
Figure 3.3.7. The Stx2a A subunit is able to form a functional toxin complex with the B subunits of both RIP-TT and RIP-HLT and induce cytotoxicity in HeLa cells.....	106

Figure S3.1. DNA sequence alignment of the *S. Stanleyville* RSE1 rip-tt locus and the *S. Typhimurium* DT104 artAB locus.175

Figure S3.2. Complete amino acid sequence alignment of the B subunits of RIP-TT, *S. Typhi* PltB and the different ArtAB toxin subtypes and PltC groups. 176

Figure S3.3. SDS-PAGE analysis of several fractions from the purification of other proteins used in this study. 177

List of Abbreviations

EPEC: Enterotoxigenic *Escherichia coli*

STEC: Shiga toxin-producing *Escherichia coli*

HUS: Haemolytic Uremic Syndrome

Neu5Ac: N-Acetylneuraminic acid

Neu5Gc: N-Glycolylneuraminic acid

SubAB: Subtilase toxin, A and B (SubA/SubB)

Ctx: Cholera toxin

Ptx: Pertussis toxin

ArtAB: ADP-ribosyl transferase A and B (ArtA/ArtB)

CdtB: Cytotoxic distending toxin B

PltA/PltB: Pertussis like toxin A/Pertussis like toxin B

LT: Heat-labile toxin

Stx: Shiga toxin

Gb3: Globotriaosylceramide

GM1: Monosialotetrahexosylganglioside

GM2: Disialotetrahexosylganglioside

ER: Endoplasmic reticulum

ERAD: Endoplasmic reticulum-associated degradation pathway

RIP: Ribosome inactivating protein

Chapter 1: General Introduction

1.1 The *Salmonella* genus and salmonellosis

Salmonella is a genus of Gram-negative bacteria which are a leading cause of foodborne infections worldwide (1). The *Salmonella* genus contains two species, *S. enterica* and *S. bongori*. *S. bongori* comprises at least 22 serotypes that mostly infect cold-blooded animals like lizards and snakes but are rarely implicated in human disease (2). *S. enterica* comprises six subspecies including *enterica* (I), *salamae* (II), *arizonae* (IIIa), *diarizonae* (IIIb), *houtenae* (IV) and *indica* (VI) that colonize and infect a range of hosts including plants, animals, and humans. *S. enterica* subspecies *enterica* which harbours over 2,600 serovars is the most studied subspecies due to its frequent association with human infections (3–5). There is immense diversity within *enterica* subspecies in terms of host range and disease outcomes and serovars can be classified based on this into typhoidal and nontyphoidal *Salmonella* (6).

1.1.1 Nontyphoidal *Salmonella*

Nontyphoidal *Salmonella* (NTS) encompass several pathogenic serovars including *S. enterica* serovar Typhimurium ((*S. Typhimurium*). Henceforth, all *S. enterica* serovars will be referred to using this shorthand: *S.* (serovar name)), *S. Enteritidis*, *S. Dublin*, *S. Infantis*, *S. Gallinarium* and *S. Choleraesuis* that infect a wide range of hosts (7). NTS infection typically presents as a self-limiting gastroenteritis with symptoms such as fever, nausea, abdominal discomfort, and diarrhoea (7) and are mainly transmitted via the consumption of contaminated food and water (8–10). There is an annual estimate of 93 million cases of salmonellosis worldwide with over 150,000 deaths (11). *S. Enteritidis* and *S. Typhimurium* are two of the

most well characterized NTS serovars that constitute the greatest disease burden globally (12–14). *S. Enteritidis* colonizes a variety of hosts but most infections due to this serovar relate to poultry, where human infection typically occurs following consumption of contaminated products like chicken and eggs (15–17). In comparison, *S. Typhimurium* generally infects a broader host range and is more frequently associated with human infection (18,19). Although NTS infections tend to be mild, severe and invasive forms of disease may occur as a result of systemic spread of the bacteria to extra-intestinal sites. There has been an increasing number of reports of invasive NTS (iNTS) infections such as bacteraemia and meningitis in several parts of the world (20). In Sub-Saharan Africa, iNTS are of particular concern, predominantly in immunocompromised individuals like those with Human Immunodeficiency Virus (HIV), diabetes, sickle cell anaemia and malignant tumours, with an annual incidence rate estimated to be between 175 to 388 per 100,000 people (10,12,20–23). Young children, elderly patients and individuals residing in regions where malnutrition and malaria are endemic also have an increased risk of developing iNTS infections (21,24). However, healthy adults are still susceptible to iNTS infections and a few cases of bacterial dissemination to deep endovascular tissues have been reported (7).

Bacteraemia is the most common clinical manifestation seen in patients with iNTS infection with other comorbidities such as hepatosplenomegaly and respiratory distress occasionally observed (23,25). Treatment of iNTS infections involve an extensive course of antimicrobial therapy for about 10 to 14 days and the majority of infected patients are able to make a full recovery with minor or no complications. However, the current rise in multi-drug resistant strains of NTS coupled with the lack of effective vaccines complicate the management of iNTS leading to disease complications and in some cases, death of affected individuals (26). The NTS

serovars mostly associated with extra-intestinal infection include *S. Typhimurium*, *S. Choleraesuis*, *S. Enteritidis* and *S. Dublin*, suggesting some sort of underlying genetic factors encoded by these serovars that may provide an advantage in terms of disease (27–30).

1.1.2 Typhoidal *Salmonella*

In contrast to NTS, typhoidal *Salmonella* serovars which include *S. Typhi* and *S. Paratyphi* (A, B and C) are human-restricted and generally cause severe infections such as typhoid and paratyphoid fever. Typhoid fever, also known as enteric fever, is a severe and life-threatening infection that infects approximately 11 to 21 million people annually, worldwide with over 120,000 associated deaths (12,21). Clinical manifestation of typhoid fever often includes symptoms such as fever, headache, malaise, loss of appetite and gastroenteritis in some cases, and disease management typically requires a course of antimicrobial treatment, fluid replacement and occasionally, surgery if intestinal damage occurs (32–34). Without immediate and appropriate treatment, typhoid fever may progress to a multi-systemic infection that involves organs such as the liver, spleen, gallbladder, lymph nodes and brain with a high fatality rate ~10 - 30% (31,35). Paratyphoid fever, a similar but less pronounced febrile illness is also a major contributor to the morbidity and mortality rates associated with typhoidal *Salmonella* with an annual estimate of five million cases occurring globally (35,36). One of the main routes of typhoidal *Salmonella* transmission is via contaminated faecal matter (37,38). Many people remain asymptomatic carriers of the bacteria following acute infection and continuously shed bacteria for prolonged periods which ranges from a few months to several years, facilitating transmission (39,40). Typhoidal *Salmonella* infection is mostly prevalent in developing

countries in Sub-Saharan Africa and certain regions of Asia where poor hygiene and sewage contamination is dominant (32,35,41).

1.2 *Salmonella* pathogenesis

Pathogenic *Salmonella* serovars employ a wide array of virulence factors to successfully invade and infect hosts. These virulence factors include fimbriae, flagella, lipopolysaccharide (LPS), secreted exotoxins and type III secretion systems (T3SS) that are encoded on chromosomal regions known as *Salmonella* pathogenicity islands ((SPI)-1 and 2) (42–44). Following ingestion of contaminated food or water, *Salmonella* bypasses the mucosal defence mechanisms of the stomach to reach the intestinal mucosa. Here, the bacteria utilizes effector proteins that are secreted by the SPI-encoded T3SS to invade M (microfold) cells and non-phagocytic epithelial cells which facilitates transmission across the intestinal epithelial barrier to the lamina propria (45). The bacteria are then phagocytosed by macrophages into *Salmonella* containing vacuoles (SCV), a process which may also be mediated by the SPI-I T3SS. In the SCV, effector proteins secreted by the SPI-2 encoded T3SS are suggested to promote intracellular survival and replication by preventing lysosomal maturation and degradation.

The host inflammatory response elicited during *Salmonella* invasion of the gut epithelium is suggested to vary between NTS and typhoidal *Salmonella* and may partly account for differences in disease outcomes. During early infection, NTS induce a robust proinflammatory response that involves neutrophil influx to the gut and the activation of cytokines such as interleukin (IL)-1, IL-6, IL-8 and tumour necrosis factor (TNF)-2 which contributes to intestinal inflammation and the subsequent establishment of a localized gastrointestinal infection (46,47). In contrast, during early infection in the gut, *S. Typhi* employs mechanisms to disrupt crucial

host cytoskeletal processes and suppress the activation of immune signalling molecules (48,49). The *S. Typhi* Vi capsular polysaccharide, which is absent in NTS, plays an important role in suppressing innate immune defence mechanisms such as neutrophil influx and inhibiting complement activation in the gut. This in turn allows the bacteria to evade immune system clearance and establish a more persistent and chronic infection (50).

The disparity in disease severity observed in the *Salmonella* genus between distinct serovars and strains indicates that there are underlying genetic factors that influence the nature of disease outcomes. In comparison to NTS, the genomes of typhoidal *Salmonella* serovars appear to have undergone extensive degradation defined by a loss of function in several homologs of essential genes encoded by NTS (51,52). Many of the functional genes encoded by *S. Typhi* and *S. Paratyphi A* are geared towards efficient colonization and invasion in humans, indicating that these serovars have adapted to specific hosts (humans) (53,54). Similarly, genomic analysis of the NTS serovars that are most implicated in more severe disease types revealed that the majority of these serovars harbour additional genes that may enhance their virulence capabilities within hosts (53,55). A thorough understanding of the genetic and molecular factors that influence the virulence properties and disease outcomes in diverse *Salmonella* strains and serovars is therefore needed in order to attain a better understanding of the pathogenic potential of highly virulent salmonellae. Bacterial AB-type toxins represent one of such virulence factors that are encoded by several enteric pathogens that are commonly associated with severe human diseases.

1.3 AB₅ toxins: structure and function

AB toxins are secreted proteins that target and enter host cells and disrupt crucial cellular and biological processes (56). AB toxins are composed of two distinct polypeptide subunits that assemble into a multimeric protein consisting of an enzymatic A (active) subunit that disrupts normal host cell functions and a B (binding, or delivery) subunit that targets cells by binding to specific receptors that are present on the host cells (57). AB-type toxins are produced by several medically relevant pathogens including *Corynebacterium diphtheria*, *Bacillus anthracis*, *Clostridium spp.*, and *Campylobacter jejuni*, where they significantly contribute to the establishment of disease (58–61).

AB toxins can be further categorized based on stoichiometry of the A and B subunits and include toxins with single or multiple A and/or B subunits. AB₅ toxins are composed of an enzymatic A subunit that is non-covalently linked to a homopentameric delivery B platform (62,63) (Figure 1.1). The A subunit includes an N-terminal A1 fragment that is attached to a smaller C-terminal A2 peptide via a disulphide bond formed between two cysteine residues (64–67) (Figure 1.1). The A1 fragment carries out the enzymatic activity of the toxin while the A2 peptide anchors the A1 fragment to the B pentamer via its C-terminal α -helical loop that inserts into the pentameric B ring and interacts with the amino acid residues that line the pore of the pentameric B subunit ring (Figure 1.1). Cellular entry of the AB₅ holotoxin is mediated by B subunit binding to specific glycan receptors present on the host cell plasma membrane (63). The AB₅ holotoxin is then internalized into endosomes via receptor-mediated endocytosis and is subsequently translocated via a retrograde pathway through the trans-Golgi network to the lumen of the endoplasmic reticulum (ER) (Figure 1.2). In the ER, enzymes such as the protein disulphide isomerase (PDI) bind and cleave the disulphide bond linking the A1 and A2 peptides,

allowing the unfolded A1 fragment to dissociate from the toxin complex (62,63). The A1 subunit traffics out from the ER to the host cytosol by hijacking the host cell ER-associated degradation (ERAD) pathway, a biosynthetic pathway that contains ER chaperones that recognize and facilitate degradation of misfolded proteins (64,68). Once in the cytosol, the A subunit refolds to become active and can then reach and modify its specific host cell target protein, leading to cellular intoxication (Figure 1.2) (69). Ultimately, this activity alters the host cell biology and triggers a cascade of immunological and biological effects that are beneficial to the bacterium and may manifest as symptoms of diseases often associated with the bacterial strains and serovars that produce these toxins. AB₅ toxins have evolved to be key players in the virulence and disease properties of a number of Gram-negative organisms such as *Vibrio cholerae*, *Bordetella pertussis*, certain *Escherichia coli* pathotypes and *Salmonella* serovars. AB₅ toxin-driven diseases range from mild cases of foodborne infections to severe and debilitating illnesses and are collectively responsible for millions of infections and hundreds of thousands of deaths each year. The biology of AB₅ toxins also make them useful tools in therapeutic disease treatment and cell biology studies. Given their importance in human health and disease, it is necessary to gain a deeper understanding of the mechanisms underlying the evolution and activity of AB₅ toxins.

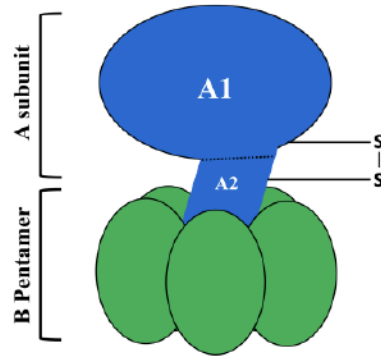


Figure 1.1. The Canonical AB₅ toxin architecture. Schematic depiction of the typical structure of a bacterial AB₅ toxin showing the catalytic A subunit (blue) which includes the A1 and the A2 moieties linked via a disulphide bond and the B subunit (green) which is made up of five monomers that form a pentameric ring.

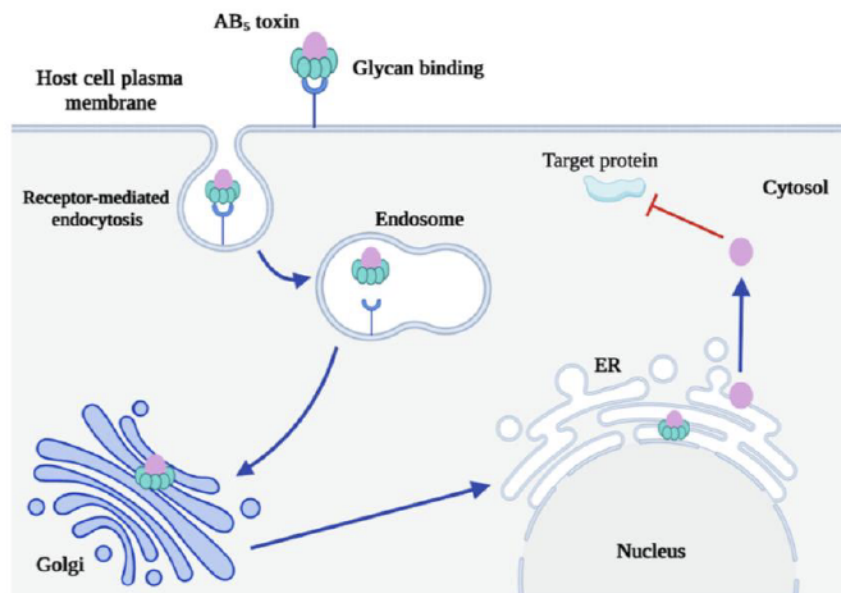


Figure 1.2. General AB₅ intoxication pathway. Cellular intoxication is initiated by B subunit binding to specific glycans on the host cell plasma membrane which results in receptor-mediated toxin uptake. The internalized holotoxin then traffics from early endosomes through the trans-Golgi network to the ER by retrograde trafficking. Once in the ER, the A subunit dissociates from the B pentamer and escapes to the cytosol via the host cell ER-associated degradation (ERAD) pathway. Here, the A subunit refolds and can then reach and modify its specific host cell target protein, leading to cellular intoxication. Created in BioRender.com.

1.4 The evolution and diversity of AB₅ toxins

All AB₅ toxins adopt a strikingly similar global structural architecture in which the A subunit sits atop a pentameric B subunit ring (Figure 1.1). Despite this, the binding and trafficking properties, as well as the enzymatic activities of AB₅ toxins can vary significantly and distinct AB₅ toxins may target different tissues or cell types and elicit very different biological effects. However, it is not uncommon for distinct AB₅ toxins to share some level of structural and functional similarity either in the enzymatic activity of their A subunits or the binding preferences of the B subunit. AB₅ toxins are often grouped based on A subunit activity and sequence identity into several families which include the Cholera family toxins, Pertussis family toxins, Shiga family toxins and Typhoid toxin (63). However, it is important to note that the binding properties of the distinct B subunits determine the cell and tissue tropism as well as the nature of hosts commonly associated with the bacterial strains that produce these toxins and cells lacking the specific binding receptors for distinct AB₅ toxins are generally resistant to intoxication. (70,71). Hence, these functional differences in glycan binding between different B subunits can significantly impact the cytotoxicity of AB₅ toxins which in turn, drives variations in their biological activity.

1.4.1 AB₅ toxins investigated in this thesis

Over the course of my thesis, I investigated several important AB₅ toxins found within the *Salmonella* genus. This includes the well-established *Salmonella* typhoid toxin (described below in section 1.4.4.1) and ArtAB toxin (described below in section 1.4.4.2) which are examined in chapter 2. In chapter 3, we present two novel AB₅ toxins found within the *Salmonella* genus that are composed of homologous subunits from various toxin families

including the Cholera family toxins, Shiga family toxins and Pertussis family toxins. In the sections below, relevant background information is given in order to provide important and sufficient context for subsequent parts of this thesis.

1.4.2 Shiga family of toxins

The Shiga family of toxins (Stxs) are potent AB₅ toxins that represent the principal virulence factors for *Shigella dysenteriae* type 1 and certain serogroups of *E. coli* known as Shiga-toxin producing *E. coli* (STEC) (72). STEC strains cause a range of infections from mild food poisoning to life-threatening illnesses like hemorrhagic colitis and hemolytic uraemic syndrome (HUS) (73,74). HUS is a debilitating disease characterized by thrombocytopenia, anaemia, and renal failure, that occasionally results in complications such as seizures and irreversible renal damage. STEC strains are estimated to cause approximately 3 million acute infections annually, and STEC induced HUS is a leading cause of acute kidney failure in infants and young children (75,76). Due to the nature and severity of diseases associated with STEC, of which Stx plays a central role, the Stx family of toxins are among the most well-studied AB₅ toxins.

The Stx holotoxin adopts the canonical AB₅ architecture composed a 32 kDa A subunit non-covalently bound to five identical 7.7 kDa B subunit monomers that make up the receptor binding B oligomer (77). The Stx A subunit is a type II ribosome-inactivating protein (RIP) with N-glycosidase activity that catalyses the depurination of ribosomes by displacing an adenine residue from the 28S ribosomal RNA of the 60S subunit of eukaryotic ribosomes, which plays a vital role in peptidyl transfer during protein synthesis (78). This activity ultimately disrupts eukaryotic protein synthesis and triggers the Ribotoxic stress response, which is characterized by the sequential activation and phosphorylation of signalling molecules like the

c-Jun NH₂ terminal kinases (JNK) and the p38 mitogen activated protein kinase (MAPK), which trigger the activation of caspases and the secretion of proinflammatory cytokines, resulting in cell death (79,80) (Figure 1.3). The RIP activity of the Stx family of toxins constitute an important part of Chapter 3 of this thesis.

The functional receptors to which the Stx B subunit bind are glycosphingolipids, in most cases showing strong specificity for globotriaosylceramide (Gb3) (81). The abundance of Gb3 varies by cell and tissue type and is known to be particularly abundant in the cell membranes of endothelial cells of the kidney and brain (82,83). Following Stx B binding to Gb3, the Stx holotoxin undergoes receptor mediated endocytosis and is trafficked to ER via a retrograde pathway where the A subunit dissociates from the B pentamer. The dislodged Stx A subunit escapes to the cytosol by hijacking the eukaryotic Endoplasmic-reticulum associated protein degradation (ERAD) where it refolds and can then reach the eukaryotic ribosome (84,85).

Following STEC colonization, secreted Stx is translocated across the intestinal barrier and through the circulatory system to renal microvascular, mesangial, and glomerular endothelial cells that are abundant with Gb3 (86). The downstream biological effects that result from Stx intoxication include intestinal inflammation that results in bloody diarrhoea and upregulation of anti-inflammatory molecules such as interleukin-1(IL-1) that boost Stx-mediated cytotoxicity and contribute to renal tissue damage (80). Stx intoxication may also result in neurological complications such as facial palsy, dysphasia and seizures and a few cases of HUS accompanied by severe neurological damage have been reported (76,87,88). However, the mechanistic details associated with the development of these symptoms are not well understood.

Stxs are classified into two evolutionarily related, but antigenically and functionally distinct subtypes known as Stx1 and Stx2 with multiple subtypes found within both groups. Stx1 is very

similar to the Stx produced by *Shigella dysenteriae* type 1 (99% amino sequence similarity) and includes subtypes Stx1a, Stx1c and Stx1d, while Stx2 shares only about 50-60% sequence identity to Stx/Stx1 and includes subtypes Stx2a, Stx2b, Stx2c, Stx2d, Stx2e, Stx2f, Stx2g as well as other recently identified subtypes (89,90). The prototypic Stx1a and Stx2a display dramatic differences in cellular and biological effects, with Stx2a being significantly more potent than Stx1a (21,22,23). STEC strains that produce Stx2a alone are associated with more severe infections like HUS compared to strains producing Stx1a or both Stx1a and Stx2a. Shiga toxin subtypes Stx1a, Stx2a, Stx2c and Stx2d are commonly isolated from human infection, while other subtypes mainly infect animals and are rarely implicated in human disease (93,94). The variation in Stx potency, host specificity and disease outcomes are mostly due to the binding properties of the B subunits or the variations in the Stx A2 subunit C-terminal residues that interact with the pentameric B ring since the enzymatic activity of the Stx A1 fragment is functionally conserved regardless of the Stx type or subtype (95,96).

The *stx* genes are encoded on diverse prophages and secretion of the assembled Stx holotoxin is primarily driven by phage-mediated bacterial cell lysis. The diversity of Stx phages significantly drives the emergence of novel Stx subtypes and is likely responsible for some of the functional differences observed in different Stx subtypes (97). The genes encoding Stx have also been identified in rare strains of other bacterial species such as *Enterobacter Cloacae*, *Shigella sonnei*, *Shigella flexneri*, *C. freundii* and *Vibrio* species, although it is not clear what roles they may play in the virulence and disease properties of these organisms (98,99).

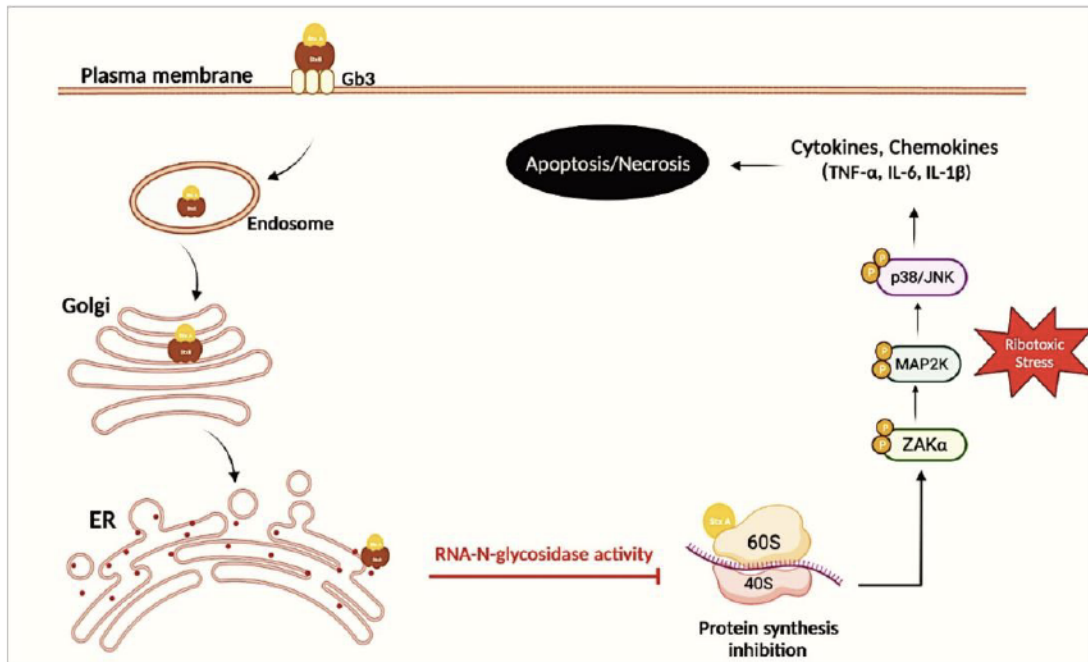


Figure 1.3. Cellular activity and effects of the ribosome inactivating Stx A subunit. Upon B subunit binding to Gb3 receptors on the host cell plasma membrane, the Stx holotoxin is internalized via receptor-mediated endocytosis. The toxin escapes the endosome and traffics intracellularly through the trans-Golgi network to the ER. In the ER, the Stx A subunit dissociates from the toxin complex and utilizes the ERAD pathway to escape to the cytosol. Here, the A1 subunit refolds and targets the 28S ribosomal RNA of the 60S ribosome via its N-glycosidase activity which leads to protein synthesis inhibition. This activity triggers the host cell Ribotoxic stress response which senses the cellular damage caused by the RIP activity of the Stx A subunit and induces a cascade of signalling events like the phosphorylation of the kinases (ZAK, MAP2K and JNK) which activates caspases and inflammatory mediators like cytokines and chemokines that drive apoptotic cell death. Stx activity may also result in necrosis, but this is less commonly observed. Created in BioRender.com.

1.4.2 The Cholera toxin family

Cholera toxin (Ctx) is the predominant virulence factor of *V. cholerae*, the causative agent of cholera, a highly virulent infection characterized by profuse watery diarrhoea, vomiting,

irritability and fatigue (100,101). Cholera affects ~3 million people annually, a significant proportion of which may result in fatality in the absence of effective treatment (101,102). The Ctx holotoxin consists of the enzymatic A subunit, CtxA non-covalently bound to a homopentamer of the binding and delivery subunit, CtxB (103). CtxA is an ADP-ribosyl transferase that covalently modifies eukaryotic membrane $G\alpha_s$ proteins, resulting in the irreversible activation of adenylate cyclase, an enzyme that disrupts eukaryotic cellular cyclic adenosine monophosphate (cAMP)- dependent ion transport. In the intestinal lumen, this disruption creates an imbalance of salt and electrolytes that eventually leads to the secretion of copious amounts of water from intestinal cells which manifests in the form of diarrhoea, the hallmark symptom for cholera (104,105,105). The drastic loss of water that ensues for Ctx activity can lead to severe dehydration and may facilitate *V. cholerae* transmission (101,106,107). Ctx entry into eukaryotic cells is primarily mediated by high affinity binding of CtxB to gangliosides, particularly Monosialotetrahexosylganglioside (GM1), cell signaling molecules that are found on the plasma membrane of intestinal epithelial cells and cells of the nervous system (108–111). The CtxB pentamer also binds with a much lower affinity to fucosylated glycoproteins, also expressed on intestinal epithelial cells and may facilitate cellular entry of the Ctx holotoxin (112).

The Ctx family of toxins includes the heat-labile enterotoxin (LT), which are important virulence factors in Enterotoxigenic *E. coli* (ETEC) pathotypes which cause a gastrointestinal illness known as traveller's diarrhoea (113). LT is divided into two antigenically distinct types, designated LT-I and LT-II with considerable diversity within both types (114,115). The LT-I holotoxin is structurally and functionally similar to Ctx and both toxins share ~ 80% amino acid sequence similarity in both the A and B subunits (116,116). LT-I-producing ETEC generally

cause a milder diarrhoeal infection to cholera, although a few cases of severe cholera-like disease have been reported (87,117). Like Ctx, the LT-I B subunit exhibits a strong affinity for GM1, and cellular entry and intoxication of LT-I is mediated by LT-I B binding to GM1 receptors present on intestinal epithelia (113,118). The LT-I A subunit also targets and modifies eukaryotic $G\alpha_s$ proteins which induces a similar cascade of cellular and biological effects to Ctx (119). LT-I has also been found to bind the related gangliosides, GM2 which does not contain the terminal galactose residue in GM1, and the sialic acid deficient asialo ganglio-N-tetraosylceramide (asialo-GM1), which is expressed on cells of the innate immune system like macrophages and basophils (65,120–122).

In Chapter 3 of this thesis, we identify and characterize an unusual AB₅-type toxin with a type II heat-labile-like B subunit. In comparison to Ctx and LT-I, the LT-II toxins are relatively recently characterized, and the *E. coli* strains that encode these toxins are rarely associated with human infection but have been isolated from farm animals and food sources (123,124). LT-II toxins are generally encoded on prophages found in diverse *E. coli* strains that have been isolated from various animal hosts and it is believed that such strains might be less adapted to infect humans. LT-II includes three subtypes, LT-IIa, LT-IIb and LT-IIc which adopt a similar structure to Ctx and LT-I and catalyse the ADP-ribosylation of $G\alpha_s$ proteins. LT-IIa and LT-IIb are the most well-studied LT-II subtypes. The A subunits of LT-IIa and LT-IIb share ~85% sequence similarity and ~60% sequence similarity to the A subunit of LT-I (114,125). However, the C-terminal sequences of the A2 peptides that mediate interactions with the pore of the pentameric LT-II B platform are ~38% identical in LT-IIa and LT-IIb and only 21% identical to the A2 sequence of LT-I (126,127). The B subunit of LT-IIa and LT-IIb exhibit ~58% sequence identity and share little to no significant sequence similarity to the Ctx and LT-I B

subunits (114,125). Despite this, the LT-II toxins exhibit a significant level of structural similarity to Ctx and LT-I and the LT-II B subunits also recognize and bind gangliosides, but with different specificity. LT-IIa and LT-IIb preferentially bind GD1 gangliosides and bind weakly to GM1 (128). However, even within the LT-II subtypes, there is significant variation in glycan binding preferences. LT-IIa exhibits high affinity binding to GD1b but also binds GD1a while LT-IIb exhibits a stronger affinity for GD1a gangliosides and binds a variety of other gangliosides including GD1b, GT1b, GM2 and GM3 albeit with a reduced affinity. Interestingly, LT-IIc which shares ~70-80% sequence similarity to the A subunits of LT-IIa and LT-IIb and ~53% sequence similarity to their B subunits has been shown to preferentially bind GM1 gangliosides with long-chain fatty acyl ceramides in murine models of infection (123,128). This binding preference is very distinct from what is usually found in LT-IIa and LT-IIb and is likely as a result of mutations in the B subunit sequence that has conferred binding specificity to different gangliosides and different hosts to what is typically observed in LT-IIa and LT-IIb. Like LT-IIa and LT-IIb, the B subunit of LT-IIc exhibits no significant similarity to those of Ctx and LT-I although their A subunits share ~57% sequence similarity to CtxA and LT-I A (128).

In addition to differences in binding preferences, LT-I and LT-II also differ in the orientation and interactions of the A and B polypeptides which may influence the assembly of individual holotoxins. Collective findings from comparisons between the architectures of LT-I and LT-II toxins, particularly the differences in amino acid sequences of their binding subunits indicate that LT-II may be evolutionarily diverged from LT-I and Ctx and *E.coli* strains encoding these toxins may have acquired a significantly different B subunit via horizontal gene transfer that is able to associate with an LT-I A subunit (125). These differences may also contribute to the variations in host range and clinical outcomes between the two LT types.

1.4.3 Pertussis family toxins

Pertussis toxin (Ptx) is a major virulence factor of *B. pertussis*, a human-restricted pathogen and the causative agent of whooping cough, an illness that mostly affects infants and young children and manifests as a low-grade fever, paroxysmal cough and vomiting (129). The currently administered DTP (diphtheria, tetanus, and pertussis) vaccines, which include purified Ptx as a major component, have been useful in protecting both children and adults against severe pertussis infection. Despite this, ~24 million people are estimated to be infected each year, a significant proportion of which result in pulmonary complications like pneumoniae and occasionally death (129,130). In certain developing countries, pertussis infection is a major cause of morbidity among non-immunized young children with approximately 400,000 deaths occurring yearly (131) .

The Ptx holotoxin is made up of five distinct subunits named S1 to S5. The S1 subunit serves as the enzymatic subunit and is coupled to a heteropentameric delivery B platform consisting of subunit S2, S3, two S4 subunits and an S5 subunit. The heteromeric nature of the Ptx delivery platform is unprecedented in the AB₅ toxin field and is thought to confer an evolutionary advantage to Ptx by expanding the pool of cell types that the toxin can bind (132). Epithelial cells of the human respiratory tract that express a variety of sialylated and non sialylated glycolipids and glycoproteins such as GD1a gangliosides, toll-like receptors, N-linked glycans and sialo-oligosaccharides are particularly sensitive to the effects of the Ptx S1 subunit which catalyzes the ADP-ribosylation of the α -subunit of heterotrimeric G_{i/o} proteins, membrane proteins that play important roles in eukaryotic cell signalling (24,118,132,133). Ultimately, S1 activity leads to an accumulation of cAMP levels (133). This can trigger a very wide range of biological effects that depend on the cell and tissue types that are intoxicated. The effects of

Ptx are thought to directly contribute to various symptoms associated with pertussis including histamine sensitization, alteration of glucose homeostasis, leukocytosis and the distinctive whooping cough that is a hallmark of pertussis infection (130,132). Ptx is suggested to be important in *B. pertussis* host-pathogen interactions and may also aid in the development of severe disease by suppressing the activation of proinflammatory cytokines during early infection (134–136).

AB-type toxins that have subunits with homology to the Ptx family of toxins have been identified in several other pathogenic bacteria including clinical isolates of *E. coli*, *Yersinia* species and *Salmonella* serovars. Despite established differences in activity, these toxins generally share significant levels of structural and functional similarities. The *Salmonella* ArtAB toxin which is particularly relevant to this thesis (discussed below) is composed of Ptx-like A and B subunits. ArtAB has been shown to bind sialic acid terminated glycoproteins and target eukaryotic G-proteins similar to Ptx.

1.4.4 *Salmonella* AB₅ toxins: ArtAB and Typhoid toxin

Pathogenic *Salmonella* serovars have not historically been thought of as having an endotoxin-driven virulence and most infections have been believed to be due to a combination of other virulence factors. Most NTS infections are also caused by serovars that lack AB-type toxins. Over the past ~15 years, two toxins, ArtA/ArtB (henceforth referred to as “ArtAB”) and typhoid toxin have been identified that appear to be important virulence factors of some particularly virulent *Salmonella* serovars and strains that cause severe infections in humans (137–139).

1.4.4.1 ArtAB toxin

ArtAB is a pertussis family toxin composed of A and B subunits that are homologous to the Ptx S1 subunit (A) and the Ptx S2 and S3 subunits (B) respectively (139–141). ArtAB was first identified in *S. Typhimurium* definitive phage-type (DT) 104, a highly virulent assortment of strains that have been isolated from humans and animals like cattle, pigs, and sheep (142,143). In animals, *S. Typhimurium* DT104 infection presents as watery or bloody diarrhoea, fever and dehydration which may progress to septicaemia (144). *S. Typhimurium* DT104 infections are endemic in England and certain European regions with an increasing number of cases being reported in the United States and Canada (143,144). In the last several decades, there has been a significant rise in multi-drug resistant strains of this pathogen to commonly used antibiotics like chloramphenicol, tetracycline, ampicillin, and trimethoprim, causing a challenge in the control of infections caused by DT104 strains (144–146). Multi-drug resistant *S. Typhimurium* DT104 has also been linked to minor outbreaks of gastroenteritis in humans, with some patients developing invasive disease and requiring hospitalization and the ArtAB toxin is suggested to impact the virulence properties of these strains (146).

ArtAB adopts the canonical AB₅ architecture with a 27 kDa A subunit (ArtA) and five 13.8 kDa B subunits that make up the pentameric B oligomer (ArtB) (140). ArtA belongs to the group of ADP-ribosylating toxins and shares significant sequence similarity with the A subunit of the Ptx and, to a lesser extent, the Ctx family toxins. Similar to these toxins, ArtA catalyses the ADP-ribosylation of eukaryotic pertussis-sensitive G proteins, presumably resulting in increased intracellular cAMP levels and biological effects that are not well-understood (140). ArtB shares approximately ~26-30% amino acid sequence similarity to the S2 and S3 subunits of Ptx but lacks the heteropentameric architecture of the Ptx B oligomer (140,142,147). ArtB

recognizes and binds sialoglycans, a chemically diverse spectrum of sialic acid-containing glycans that are widely distributed in several mammalian cells and tissues and other vertebrates with varying affinity (70,148,149). While the specific natural receptor(s) for ArtB remains unclear, it has been shown to bind both N-acetylneuraminic acid (Neu5Ac) and N-glycolylneuraminic acid (Neu5Gc) terminated sialoglycans which are found in many mammalian glycolipids and glycoproteins (149–151). Neu5Ac is a dominant sialic acid in humans and plays a role in host susceptibility to bacterial and viral infections. Neu5Gc, which differs from Neu5Ac by an additional hydroxyl group is not synthesized by humans but is present in many animals (152).

In *S. Typhimurium* DT104, the genes that encode the ArtAB toxin are located on a gifsy-1 prophage and the expression of the *artA* and *artB* genes is dependent on prophage induction, which also results in bacterial cell lysis and thus release of the assembled holotoxin. In *S. Typhimurium* DT104 it has been shown that adding compounds to bacterial cultures that induce the SOS response and trigger prophage induction, such as mitomycin C and hydrogen peroxide (H₂O₂), triggers the expression of the *artAB* genes (142,153). Although several studies have proposed a role for ArtAB toxin in pathogenesis, the precise contribution of this toxin to disease development is not known. ArtAB toxin has been shown to be cytotoxic in various cell lines including HeLa cells, Vero cells, Chinese Hamster Ovary (CHO) cells and colonic human epithelial and brain microvascular cells. Cellular intoxication has been shown to result in the upregulation of pro-inflammatory chemokines and cytokines at both local and systemic sites, which might contribute to disease. (62,154,155). Collectively, these studies highlight a potential role for ArtAB in *Salmonella* pathogenesis through modulation of host inflammatory response promote infection and potentially a greater propensity to cause invasive disease.

1.4.4.2 Typhoid toxin

S. Typhi produces a unique A₂B₅ toxin known as typhoid toxin which plays a crucial role in the development of typhoid fever (147,156,157). Typhoid toxin is composed of two distinct enzymatic subunits, PltA and CdtB that form a complex with the pentameric delivery B subunit, PltB (Figure 1.4) (156). Like ArtA and ArtB, PltA and PltB are Pertussis toxin-like subunits and both subunits share ~30% sequence similarity to Ptx S1, S2 and S3. PltA exhibits a higher sequence similarity to ArtA (~60%) while the PltB and ArtB sequences are ~30% identical. PltA possesses ADP-ribosyl transferase activity, however its cellular target is yet to be identified (154,158). PltB also binds cell surface sialoglycans similar to ArtB, although it has been shown to have a narrower specificity for Neu5Ac-terminated glycans and is unable to bind Neu5Gc. CdtB, the second enzymatic subunit of typhoid toxin, is a homolog of the active subunit of an AB-type toxin known as Cytolethal Distending Toxin (CDT) which is produced by several Gram-negative pathogens (Figure 1.4) (61). CdtB is a deoxyribonuclease (DNase) that induces double-stranded breaks in eukaryotic cellular DNA resulting in cell cycle arrest in the G2/M phase and eventually, cell death and the cellular effects observed in cells treated with the typhoid holotoxin is mainly attributed to CdtB (159,160). PltA interacts with the hydrophobic pore of the PltB pentamer via insertion of its C-terminal helix and serves as the major structural link between CdtB and PltB (63,156).

Due to the host-restrictive nature of *S. Typhi*, elucidating the role of typhoid toxin in *S. Typhi* pathogenesis is considerably hindered by the lack of suitable animal models of infection that are necessary to study several key aspects of the biology of *S. Typhi*. Several studies have implicated the use of cytidine monophospho-N-acetylneuraminic acid hydroxylase (CMAH)-null mice that lack the CMAH enzyme required in the synthesis of Neu5Gc glycans, which is

also absent in humans (137,161). Administration of purified typhoid toxin to CMAH-null mice has been shown to reproduce some of the symptoms of typhoid fever including leucocytosis, malaise, loss of appetite and central nervous system impairment (150,156). The CdtB-induced cellular DNA damage is suggested to contribute to the chronic colonization and there is some evidence that typhoid toxin may enable *S. Typhi* may play a role in suppressing the host intestinal inflammatory response, which may facilitate establishment of a persistent infection (162,163). In summary, collective findings so far indicate that typhoid toxin likely plays a bigger role in the development and progression of chronic typhoid fever and may be less important during the early stages of infection.

Typhoid toxin is unique amongst characterized AB₅ toxins in that it is produced by intracellular bacteria (*S. Typhi* that reside in a SCV within a host cell) (164–166). The expression of the typhoid toxin genes is tightly controlled by regulatory systems which are induced by environmental stressors present within the SCV that ensure that the toxin is exclusively produced from within this environment. The PhoP/PhoQ two-component system has been identified as the master regulator of typhoid toxin gene expression in the SCV. In low magnesium and low pH conditions, the inner membrane sensor, PhoQ activates the response regulator, PhoP via phosphorylation, which results in the transcription of the typhoid toxin genes and assembly of the A₂B₅ complex (164,167). Following its production, typhoid toxin is secreted using a unique mechanism that involves remodelling the cell wall to permit slow toxin release upon perturbation of the outer membrane by agonists present in the SCV. Once in the SCV lumen, the holotoxin is then packaged into vesicle carriers which are then trafficked out of the cell to the extracellular space (165,166,168). From this environment, typhoid toxin can adopt the traditional AB₅ intoxication mechanisms, binding receptors on the surface of target

cells. Cellular activities that interfere with the expression, sorting or trafficking of typhoid toxin have been shown to result in an unproductive intoxication, emphasizing the importance of these features in the biology and function of typhoid toxin(165,169).

Another unique aspect of typhoid toxin's biology was recently revealed when it was discovered that *S. Typhi* produce two different typhoid toxins. In addition to the "PltB typhoid toxin" described above, *S. Typhi* also encodes another B subunit, PltC, which is able to assemble an AB₅ complex with PltA and CdtB, replacing PltB as the homopentameric B subunit in the typhoid toxin complex (170). Although PltC shares only ~30% amino acid sequence similarity to PltB, the underlying molecular factors governing the interactions of PltB and PltC with PltA are relatively well conserved, allowing both subunits to compete for inclusion in the typhoid toxin complex. The two forms of typhoid toxin differ in their downstream biological effects following cellular intoxication. The PltC-typhoid toxin is more strongly linked to the suppression of host immune response in animal models of infection but does not elicit the extensive neurological damage observed in mice administered the PltB-typhoid toxin (170). Although *pltC* expression also requires the intracellular conditions of the SCV, the two toxins are differentially regulated and *pltC* expression is mainly controlled by the SSrA/SSrB two-component regulatory system, which also regulates the expression of the SPI-2 T3SS (44,170,171). In this system, the inner membrane histidine kinases, SSrA phosphorylates the SSrB response regulator under certain conditions which may include acidic pH and phosphate starvation, resulting in the expression of *pltC* (170–172). In support of this, mutations in *ssrA/ssrB* have been shown to substantially reduce the expression levels of *pltC* in *S. Typhi* infected epithelial cells. The PhoP/PhoQ two-component system has also been found to activate the expression of *ssrA* and *ssrB* and may indirectly play a much lesser role in *pltC* expression

(173,174). Because both versions of typhoid toxin retain their A subunit structure and function, the observed differences between the PltB- and PltC-typhoid toxins are due to functional variations in their B subunits. PltC does not exhibit the Neu5Ac specificity observed for PltB and binds an assortment of Neu5Ac and Neu5Gc terminated glycans (70). Structural analyses have revealed that PltC and its evolutionary cousin, ArtB share ~70% sequence similarity and both subunits contain an extra glycan binding pocket compared to PltB that is located on the basal side of the B oligomer that likely contributes to the binding differences between these proteins (70). The remarkable evolutionary twist of producing two different AB₅ toxins diversifies the function of typhoid toxin, although we do not yet have a complete understanding of the biological ramifications of this.

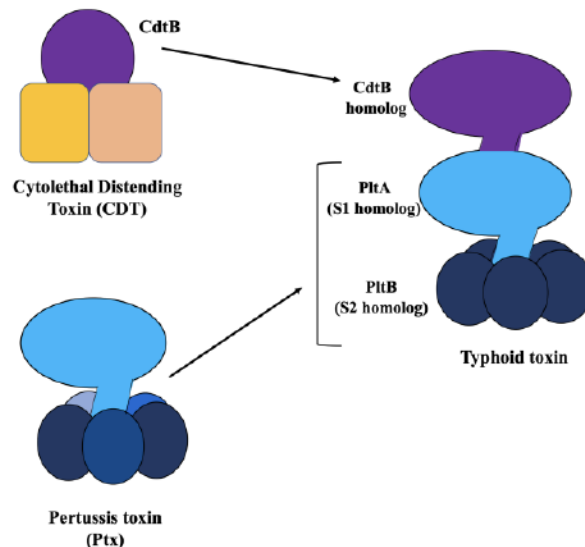


Figure 1.4. Schematic diagram depicting the unique architecture of the *Salmonella* typhoid toxin that resulted through a combination of homologous A and B subunits from two distinct AB-type toxins. The unique architecture of typhoid toxin is as a result of the amalgamation of homologs of the *B. pertussis* S1 and S2 subunits which make up the PltA/PltB core of typhoid toxin with the enzymatic subunit of Cytotolethal distending toxins (CdtB), an AB₂-type toxin from a different organism in a single toxin. (Adapted from (175)).

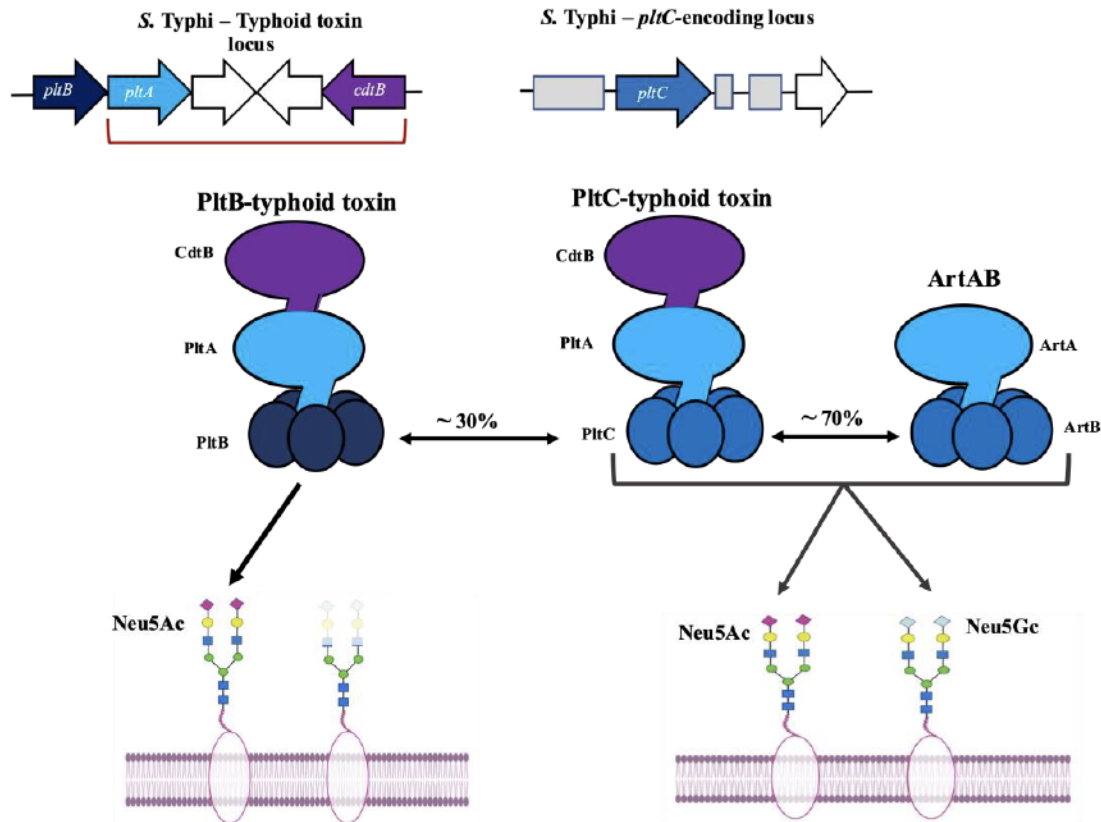


Figure 1.5. *S. Typhi* produces two forms of typhoid toxin with identical enzymatic A subunits but different binding B subunits. Schematic illustration of the *S. Typhi* *pltB* typhoid toxin locus that contains the genes encoding the PltB- typhoid holotoxin and the distant locus that encodes, PltC which serves as an alternate delivery subunit in the typhoid toxin complex and confers additional binding specificity to the typhoid toxin. PltC exhibits a higher sequence similarity to the ArtB subunit from the *S. Typhimurium* DT104 ArtAB toxin (~70%) compared to PltB (~30%). All three B subunits can bind an assortment of Neu5Ac-terminated glycans, however PltC and ArtB can also bind Neu5Gc-terminated glycans which PltB does not bind. Coloured arrows in the gene diagrams depict the structural genes that encode the A and B subunits of both versions of the typhoid holotoxin (PltB and PltC-typhoid toxin). Genes situated within the red bar indicate shared subunits between both toxins (CdtB and PltA). The grey boxes depict pseudogenes while white arrows indicate other functional genes found on both loci. (Adapted from (170)).

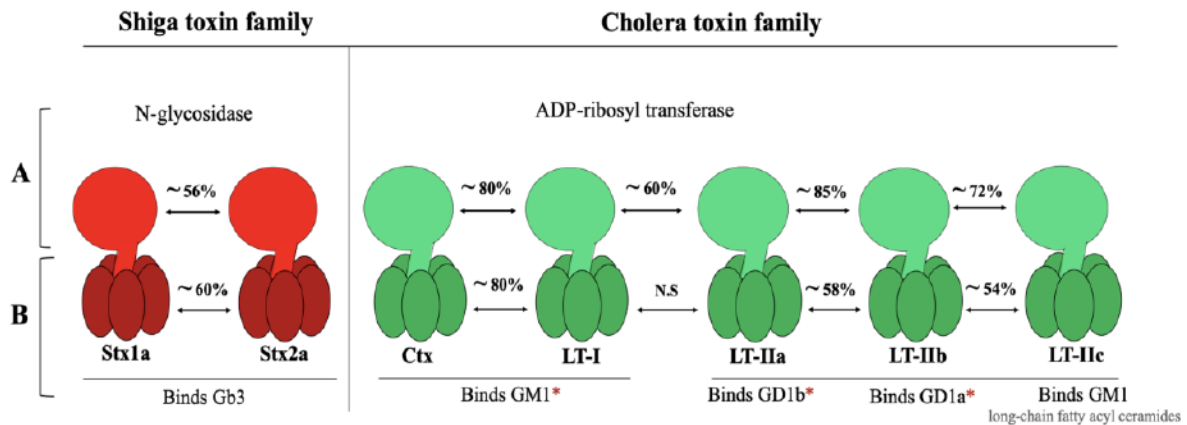


Figure 1.6. Schematic diagram showing the sequence diversity found in the Shiga and Cholera family toxins. Shiga and Cholera/Heat-labile toxins are a major part of Chapter 3 of this thesis. Both toxin families exhibit very different enzymatic activities (N-glycosidase vs. ADP-ribosyl transferase) and bind different glycans. The major Stx subtypes, Stx1a and Stx2a which share ~56-60% sequence similarity preferentially bind Gb3 receptors. In contrast, the Ctx family of toxins exhibit high affinity binding to a range of gangliosides. Ctx and LT-I which share roughly 80% sequence identity bind most strongly to GM1 gangliosides, while the major LT-II subtypes (LT-IIa and LT-IIb) exhibit high affinity binding to GD1 gangliosides. LT-IIc which is a relatively recently characterized LT-II subtype has been shown to specifically bind GM1 gangliosides with long-chain fatty acyl ceramides. The LT-II toxins exhibit higher sequence similarities in their A subunits (~ 60-85%) compared to the B subunits (~54-58%). The A subunits of LT-II toxins also share ~ 60% sequence similarity to those of LT-I but no significant sequence similarity is observed in their B subunits (N.S = Not Significant). Asterisks (*) indicate that these toxins bind other gangliosides (with lesser affinity) other than those stated here.

1.4.4.3 Diversity of *Salmonella* AB₅ toxins

Most of our current knowledge about typhoid toxin comes from *S. Typhi*, but the typhoid toxin genes are also sporadically distributed in various *S. enterica* serovars belonging to distinct lineages or clades (176–179). *S. Javiana*, a major NTS serovar that causes food-borne infections worldwide, has served as a model system for studying typhoid toxin outside of *S. Typhi*.

Although genetically similar, the *S. Javiana* typhoid toxin exhibits functional differences in both cell culture and animal models of infection compared to the *S. Typhi* typhoid toxin that have been traced to a few amino acid differences in the B subunits (179,180). These findings provide a glimpse into the enormous functional diversity amongst *Salmonella* typhoid toxins. An important but largely unexplored aspect of *Salmonella* pathogenesis is to understand the role that diverse AB₅-type toxins play in dictating the nature and severity of infections. However, investigating the potential contributions of AB₅ toxins in diverse *Salmonella* strains and serovars has been hindered by the immense diversity and irregular distribution of AB₅ toxin genes in *Salmonella*. In Chapter 2 of this thesis, we take an *in silico* approach to explore the evolution, distribution and functional implications of the diverse collection of the ArtAB and typhoid toxin genes in *Salmonella* as a fundamental step in deciphering the potential roles of ArtAB and typhoid toxin in other virulent *Salmonella* strains and serovars.

1.5 Functional implications of AB₅ toxin evolution and flexibility

Although all characterized AB₅ toxins exhibit structural similarities and utilize similar mechanisms to enter cells and reach their targets, there is a considerable amount of diversity amongst the different AB₅ toxin families and also within distinct families that has resulted in variations in the cellular and biological effects of distantly and closely related AB₅ toxins (63,181). The evolution and diversity of AB₅ toxins may be driven by horizontal gene transfer of prophage encoded AB₅ genetic elements, genetic recombination events, functional mutations in the A or B polypeptides and the spread of mobile genetic elements (182,183). In some cases, the resulting effect is the emergence of novel AB₅-type toxins that assemble from homologous components or subunits from distinct toxin families or novel AB₅-type toxins with newly

acquired subunits. Novel AB₅-type toxins with newly acquired A subunits in combination with homologs of B subunits from well-characterized toxin families leads to differences in enzymatic activities of these toxins which may have severe biological consequences. For example, the CfxAB and EcxAB toxins which have been identified in certain strains of *Citrobacter freundii* and *E. coli* are both composed of a Ctx/LT-I B subunit. However, their A subunits share no similarity to the Ctx family of toxins (184). Both CtxAB and EcxAB have been shown to assemble into a functional AB₅ complex that can induce morphological changes in certain cell lines (185). Subtilase toxin (SubAB), a relatively recently emerged AB₅ toxin produced by a certain STEC strains is composed of a B subunit (SubB) that shares similarities with the Ptx S2 subunit. However, the A subunit, SubA is a serine protease that targets an endoplasmic reticulum chaperone known as Bip and is functionally distinct from the Ptx S1 subunit. The genes encoding SubAB have since been identified in over 30 STEC strains, a few of which have been associated with severe disease (186,187). Conversely, newly acquired B subunits may result in toxins that bind very different glycans and cell types or exhibit subtle differences in binding specificities to their homologs which can also have serious implications.

In Chapter 3 of this thesis, we highlight some of the functional implications of AB₅ evolution by characterizing two novel “hybrid” toxins, each with unique subunit combinations that can assemble into potent AB₅ complexes capable of intoxicating cells.

1.6 Thesis objectives

1. To explore the evolution, distribution and functional implications of the diverse assortment of *Salmonella artAB*-like genetic elements using a variety of *in silico* methods.

2. To investigate the evolution and activity of novel “hybrid” AB₅-type toxins found within the *Salmonella* genus through a combination of bioinformatic and experimental analyses.

The objectives outlined above were addressed through two separate, but related projects aimed at providing a better understanding of AB₅ toxin evolution. Research addressing objective 1 is described in Chapter 2 and Research addressing objective 2 is described in Chapter 3.

Chapter 2: The evolutionary diversification of the *Salmonella artAB* toxin locus

By: Adaobi Ojiakor, Rachel N. Gibbs, Zhe Chen, Xiang Gao, and Casey C. Fowler

Preface

This chapter explores the evolutionary diversification of *Salmonella artAB*-like genetic elements and is modified from a paper published under a Creative Commons CC-BY licence in *Frontiers in Microbiology* in November, 2022 as: [Adaobi Ojiakor](#), [Rachel N. Gibbs](#), [Zhe Chen](#), [Xiang Gao](#), and [Casey C. Fowler](#) (2022) “The evolutionary diversification of the *Salmonella artAB* toxin locus” and is available at doi: [10.3389/fmicb.2022.1016438](https://doi.org/10.3389/fmicb.2022.1016438).

This work was a collaboration between the Fowler lab and Gao lab. My contributions to this study were primarily data extraction, sequence analyses, data interpretation, and being involved in producing figures/tables. To be more specific, my contributions to this work include compiling sequence data from the different ArtAB and PltC groups from large numbers of salmonellae, as well as analyzing these data by the generation of percent identity matrices and phylogenetic trees showing predicted evolutionary relationships between the 7 ArtAB subtypes and the four PltC groups. I additionally contributed to the analyses of their genome localizations and their association with prophages and the analysis of these prophages. This work and the tables/figures generated are found both in the main article (Figures 1 and 3, which are presented as Figures 2.3.1 and 2.3.3 in this thesis) and in supplementary files including the supplementary data files (containing the raw data used for the study) and the supplementary Figures/tables (S2.1, S2.2, S2.5, S2.6 and Table S2.1).

My supervisor, Dr. Fowler, and other authors contributed to writing and editing the manuscript and I provided feedback and edits for the manuscript. Specific contributions of other authors are available at: <https://doi.org/10.3389/fmicb.2022.1016438>.

2.1 Introduction

Salmonella enterica is a widespread species of enteric bacteria that can be broken into six subspecies and more than 2,500 serological variants (serovars), a subset of which are important human pathogens (2,6,18). The human adapted Typhi and Paratyphi A serovars cause prolonged systemic infections that underlie the disease (para)typhoid fever, a major health issue in the economically developing world (31,33,34,188). Certain other lineages, most notably *Salmonella* Typhimurium sequence type 313 (ST313), cause invasive non-typhoidal salmonellosis, which is predominantly endemic to Africa where it causes significant morbidity and mortality (189,190). In the economically developed world, however, *Salmonella* is best known as a leading cause of food poisoning, which typically presents as a self-limited gastroenteritis but can also trigger more serious complications, particularly in young children, older adults or immunocompromised individuals (7). Although a few serovars, such as Typhimurium and Enteritidis, account for a significant proportion of all *Salmonella* gastroenteritis cases, a very wide range of other salmonellae also routinely cause non-typhoidal disease (139,191,192). The proportion of infections caused by different serovars varies significantly across geographic regions and over time, and the host ranges and disease properties of different salmonellae are known to be variable at both the serovar and strain levels (139,191,193,194). Identifying genetic characteristics that confer more severe virulence properties will have important implications for our ability to diagnose, prevent and treat salmonellosis worldwide.

Recently, AB₅-type protein toxins have emerged as a key factor underlying the diversity of *Salmonella* virulence properties. These secreted, proteinaceous toxins consist of two distinct subunits or domains: A (or active) subunits that modify specific host cell target molecules or

structures and B (or delivery) subunits that mediate the binding of the toxin to receptors – typically glycans - on the surface of the host cell, resulting in the uptake and trafficking of the toxin to its site of activity (63,67,195). AB₅-type toxins adopt a common structural configuration wherein an active subunit sits atop a donut-shaped delivery platform comprised of five B subunits. Numerous AB₅-type toxins with heterogeneous sequences and biological activities have been identified and characterized, many of which are affiliated with enteric pathogens (132,187,196–198). Despite little or no significant sequence similarity between different families of AB₅ toxins, their common architecture suggests they are likely to be evolutionarily connected (63,67,195,199). The considerable diversity that exists both within and between the different AB₅ toxin families indicates that the AB₅ scaffold has been particularly amenable to evolutionary diversification, yielding a large, versatile arsenal of toxins that utilize this common structural arrangement. AB₅-type toxins play a major role in shaping the virulence properties of bacterial pathogens such as *Bordetella pertussis*, *Vibrio cholerae*, *Shigella dysenteriae* and certain *Escherichia coli* pathotypes and thus have a major impact on human health (113,132,187,196,197,200–202). Two AB₅-type toxins have been identified in *Salmonella*: typhoid toxin and ArtA/ArtB (henceforth ArtAB) toxin (137–139). Both of these toxins were identified within highly virulent salmonellae and have been implicated in their more severe disease properties (140–142,156,166,170,203).

Typhoid toxin was originally identified in *S. Typhi* as a unique A₂B₅ toxin comprised of three subunits: PltB, the delivery subunit, and two active subunits, PltA and CdtB (166). PltB and PltA are members of the pertussis family of toxins and assemble into a canonical AB₅ structure (156) CdtB, a homolog of the active subunit of Cytotoxic distending toxin, does not directly contact the delivery platform, but is stably incorporated into the toxin *via* a single

disulfide bond that covalently attaches CdtB and PltA, giving typhoid toxin its unusual A₂B₅ conformation (204). PltA is an ADP-ribosyl transferase, however its host cell target(s) have not yet been identified and all phenotypes currently associated with typhoid toxin stem from the activity of CdtB, a DNase that induces double-stranded breaks in host cell genomic DNA, leading to cell cycle arrest or cell death (160,166,204). Typhoid toxin is delivered using its PltB pentamer, which binds receptors containing N-Acetylneuraminic acid- (Neu5Ac) terminated glycans to mediate toxin uptake and trafficking (150,204). Typhoid toxin is highly unusual in that it is produced by intracellular bacteria, and PltB also mediates typhoid toxin exocytosis from the intracellular compartment where it is produced (139,164,166). A significant pool of evidence indicates that typhoid toxin is a key virulence factor for *S. Typhi* and that it may be directly responsible for some symptoms associated with severe typhoid fever (160,166,170,180,203–205). Typhoid toxin is not encoded by *Salmonella* serovars such as Typhimurium and Enteritidis that most commonly cause gastroenteritis, but it is widely (but sporadically) distributed in the *Salmonella* genus and it is clear that typhoid toxin is not the sole factor that confers the typhoidal serovars with their unique virulence properties (170,176,177,206). Typhoid toxin is not thought to play an important role in the early stages of *S. Typhi* infection, but is proposed to play a key role at the later (systemic) stages of infection (138,207). Certain nontyphoidal serovars that encode typhoid toxin have been observed to cause invasive disease at a higher rate than the Typhimurium and Enteritidis serovars, which is consistent with experimental data that indicate typhoid toxin can promote systemic spread or persistence in animal models of infection (162,179,191,193,194,203). These more invasive lineages elicit a range of severe disease outcomes, including those clinically-similar to typhoid fever (139,193,208,209). Sequence differences in the typhoid toxins produced by nontyphoidal

serovars can significantly alter their activity compared to *S. Typhi* typhoid toxin in cell culture and animal models of intoxication (180). This is not unexpected since it is well-known that different AB toxin sequence variants (subtypes) can elicit very different virulence or disease properties (93,210,211). The genetic variation in typhoid toxins and how different variants contribute to disease in nontyphoidal salmonellae is an important and largely unexplored subject.

ArtAB is an ADP-ribosyl transferase toxin that was originally identified in *Salmonella enterica* serovar Typhimurium definitive phage type 104 (*S. Typhimurium* DT104) (142). Like PltA/PltB, the ArtAB toxin is a member of the pertussis family of AB₅ toxins; ArtA is ~60% identical to PltA and ArtB is ~30% identical to PltB, suggesting that, although they have diverged significantly, the AB₅ core of typhoid toxin and ArtAB share a common ancestry (147). ArtAB is cytotoxic in cell culture models of intoxication and ArtA has been reported to target the α -subunit of host G-proteins, similar to pertussis toxin (140,141). ArtAB elicits toxicity in animal models of intoxication and provokes some of the same symptomology as pertussis toxin, although it does not induce leukocytosis, suggesting there are important functional differences between ArtAB and pertussis toxin (140). Although the function of ArtAB and how its activity might influence disease outcomes is not yet clear, it has been proposed that this toxin might play a role in manipulating the host immune response following *Salmonella*-induced intestinal inflammation (139).

Previous reports have shown that diverse *Salmonella* strains encode an ArtAB toxin and that there can be variability amongst these toxins (140). In addition, recent reports have shown that certain *Salmonella* lineages harbour an *artAB*- like locus in which the *artA* gene is degraded (a pseudogene) and the B subunit has evolved to serve as an alternate delivery subunit for typhoid

toxin, replacing PltB in an analogous complex with PltA and CdtB (70,170,176,179). Because these ArtB homologs serve a different function, they have been named PltC to reflect their involvement in typhoid toxin biology. The version of typhoid toxin featuring PltC as its delivery subunit has been shown to adopt a similar overall structure compared to the PltB version of typhoid toxin, but the PltC version has distinct glycan binding properties, distinct trafficking properties in cell culture models of *S. Typhi* infection, and elicits different symptomology in animal models of intoxication (70,170). These studies illustrate that the evolution of PltC as an alternate delivery platform has conferred significant functional versatility to typhoid toxin. There is therefore substantial evidence that *artAB/pltC*-like genetic elements can play an important role in the pathogenesis of the *Salmonella* lineages that produce them. However, deciphering the impact of *artAB/pltC* is complicated by the considerable genetic and functional diversity amongst these elements, as well as their discontinuous phylogenetic distribution.

In this study, we employ an array of *in silico* approaches to analyze the collection of *artAB/pltC* toxin genetic elements, how they are distributed within the *Salmonella* genus, how they may have evolved, and the functional implications of this diversity. Our results provide a framework for assessing the biology of the surprisingly diverse assortment *pltC* and *artAB* elements in the *Salmonella* lineage and provide insights into the mechanisms of evolutionary diversification of AB5-type toxins.

2.2 Materials and methods

2.2.1 Identification and analysis of *artAB* genetic elements and ArtAB toxin subtypes

In order to identify ArtAB toxins, the *S. Typhimurium* DT104 ArtA and ArtB sequences were used as the query sequence for tBLASTn searches of complete *Salmonella* genomes within the NCBI nonredundant nucleotide (nr/nt) DNA sequence database (which contains >2000 such sequences from diverse *Salmonella* lineages). These searches (and analogous searches of this database described below) were performed in December 2021. For the ArtA search, a sequence identity threshold of 65% and a query coverage threshold of 80% were set in order to exclude PltA (~60% identical to ArtA) from the results; all hits with an e value less than 0.05 were considered for the ArtB search. The complete set of ArtA-encoding genomes was then cross-referenced with the ArtB search results in order to identify genomes with an *artAB* toxin locus. To analyze the sequences of ArtAB toxins identified and to group them into toxin subtypes, the complete collection of ArtA and ArtB sequences were analyzed using iterative tBLASTn searches of individual toxin subunits from this collection. ArtAB toxins in which the ArtA and ArtB subunits were both more than 90% identical were then grouped into a toxin subtype. This threshold was guided in part by the natural spread (break points) in the sequence diversity observed, and strikes a reasonable balance between ensuring there is substantial sequence diversity between different subtypes, but without grouping genetically divergent sequences into a single group. This threshold (90%) was also used for *pltC* groupings. To compare the DNA and protein sequences of the different toxin subtypes, a single representative member of each group was selected. The selections of representative members here and elsewhere were arbitrary, but were guided by the results of the iterative BLAST searches in order to avoid selecting members whose sequences were outliers from the group at large. Multiple sequence

alignments of the representative members were then conducted using the EMBL-EBI suite of alignment tools using Clustal Omega (default parameters; Gonnet transition matrix, 6 bit gap opening penalty, 1 bit gap extension penalty) (212). The results of these alignments were then used to generate percent identity matrices, as well as to generate phylogenetic trees using the MEGA (Molecular Evolutionary Genetics Analysis) V11 software with the parameters noted in the Figure legends (213). The NCBI nr/nt database was selected for these analyses - as well as the *pltC* analyses described below – because it contains a large number of complete genome sequences from diverse *Salmonella* subspecies and serovars, and because it is accessible/compatible with a range of bioinformatic tools (such as NCBI sequence comparison and analysis tools and PHASTER) that we used to analyze this data set. To determine which *artAB*- encoding genomes (and *pltC*-encoding genomes) also encode typhoid toxin, the complete sequence of the *S. Typhi* TY2 typhoid toxin (start of *cdtB* coding sequence through start of *pltB* coding sequence) islet was used for BLASTn searches that were cross- referenced with our list of *artAB*-encoding genomes (or *pltC*- encoding genomes). Genomes that aligned significantly over >80% of the input sequence were considered to have a typhoid toxin islet. To ensure that typhoid toxin islets with divergent sequences were not being missed by this analysis, searches were also conducted with divergent typhoid toxin islet sequences from the *S. bongori* and subsp. *diarizonae* lineages; these searches yielded the same results as those using the Typhi islet.

2.2.2 Identification and analysis of *pltC* genetic elements

Complete *Salmonella* genomes within the NCBI nonredundant nucleotide (nr/nt) DNA sequence database that encode a *pltC* genetic element were identified using BLASTn searches

using the *S. Typhi* TY2 sequence spanning from the start of the *sty1362* sequence through the end of the *pltC* sequence. Only hits that resulted in a single alignment that spanned >90% of the full query sequence were considered further. To determine whether the identified sequences encode an intact PltC homolog, the results were cross-referenced with a tBLASTn search using *S. Typhi* PltC as the query sequence. The (few) strains in which *pltC* was found to be a pseudogene were excluded from further analysis. To determine which *pltC* elements were located within an islet at the *sap* locus, we did a BLAST search of the *S. Typhi* sequence spanning *pltC* through *sapB* and cross-referenced this list with our master list of hits. The genomic locations of any *pltC* elements that were not identified to be at the *sap* locus using this approach were manually inspected using the NCBI genome browser. PltC sequence comparisons were conducted as described above for ArtA and ArtB.

2.2.3 Analyzing rates of non-synonymous and synonymous mutations (dN/dS)

To explore whether there is evidence that the ArtB/PltC B subunits have been subjected to positive (diversifying) selection, we analyzed the DNA sequences of type 1 *artB* genes and *pltC* genes using the BUSTED analysis tool (hosted by webmonkey.org) (214). This tool uses the rates of non-synonymous and synonymous mutations amongst homologous genes to determine whether there is evidence (on a gene-wide level) that the gene has been subjected to diversifying selection. For this analysis, we used the DNA sequences of each of the representative *pltC* groups (*pltCsap*, *pltCphage1*, *pltCphage2*, *pltCphage3*) and each of the type 1 *artB* groups (1a, 1b, 1c, 1d). Type 2 *artB* sequences were not included since they share minimal protein sequence similarity and no significant DNA sequence similarity. Because this tool works better with larger and more diverse datasets, we also included the sequence of the most divergent member

of each of these groups/subtypes (member with the lowest % amino acid sequence identity compared to the representative member) in the analysis for any groups/subtypes where at least one member of the group is <98% identical to the representative member. The accession numbers of the “divergent” members used were: *pltC*_{sap} (CP082381.1), *pltC*_{phage2} (CP042441.1) and *pltC*_{phage3} (CP014996.1). DNA sequences for each of the genes described above were aligned using Clustal omega and this alignment file was submitted to BUSTED for analysis *via* the webmonkey.org web server.

2.2.4 Identification and analysis of prophages encoding *artAB* and *pltC*

To determine whether identified toxins were encoded from within prophage, we used the PHASTER web-based phage identification and analysis tool (215,216). PHASTER was used to identify the complete set of prophages in each of the genomes encoding an ArtAB toxin as well as all PltC-encoding genomes where *pltC* was found to be outside the sap locus. The genomic locations of all of the identified prophages within each of these genomes were then cross-referenced with the genomic locations of the toxin loci. To analyze and compare the phage, their complete sequences were exported from PHASTER and compared using iterative sequence alignments using the BLASTn pairwise sequence alignment tool to compare query phages to all other identified phages. Phages which exhibited significant sequence similarity that spanned >80% of the smaller phage and >50% of the larger phage were deemed to be in the same group (different thresholds were necessary since the sizes of the prophages identified were highly variable). This threshold allowed us to capture the substantial phage diversity that exists in our dataset without parsing apart genetically similar phages with only subtle variations. Phage sequence comparison diagrams were generated with the assistance of EasyFigure V2.2.2 (217).

2.2.5 Structural analysis of B subunit interactions with A subunits and with glycans

Structural analyses, including structural alignments and modelling, were conducted using Pymol V2.0 (Pymol, 2015). Analysis of the A-B interactions was conducted using the structure of PltC typhoid holotoxin (PDB ID: 7EE6) and the structure of the ArtB homopentamer (PDB ID: 5WHV), where the interface between ArtB and PltA was modelled by displaying each chain of the B subunit individually and measuring its interactions with the A subunit. Analysis of glycan interactions utilized the Neu5Aca2- 3Galb1-3Glc-bound structures of both ArtB (PDB ID: 5WHU) and PltC (PDB ID: 7EE5).

2.3 Results

2.3.1 Multiple subtypes of the ArtAB toxin are encoded by diverse prophages within the *Salmonella* lineage

It has been observed that assorted *Salmonella* strains produce ArtAB toxins that in some instances have different sequences, however the sequence diversity and phylogenetic distributions of *Salmonella* ArtAB toxins have not been comprehensively analyzed (140). To explore this issue, we mined the NCBI nr DNA sequence database and compiled a complete list of all *Salmonella* genomes in this database that encode an intact, full-length homolog of *S. Typhimurium* DT104 ArtA. Using a 65% sequence identity cut-off to omit PltA from our analysis, we identified a total of 60 genomes that encode ArtA. We found that an intact ArtB is encoded immediately adjacent to ArtA in 59 of the 60 strains, suggesting these strains have the capacity to produce an ArtAB toxin (an *artB* gene is present in the other strain - *S. bongori* strain NCTC12419 accession number LR134137.1 - but it is a pseudogene and thus this strain was excluded from further analysis). We then compared the amino acid sequences of the 59 ArtA and ArtB proteins and found that there is considerable diversity amongst the toxins encoded by these strains. In accordance with the nomenclature established for other AB5-type toxins, we divided these different ArtAB toxins into distinct types and subtypes. On the basis of both sequence similarity and gene order (*artAB* versus *artBA*), the identified toxins overtly clustered into two clades, which we have dubbed type 1 and type 2 (Figure 2.3.1A; Supplementary Figure S2.1). The grouping of ArtAB toxins into these two types is also supported by phylogenetic analyses using both ArtA and ArtB amino acid sequences (Supplementary Figure S2.2). To define subtypes, we set a threshold of <90% amino acid sequence identity to existing subtypes for at least one of the two subunits. The 59 ArtAB toxins

identified clustered into seven subtypes, 1a-1d and 2a-2c (Figure 1A). Other than type 2a, where a modest amount of sequence diversity was observed, all members of the other subtypes were >99% identical to one another at the amino acid level for both ArtA and ArtB, indicating that the subtypes were mostly homogeneous. To analyze the sequence diversity between subtypes, we performed multiple sequence alignments for ArtA and ArtB using one representative from each subtype (Supplementary Figure S2.1) and compiled pairwise percent identity matrices and generated phylogenetic trees (Figures 2.3.1B,C; Supplementary Figure S2.2). Interestingly, we found that there was considerably more sequence variation amongst the B subunits than the A subunits. Indeed, the average percent identity amongst A subunits from the different subtypes was well over 80%, whereas B subunits averaged ~50% identity between subtypes. This disparity in the conservation of the A and B subunits is evident when comparing within the two major types (e.g., comparing type 1 subtypes to one another), but is most overt when comparing type 1 toxins to type 2. Indeed, some combinations of type 1/type 2 toxins have ArtA subunits that are >90% identical, but ArtB subunits that are <30% identical. Collectively, these data indicate that salmonellae encode a diverse collection of ArtAB toxin subtypes and that most of this diversity is found within the delivery subunits of these toxins.

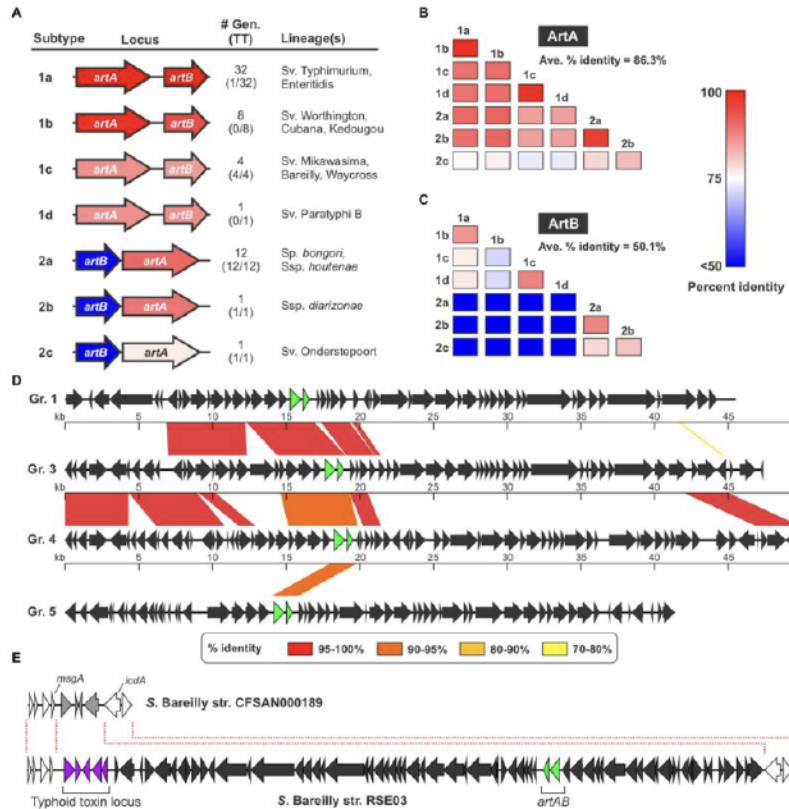


Figure 2.3.1. Several different ArtAB toxin subtypes are encoded by diverse prophages in *Salmonella*. (A) Summary of the seven ArtAB toxin subtypes identified in this study including: a gene diagram that uses a colour scale to show the percent sequence identities of the *artA* and *artB* genes compared to *S. Typhimurium* DT104 *artA/artB*, the number of genomes in the NCBI nr DNA sequence database that encode that subtype and how many of those genomes also encode a typhoid toxin islet [#Gen (TT)], and the *Salmonella* lineage (s) identified that encode this subtype. Percent identity values determined using a single representative of each toxin subtype. (B,C) Percent amino acid sequence identity matrices comparing the different ArtAB toxin subtypes for ArtA (B) and ArtB (C). Values generated using multiple sequence alignments of the representative member of each toxin. (D) Genome diagrams conveying the mosaic nature of the prophages that encode ArtAB toxins. Diagrams are shown for four representative ArtAB-encoding prophage groups (Gr.); regions of significant sequence similarity between combinations of these prophages are shown using a color scale to indicate the percent sequence identity. The *artA* and *artB* genes are shown in green. (E) Gene diagrams showing the Type 1c ArtAB toxin-encoding prophage locus in *S. Bareilly* strain RSE03, and the same genomic locus in a strain from this serovar that lacks this prophage. This comparison suggests that a typhoid toxin islet is part of the *artAB*-encoding prophage.

ArtAB from *S. Typhimurium* DT104 is known to be encoded by a Gifsy-1-like prophage, and given their irregular phylogenetic distribution, we reasoned that many or all the other identified ArtAB toxins might also be phage-encoded (142,218). To explore this hypothesis, we used the PHASTER web server, a well-established tool for identifying prophages in bacterial genomic DNA sequences, to predict the complete set of prophages present in each of the genomes where a putative ArtAB toxin was identified (215,216). Using this approach, we determined that all of the identified *artAB* loci map to predicted prophages, although some phages were predicted to be incomplete. A comparison of the various prophages indicated that, although there are evolutionary relationships between many of the phages identified, a heterogeneous assortment of different phages carry *artAB* in *Salmonella*. Setting a threshold of >80% sequence identity over >80% of the prophage sequence, we categorised the identified phages into 11 different groups. While these phage groupings correlate well with the toxin subtypes found within, there are instances where phages within a single grouping encode different toxin subtypes. Consistent with phage mosaicism and the prominent role that horizontal gene transfer plays in phage evolution, the different phage groups share stretches of high sequence homology with other groups (219). The extent of sequence homology between different phage groups varies widely from 78% of the full locus down to less than 1% (Figure 2.3.1D; Supplementary Table S2.1).

The strains we identified that encode *artAB* are widely distributed across the *Salmonella* genus. Type 1 toxins were generally found in strains from *S. enterica* subsp. *enterica*, while type 2 toxins were generally encoded by *Salmonella bongori* or by *S. enterica* subspecies other than *enterica* (Figure 2.3.1A). Interestingly, we found that certain ArtAB toxin subtypes were invariably encoded by strains that also encode typhoid toxin, whereas other subtypes were rarely

or never found in genomes with a typhoid toxin islet (Figure 2.3.1A). All 14 type 2 ArtAB toxins identified here are found in typhoid toxin-encoding strains, while type 1 toxins are generally in strains that lack typhoid toxin. Indeed, typhoid toxin is only encoded by 1 of the 41 genomes with type 1a, 1b or 1d ArtAB toxins, subtypes that are generally encoded by nontyphoidal serovars from subsp. *enterica* clade A; it has previously been noted that such serovars very rarely encode typhoid toxin (177). Surprisingly, all four types 1c ArtAB toxins are found in strains that encode a typhoid toxin islet, despite being from subspecies *enterica*, clade A. A closer inspection of these genomes revealed that the typhoid toxin islet is immediately adjacent to the *artAB* prophage boundary identified by PHASTER. Based on genome comparisons with other strains from these serovars that lack this prophage, it is likely that this typhoid toxin islet is a part of the *pltC*-encoding prophage (Figure 2.3.1E). Taken together, these data indicate that *artAB* toxins have been extensively transferred amongst prophages, providing a vehicle for their evolutionary diversification, and further suggest that there is a correlation between encoding ArtAB and encoding typhoid toxin that is dependent on ArtAB toxin subtype.

2.3.2 Evolutionary adaptations of the *pltC* locus

In addition to genetic elements that encode an ArtAB toxin, a related element that exhibits a high degree of sequence similarity is also found in *Salmonella* as a *pltC* locus. Despite their close evolutionary relationship, the *pltC* genetic element has been demonstrated to be functionally distinct from intact *artAB* elements, since their A subunit is a pseudogene and their B subunit serves as a typhoid toxin delivery subunit (170,179). We set out to identify and characterize the differences between the *pltC* and *artAB* genetic elements to shed light on the evolutionary exaptation of this locus. We selected the *S. Typhi* *pltC* locus and the *S.*

S. Typhimurium DT104 *artAB* locus for these analyses since these are the best-studied representatives and because they exhibit a high level of DNA sequence identity, suggesting a close evolutionary relationship (Supplementary Figure S2.3). The *artAB* genes in *S. Typhimurium* DT104 are located within a Gifsy-1 prophage downstream of a putative antitermination protein and upstream of phage holin/endolysin genes involved in bacterial cell lysis (Figure 2.3.2 A). This is a common synteny also observed for some other phage-encoded bacterial toxins, such as *E. coli* heat labile toxin and Shiga toxin (220,221). This localization provides a mechanism for these toxins to be expressed and subsequently released from the bacterial cell; upon phage activation their expression is driven by an upstream phage promoter and the toxin's release is facilitated by phage-mediated cell lysis (220–222). Consistent with this, the production of ArtAB toxins and their release into culture supernatants has been shown to be activated by agents known to trigger phage induction, such as mitomycin C and quinolone-family antibiotics (142,223). The *S. Typhi* *pltC* locus, by contrast, is found within a small genomic islet that interrupts the *sapA-sapE* operon (170). This islet does not contain the phage elements that neighbour *artAB* but does contain an assortment of DNA sequences that appear to represent remnants of genes associated with mobile genetic elements, including phage elements (Figure 2.3.2 A). The *pltC*-encoding islet is replete with pseudogenes, including the *artA* pseudogene *sty1362*; other than small (<50 amino acids) putative ORFs of unknown function, the only gene that is intact in this islet is *pltC*. The region where significant homology can be found between the *pltC* and *artAB* elements is limited to the two-gene toxin locus and short segments immediately upstream and downstream (Figure 2.3.2 A; Supplementary Figure S2.3). Within the homologous region, most striking difference is a 359 bp deletion in the *pltC* locus that spans the final 252 bp of *artA* through the first 107 bp of

the intergenic region between *artA* and *artB* (Figure 2.3.2 A). Another salient feature of *sty1362* is a frameshift created by a 1 nt deletion that produces a stop codon five codons into the *sty1362* sequence (Figure 2.3.2 A; Supplementary Figure S2.3;(176)).

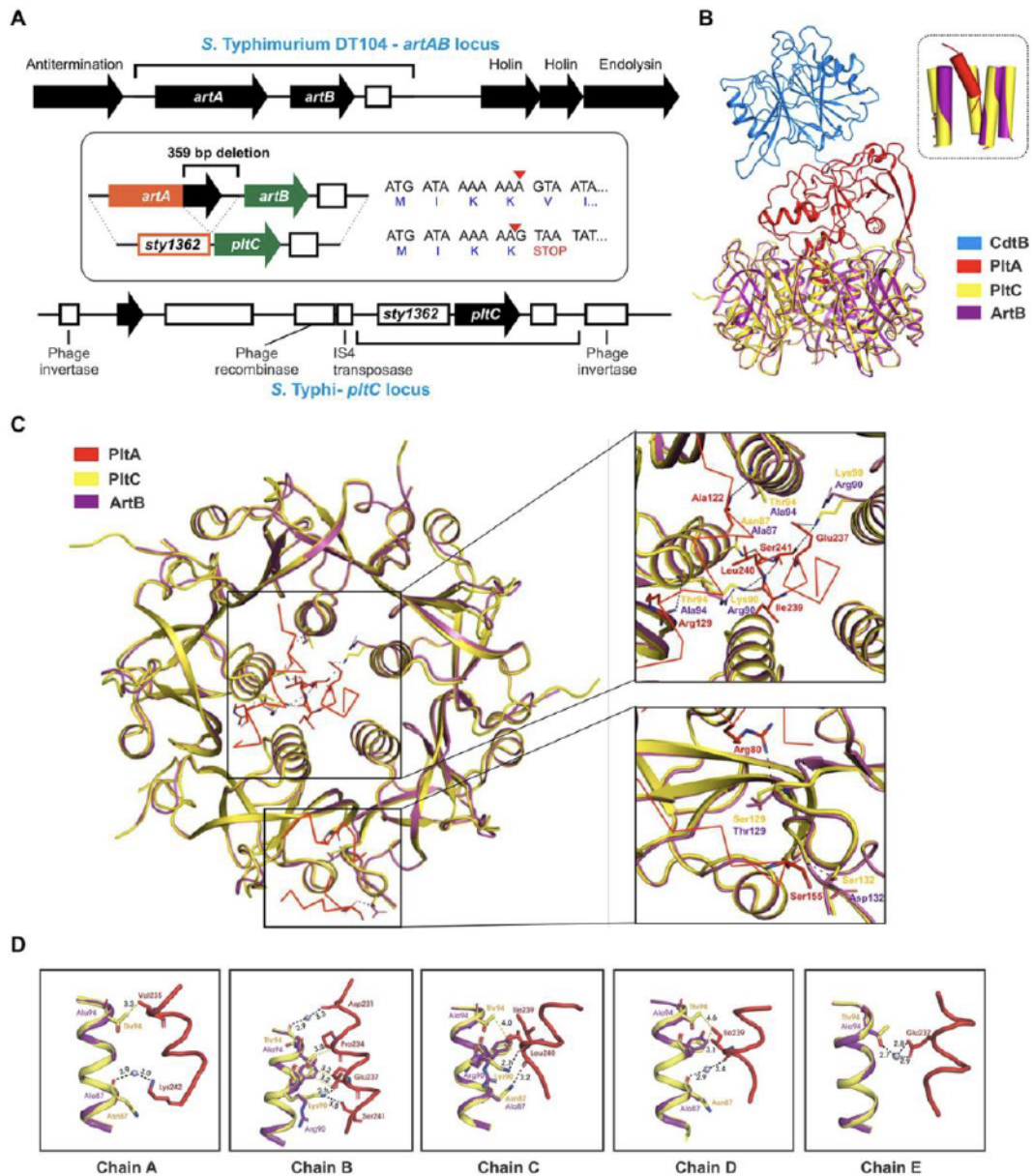


Figure 2.3.2. Evolutionary divergence of the *pltC* and *artB* genetic elements. (A) Comparison of the *S. Typhimurium* DT104 *artAB* and *S. Typhi* *pltC* genomic loci. The homologous region shared by these two loci is shown using black brackets and this region is further dissected in the inset. The inset highlights key differences between these loci, which includes a 359 bp deletion in the *pltC* locus, and a single base deletion (red arrow head) in the *artA* pseudogene *sty1362* that results in a premature stop codon after only 4 amino acids. Intact genes are shown as black arrows and pseudogenes as white boxes. (B) Ribbon diagram showing the structure of PltC typhoid toxin (PDB ID: 7EE6) overlaid with the structure of the modelled typhoid toxin that features ArtB (PDB ID: 5WHU) in place of PltC. The inset shows the very similar structures of the central pores of the B subunit homopentamers of PltC and ArtB and the orientation of the PltA C-terminal helix within these pores. (C) Cut-away top-down view of the A-B interactions in the structures described for (B) featuring detailed views of key intermolecular interactions within the B subunit pore and on the apical surface of the B subunit homopentamer. (D) Ribbon diagram of the structures described for (B) showing the interactions involving the PltC residues Asn87, Lys90 and Thr94 with the C-terminal helix of PltA, and the absence of many of these interactions in the modelled ArtB structure. Boxes show the individual PltC/ArtB chains that make up the homopentamer.

A DNA sequence comparison of the *pltC* and type 1 *artAB* elements indicates that there is a higher degree of similarity within the *artA/sty1362* region than within the *artB/pltC* region (Supplementary Figure S2.3). Pseudogenes (such as *sty1362*) are generally considered to be neutral to genetic drift, and thus accumulate mutations faster than most functional genes in a genome, which are subject to negative (purifying) selection (224,225). By contrast, genes under positive selection (i.e., there is a selective benefit to modify their sequence/ properties) would be predicted to accumulate mutations faster than non-functional DNA, such as a pseudogene (224,225). To further explore the possibility that *pltC* has been subjected to positive selective pressure, we analyzed diverse *pltC* and type 1 *artB* sequences using BUSTED, which uses the rates of non-synonymous and synonymous mutations (dN/dS) amongst homologous genes to

determine if there is evidence for positive (diversifying) selection (214). This analysis found evidence (value of $p < 0.05$) of gene-wide episodic diversifying selection (see methods section). Collectively, our data therefore suggest that *pltC* has been subjected to selective pressure to adapt to its newfound role as a typhoid toxin delivery subunit.

PltC's evolutionary adaptations presumably included the need to adapt to optimally engage with PltA (rather than ArtA) in order to form a typhoid toxin complex. To explore how the sequence differences in PltC relative to ArtB could potentially enhance PltC's ability to form a complex with PltA, we took advantage of the high-resolution structures that have been generated for the PltC holotoxin and the ArtB homopentamer (70,147). Like other AB₅-type toxins, the primary A-B interactions in the PltC typhoid toxin involve the C-terminal A-helix of the A subunit, which inserts into the central pore of the B pentamer, interacting with the helices that line this pore. We modelled ArtB into the PltC holotoxin structure and found that ArtB exhibits shape complementarity with PltA and that ArtB forms a central pore that is compatible with PltA, forming stabilizing interactions with its C-terminal helix (Figure 2.3.2B; Supplementary Figure S4). This is consistent with previous experimental findings that have found that ArtB can assemble into a stable AB₅ toxin with PltA (147). However, we observed that many of the PltC residues that form intermolecular interactions with PltA are different in ArtB (Figures 2.3.2C,D). Of particular note are Asn87 and Thr94 of PltC, which line the PltC central pore and form key interactions with the C-terminal PltA helix; ArtB has alanine residues at these two positions and thus many of these interactions are not observed in the modelled ArtB structure (Figures 2.3.2C,D). Additionally, Lys90 in PltC forms direct hydrogen bonds with PltA Glu237, Ile239, Leu240 and Ser241 through its side chain that are not observed in ArtB, which has an arginine at this position. Interestingly, in ArtB, Arg90 plays a role in

Pentamerization, suggesting that the function of this residue has been diverted from stabilizing the B subunit pentamer in ArtB to stabilizing the A subunit interaction in PltC. PltC also interacts with PltA *via* its apical surface, and there are also interactions at this location that are not observed in the modelled ArtB structure. Specifically, Ser129 and Ser132 in PltC (Thr 129 and Asp132 in ArtB) form direct hydrogen bonds with Arg 80 and Ser155 of PltA that are lost with ArtB (Figure 2.3.2C). Collectively, these data suggest that PltC evolved from an ArtB-like precursor that had the capacity to interact with PltA, but that PltC has since adapted to yield numerous additional chemical interactions with PltA that enhance its capacity to form a stable typhoid toxin complex.

2.3.3 Widespread distribution of *pltC* elements indicates a pervasive role in expanding the functional versatility of typhoid toxins

Experimental evidence has demonstrated that PltC is a *bona fide* typhoid toxin subunit for both the Typhi and Javiana serovars and previous reports have suggested that PltC's role in typhoid toxin biology is likely to be widespread in *Salmonella* (70,170,176,179). We compared the DNA sequences of the *pltC* elements (spanning from the *artA* pseudogene through *pltC*) from the Typhi and Javiana serovars and found that they are ~97.5% identical and that the marquee characteristics that distinguish the *pltC* and *artAB* loci noted above - the 359 bp deletion and the stop codon a few amino acids into the *artA* pseudogene - were conserved in the Javiana sequence as well (Supplementary Figure S2.3). To further explore the diversity and distribution of this genetic element, we mined the NCBI nr DNA sequence database to identify the complete set of genomes within this database that encode a *pltC* locus. The 359 bp deletion in *pltC* served as a distinguishing characteristic that allowed us to readily extricate *pltC* genetic

elements from intact *artAB* sequences. We identified a total of 383 genomes that encode a *pltC* element, a number which far exceeds the number of genomes that encode *artAB* elements (59) in this database. We analyzed the genomic locations of the *pltC* elements and determined that, consistent with previous findings, in most genomes *pltC* is localized within a genomic islet that interrupts the *sap* locus. Data presented here and elsewhere indicates that encoding a *pltC* islet that interrupts the *sap* locus is a highly conserved feature of the genomes of both the Typhi/Paratyphi A serovars and of the subsp. *enterica* clade B lineage (170,177). However, we also identified 24 genomes outside of these phylogenies that encode a *pltC* element that is not found at the *sap* locus, including strains from (nontyphoidal) subsp. *enterica* clade A serovars such as Inverness and Weltevreden, and strains from subsp. *salamae* and *houtenae*. Interestingly, 9 of these 24 strains encode *pltC* at two different genome locations. Importantly, the 359bp deletion is conserved in all *pltC* elements regardless of their genomic location, indicating that they likely all descend from a common ancestral sequence that featured a degraded *artA* gene and an orphan B subunit. Consistent with *PltC*'s functional association with typhoid toxin, we found that 382 of the 383 genomes that encode *pltC* also encode a typhoid toxin locus (>99.7%); the sole exception was a *S. Typhi* strain that has a fragment of the typhoid toxin islet and an IS200-type transposase at the typical typhoid toxin locus, suggesting that the typhoid toxin locus was recently lost from this strain. Coupled with recent experimental findings, this strongly indicates that, regardless of its genomic or phylogenetic context, *PltC* functions as a typhoid toxin delivery subunit and that *pltC* is functionally distinct from closely-related *artAB* genetic elements.

Given *pltC*'s evolutionary connection with *artAB* and the invariable association of *artAB* with prophage, we reasoned that *pltC* might be carried by prophage in the strains where *pltC* is

encoded outside of the *sap* locus. Using PHASTER, we found that all 33 of the *pltC* genetic elements (in 24 different genomes) that we identified that are encoded outside the *sap* locus are located within predicted prophage, although some of these phages were identified as incomplete. To explore whether there are genetic differences between *sap* locus-encoded and prophage-encoded PltC, we analyzed all 392 PltC sequences. Using a threshold of <90% sequence identity, we found that all identified sequences sorted into four groups (Figure 2.3.3A; Supplementary Figure S2.5). The phage- encoded PltC sequences fell into 3 groups (PltCphage1-PltCphage3), and all PltC sequences encoded at the *sap* locus clustered into a single group (PltC_{sap}). It is noteworthy that the segment of the *pltC* locus that contains the PltC coding sequence is much more variable amongst the four *pltC* groups than the segment that contains the *artA* pseudogene, suggesting that there has been selective pressure for functional changes in PltC (Figure 2.3.3A). Phylogenetic analysis based on DNA sequences comparisons of the four groups of *pltC* loci and the group 1 *artAB* subtypes (*pltC* sequences are all highly divergent from type 2 *artAB*s) suggest that the *pltC* allele likely evolved from an *artAB* type 1a/1b-like ancestor (Supplementary Figure S2.6). However, sequence comparisons of these genetic elements reveal that the various *pltC* groups are all approximately equally divergent from *artAB* and, if the 359 bp deletion is disregarded, some *pltC* loci share as much sequence identity with *artAB* as they do with each other (Figure 2.3.3A). By the same token, a pairwise amino acid sequence comparison of all type 1 ArtB subtypes and all PltC groups reveals that, with few exceptions, ArtB subtypes are as similar to the various PltCs as they are to each other, and vice versa (Figure 2.3.3B). Coupled with previous studies that show that *pltC* is almost ubiquitous in clade B of the *enterica* subspecies, implying that it was present in the most recent common ancestor of this lineage, this suggests that *pltC* diverged from *artAB* long ago and that

both of these genetic elements have since undergone considerable evolutionary diversification (177).

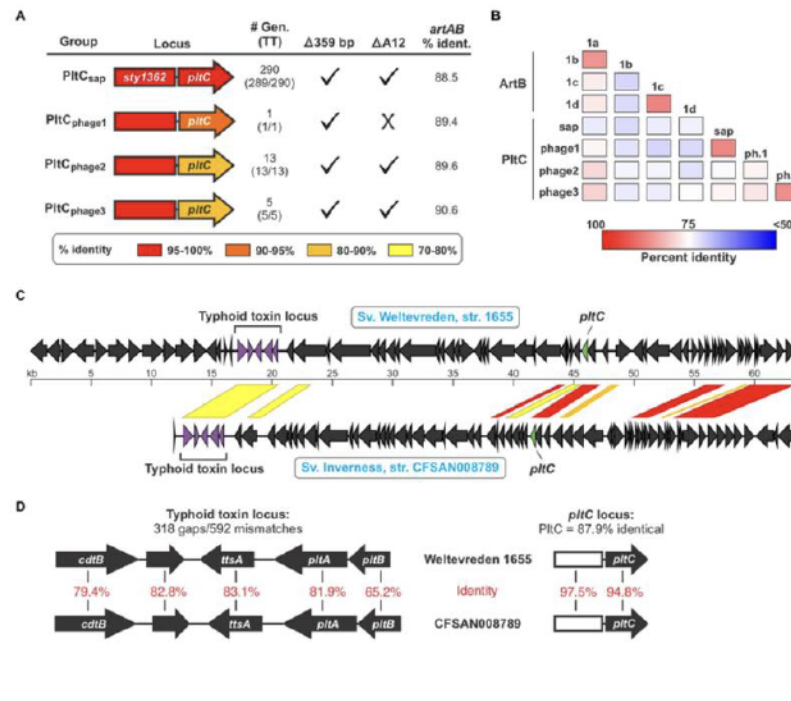


Figure 2.3.3. The *pltC* genetic element has been subject to significant diversification and horizontal transfer within the *Salmonella* lineage. (A) Summary of key features and data for the different groups of *pltC* genetic elements identified in this study including: a gene diagram that uses a colour scale to show the percent sequence identities of the *artA* pseudogenes and *pltC* genes compared to the *S. Typhi* locus (the representative member of the PltC_{sap} group), the number of genomes in the NCBI nr DNA sequence database that encode that subtype and how many of those genomes also encode a typhoid toxin islet [#Gen (TT)], whether or not these subtypes have the salient *pltC*-specific features highlighted in Figure 2A including the 359 bp deletion and the deletion of the 12th base pair of the *artA* coding sequence, and the percent DNA sequence identity of these genetic elements compared to *S. Typhimurium* DT104 *artAB* (disregarding the 359 bp deletion). For sequence comparisons, the representative member of each *pltC* group was used. (B) Percent protein sequence identity matrices comparing the different *ArtB* subtypes and PltC groups. Values generated using multiple sequence alignments of the representative member of each subtype/group. (C) Gene diagrams comparing divergent prophages that encode both a *pltC* locus and a typhoid toxin locus. Regions of significant sequence similarity between these prophages are shown using a color scale to indicate the percent sequence identity. (D) Gene diagrams and DNA sequence comparisons of the typhoid toxin and *pltC* loci of the prophages shown in (C).

Analysis of the *pltC*-encoding phages identified a heterogeneous group of phages that share highly variable extents of sequence overlap, similar to what we observed for the *artAB*-encoding phages (Supplementary Table S2.1). Most phages that carry *pltC* also encode a typhoid toxin islet at a distinct (and distant) locus within the prophage. Our analysis reveals that amongst phages that carry both of these toxin loci, there is substantial diversity in the typhoid toxin loci, in the *pltC* loci, and in the core phage genes. This indicates that these two toxin loci have been subject to extensive horizontal gene transfer amongst phages, and that *pltC* elements are consistently found on typhoid toxin-encoding phages despite their distant genetic locations within phages. As an example of the diversity in *pltC*-encoding phages, we compared the prophages found in serovar Weltevreden strain 1655 and serovar Inverness strain CFSAN008789; both of these serovars are from subsp. *enterica* clade A and generally do not encode *pltC* or typhoid toxin genes (Figure 2.3.3C). Interestingly, the typhoid toxin loci found within these two phages are highly divergent throughout the entire toxin gene cluster, exhibiting an average of only ~75% DNA sequence identity (Figure 2.3.3D). The *pltC* loci within these two phages exhibit a very high level of DNA sequence identity (~96%), but despite this, the PltC proteins share only ~88% sequence identity (Figure 2.3.3D). Outside of the regions that encode *pltC* and typhoid toxin, these two phages are very different and share only a few short regions of significant sequence overlap (Figure 2.3.3C). Collectively, these results indicate that *Salmonella* lineages that do not typically encode typhoid toxin can carry different prophages that confer the ability to produce typhoid toxins with diverse sequences.

2.3.4 Sequence diversity amongst ArtB/PltC glycan binding residues

As noted above, the B subunits of the *artAB/pltC* genetic elements identified here exhibit markedly more sequence diversity than the associated A subunits, even amongst the *pltC* elements where the A subunit is a pseudogene (Figures 2.3.1B,C, 2.3.3A,B). To explore the functional implications of this diversity, we exploited the high-resolution structures of glycan-bound *S. Typhimurium* DT104 ArtB and *S. Typhi* PltC to examine how this sequence variation could impact receptor binding (70,147). Both of these B subunits have two glycan binding sites: (i) a binding site located on the lateral side of the protein that is also found in more distantly-related homologs such as PltB (typhoid toxin) and SubB (subtilase toxin); this site contains a conserved serine residue (Ser31 in ArtB/PltC) that is essential for ligand binding at this site, and (ii) a binding site located on the basal side of the protein that is formed in large part by a four amino acid insertion (relative to PltB, for example) in ArtB/PltC which forms an extended “spoon-like” loop. This loop contains a serine residue (Ser45 in ArtB/PltC) which plays an essential role in ligand binding at this site (Figure 2.3.4A; (70,147,150)). We analyzed the sequences of the B subunits from each of the ArtAB subtypes and PltC groups to determine whether these two binding sites are conserved. We found that the key serine residues for both the lateral and the basal sites are conserved amongst all PltC groups and type 1 ArtB subtypes (PltCphage3 has a Thr45 residue, a conservative substitution which retains the crucial hydroxyl side group), as is the four amino acid insertion that comprises the extended loop at the basal site (Figures 2.3.4A,B). This suggests that all PltC groups and ArtB type 1 subtypes use the two previously identified binding pockets to recognize host glycans, and that they likely all selectively bind sialic acid terminated glycans. Interestingly, however, we find that neither of the critical serine residues are conserved in any of the ArtB type 2 subtypes, and that the

extended loop that forms that basal binding pocket is also absent. This suggests that the glycan binding mechanisms, as well as the nature of the glycans recognized, are likely to differ for type 2 ArtAB toxins.

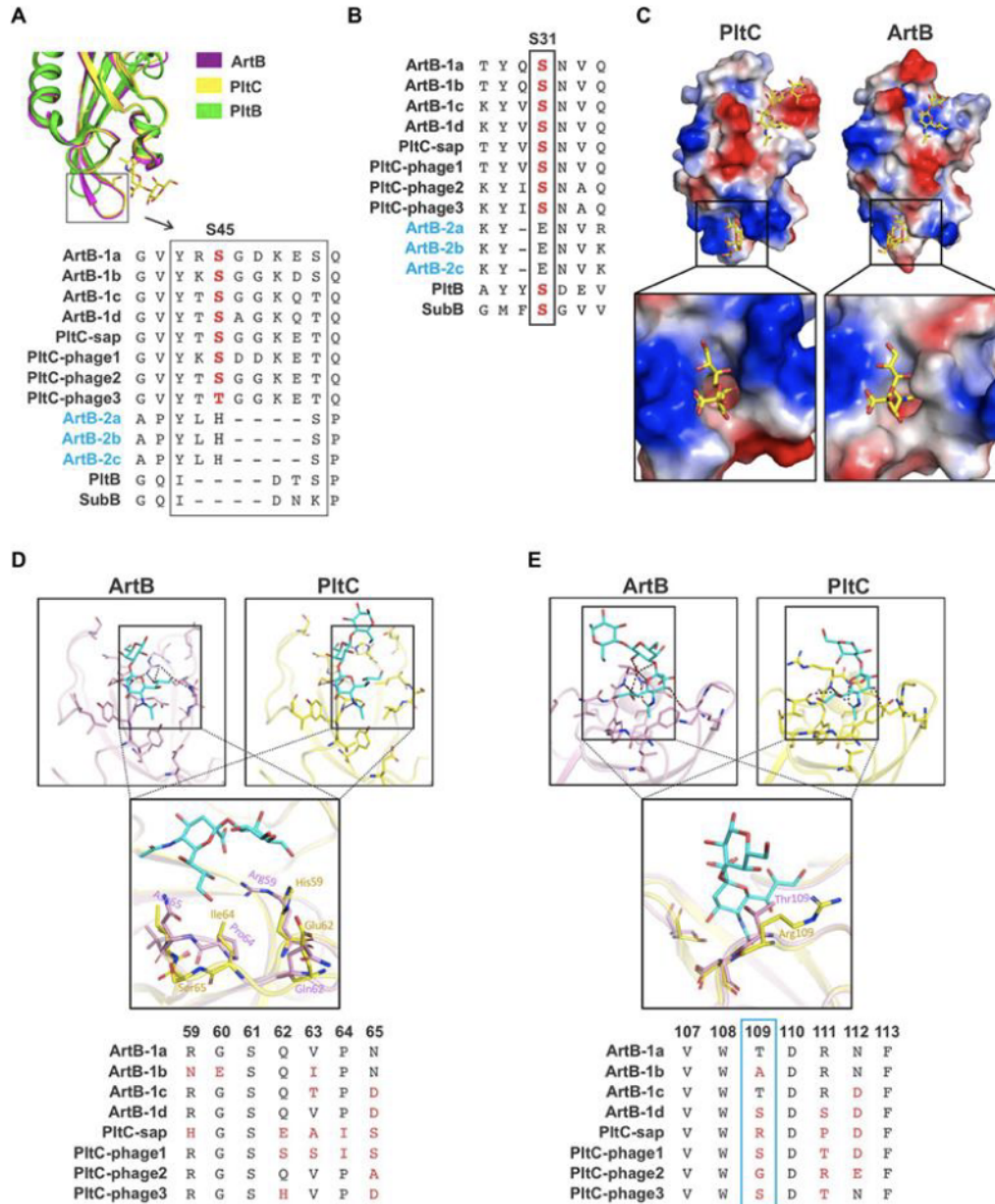


Figure 2.3.4. Analysis of the diversity within the glycan binding pockets of different *Salmonella* ArtB subtypes and PltC groups. (A) Conservation of the basal glycan binding site. Ribbon diagram shows the overlaid structures of the basal binding sites from *S. Typhimurium* DT104 ArtB and *S. Typhi* PltC as well as the structure of PltB, which lacks the basal binding site. Sequence alignments of each ArtB subtype and PltC group show the four amino acid insertion that yields the extended loop that forms a key structure of the basal binding site, as well as the critical glycan-binding serine residue within this loop. The absence of these features in type 2 ArtB subtypes suggests that they lack this binding site. (B) Conservation of the lateral glycan binding pocket. Sequence alignment shows the conservation of a serine residue (labelled S31, its position in PltC/ArtB) that is essential for glycan binding at this site in various B subunits from this family of toxins, including each type 1 ArtB subtype and PltC group. This alignment suggests that type 2 ArtB subtypes might lack this binding pocket, or that it might vary substantially from the pocket in type 1 ArtB subtypes. (C) Electrostatic potential surface view of the Neu5Aca2-3Galb1-3Glc-bound structures of *S. Typhi* PltC and *S. Typhimurium* DT104 ArtB (sugars are shown as sticks), highlighting the shape and charge distribution within their glycan binding pockets. Inset shows a zoomed in view of the basal (S45) binding site. (D,E) Ribbon diagrams of the binding pockets of *S. Typhi* PltC and *S. Typhimurium* DT104 ArtB and overlays that highlight key variable regions of these pockets. Accompanying sequence alignments show the pertinent region of each type 1 ArtB subtype and PltC group. (D) The lateral binding site. (E) The basal binding site. The PDB identifiers for the structures shown are: ArtB; 5WHU, PltC; 7EE4, PltB; 5WHT.

A comparison of the glycan binding pockets in the structures of *S. Typhimurium* DT104 ArtB and *S. Typhi* PltC reveals that, although they are overall quite similar, there are differences in the geometry and charge distributions at both binding sites (Figure 2.3.4 C). To explore the potential diversification of this pocket amongst PltC and ArtB (type 1) sequences, we analyzed the sequences of amino acid residues that are involved in glycan binding at the lateral and basal binding sites. Consistent with the notion that these proteins all recognize sialic acid terminated glycans, several residues that contact core sialic acid moieties (in addition to the Ser31/Ser45 residues noted above) are conserved amongst all PltC/ArtB type 1 subtypes (Supplementary

Figure S2.7). The strict conservation of Tyr103 in the lateral binding pocket is noteworthy, since this residue forms a key hydrogen bond with the extra hydroxyl group that distinguishes Neu5Gc from Neu5Ac (70,150). This tyrosine residue is conserved amongst members of this family that are able to bind Neu5Gc-terminated sialic acids (ArtB, PltC, SubB) but not in PltB, which exclusively binds Neu5Ac (70,149,150). In contrast to amino acids that contact the sialic acid core, residues that contact peripheral sialic acid functional groups are some of the most variable positions amongst PltC/ArtB type 1 proteins (Figures 2.3.4D,E; Supplementary Figure S2.7). Of particular note is the highly variable stretch running from amino acids 59–65, which defines one boundary of the lateral binding site; the only conserved residue in this stretch, Ser61, does not face the binding pocket (Figure 2.4D). This portion of the binding pocket forms the environment that surrounds (and directly contacts) the C7-C9 positions of the sialic acid, which are known to be common sites where sialic acids are chemically modified (226). Although the basal binding site is better conserved than the lateral site, there is variability at positions 46, 50 and 75, which are residues that play a role in glycan binding in the PltC and/or ArtB structures. But the most conspicuous variability in the basal binding pocket is at residue 109 (Thr in type 1a ArtB), which is one of the most variable positions amongst these proteins despite engaging in substantial polar interactions with the glycan in the *S. Typhimurium* DT104 ArtB structure. Collectively, these data indicate that type 1 ArtB and PltC glycan binding pockets have undergone an evolutionary “fine tuning,” and that type 2 ArtAB toxins appear to have very different mechanisms of glycan binding compared to the rest of this family.

2.4 Discussion

In this study, we identify three categories of ArtAB-like genetic elements within the *Salmonella* genus: those that encode a type 1 ArtAB toxin, those that encode a type 2 ArtAB toxin, and those that encode PltC. Type 1 ArtAB toxins are generally encoded by subspecies *enterica* clade A serovars that do not encode typhoid toxin, including those which commonly cause gastroenteritis in humans, such as Typhimurium. Type 2 ArtAB toxins have similar ArtA sequences as type 1 ArtAB toxins but can be distinguished from type 1 based on their reversed gene order and their substantially different B subunit sequences. Unlike type 1 toxins, genomes encoding type 2 ArtAB toxins also generally encode typhoid toxin. Type 2 ArtAB toxins are typically found outside of *S. enterica* subsp. *enterica* and are common in the *S. bongori* species. These lineages generally infect or colonize cold-blooded hosts such as reptiles, implying that these toxins have not evolved to target a mammalian host and therefore might be less potent against these hosts (227). This is supported by recent experimental data comparing the effects of purified ArtAB toxins from *S. bongori* (type 2a ArtAB) to ArtAB toxins from *S. Typhimurium* DT104 and *S. Worthington* (type 1a and 1b toxins respectively) in a murine model of intoxication, where the LD₅₀ for the type 2 toxin was ~10-fold higher than the type 1 toxins (140). ArtAB type 1 and type 2 toxins are both invariably encoded by prophages, and the diversity of these phages indicates that these toxins have been subject to extensive horizontal gene transfer. *pltC* genetic elements, by contrast, can be found in a small genomic islet that interrupts the *sap* locus in certain lineages (such as subspecies *enterica* clade B serovars and the Typhi/Paratyphi A serovars) and within prophages in other lineages. *pltC* genetic elements are genetically similar to *artAB*, but the *artA* homolog is degraded (a pseudogene) and *pltC* elements can be readily distinguished by the conserved 359 bp deletion of the C-terminal portion

of the A subunit gene. PltC proteins and type 1 ArtB proteins have similar sequences; in fact, the sequences of some PltC groups are just as similar to some type 1 ArtB subtypes as they are to each other. However, in stark contrast to type 1 ArtAB toxins, PltC is consistently found in genomes that encode typhoid toxin, regardless of the lineage or the genetic context. This study therefore further solidifies that PltC is a typhoid toxin subunit and is functionally distinct from ArtB (70,170,176,179).

In addition to the variation between the three categories of ArtAB-like genetic elements outlined above, there is also substantial sequence variation (subtypes or groups) within each category. The NCBI nr DNA sequence database used here to identify *artAB*-like genetic elements contains ~2,000 complete *Salmonella* genomes, and although clinically-relevant lineages are over-represented, this dataset includes substantial diversity on the species, subspecies and serovar levels. Using this database, we have unveiled substantial *pltC* and *artAB* sequence diversity that provides a framework for understanding the variation that exists in these toxin subunits. However, given the remarkable diversity present within the *Salmonella* lineage, there are unquestionably *artAB* and *pltC* sequence variants that are not captured by the dataset used here. We believe that the provisional subtypes/groups proposed here, which are based on amino acid sequence differences, will be useful for future studies that explore *Salmonella* toxin diversity. However, as additional sequence variants are identified and as we gain a better understanding of the phenotypic properties of these assorted toxins, re-classifying these toxin subunits on the basis of their functional characteristics might prove to be more practical.

The evolution of different subtypes has been observed for different families of AB-type toxins and can have important functional implications. For example, Shiga toxin subtypes that vary by only a few amino acids can differ in potency by orders of magnitude in animal models

of intoxication, which is also reflected in the propensities of strains encoding these subtypes to cause severe disease in humans (93). The properties and potencies of the various ArtAB toxins and PltC typhoid toxins identified here might therefore vary substantially from the *S. Typhimurium* DT104 and *S. Typhi* toxins that have been studied. *Salmonella* infects or colonize a wide variety of animal hosts and different lineages can have very different host ranges and ecologies (227,228). Our data suggest that different PltC groups and type 1 ArtB subtypes have evolved to fine tune their glycan binding pockets, which presumably has enabled these toxins to adapt to effectively target specific cell or tissue types in different host species. PltC/ArtB are members of a family of B subunits that recognize sialic acid terminated glycans, a broad distinction that encompasses tremendously diverse glycolipids and glycoproteins that can be found on the surfaces of cells. Further sialoglycan diversity can be conferred through chemical modifications to the sialic acid residues themselves, and a very broad spectrum of such modifications are known to be produced naturally by animal cells (226). Indeed, such modifications were recently found to play a role in receptor binding for typhoid toxins (229). Finally, PltB and ArtB toxins contain a total of 10 glycan binding sites (two for each monomer) and simultaneously engaging multiple receptors is thought to be important for AB₅ toxins to provide a sufficient binding avidity to efficiently bind and enter target cells (76). The geometry and flexibility required within glycan binding sites in order to simultaneously engage multiple receptors is therefore an important layer of complexity that is not captured by the available structural data. Given this complex array of factors, the considerable binding subunit sequence diversity identified here is not surprising. Future studies will be required to explore the hypotheses generated here regarding the functional implications of the observed sequence

diversity. Exploring how this diversity impacts the properties of these toxins as well as their role in human disease will be an important area of future research.

The analyses presented here provide insight into how the diverse assortment of *artAB*-like genetic elements that we see today might have evolved. Based on these observations, we hypothesize that PltC evolved to serve as an alternate typhoid toxin delivery subunit in the context of a phage that carried both a type 1 ArtAB toxin and a typhoid toxin locus. In this scenario, the ArtB gene, which we show is structurally-compatible with PltA, provided an evolutionary advantage as a typhoid toxin delivery mechanism that outweighed any advantage it provided as an ArtA delivery mechanism. This would have led to a selective pressure to disrupt *artA* in order to prevent it from competing with typhoid toxin for ArtB. PltC subsequently evolved numerous additional intermolecular interactions to enhance its ability to form a complex with PltA, allowing it to more effectively compete with PltB to form a second pool of typhoid toxin with distinct receptor-binding properties. This hypothesis is supported by our identification of individual phages that carry both ArtAB toxin and typhoid toxin, as well as numerous phages that carry both typhoid toxin and *pltC*.

Our results also highlight a potential evolutionary path for the two ArtAB toxin types that we identified. Discounting N-terminal amino acids predicted to be removed by Sec secretion machinery, the subtype 1a and 2a ArtA sequences are >96% identical over the C-terminal 225 amino acids of the protein, but their B subunits share only ~26% sequence identity. Coupled with the reversed gene order between these loci, this suggests that the two distinct ArtAB types likely evolved as a result of a horizontal gene transfer event. A closer inspection of the type 2 *artAB* toxin loci revealed that in some instances an IS605-family transposase is encoded immediately downstream of *artA* (e.g., EWI73_18225 from *S. bongori* str. 04-0440),

suggesting that *artA* may have been transferred *via* transposition to a locus that encoded an evolutionarily distinct B subunit, resulting in the emergence of type 2 ArtAB toxins. Consistent with this, we found that many strains of *S. bongori* (a lineage that commonly encodes type 2 ArtAB toxins) encode a putative protein that exhibits ~70% sequence homology to type 2 ArtB at a distinct genomic locus (e.g., EWI73_01245 from *S. bongori* str. 04-0440); a relative of this gene therefore might have served as the evolutionary source of the type 2 ArtB. The evolution of PltC and of type 2 ArtAB toxins therefore showcases the flexibility of the A-B interface of AB₅-type toxins and how this can be exploited by evolution to yield novel toxins with distinct properties.

2.5 General conclusions and link to Chapter 3

Our use of bioinformatic and structural tools as an approach to explore the evolutionary diversification of *artAB/pltC* genetic elements in *Salmonella* revealed important findings that may be useful in deciphering the roles of ArtAB and typhoid toxin in *Salmonella* pathogenesis and disease. The functional implications associated with the biology and flexibility of AB₅ toxins is becoming more evident as novel AB₅-type toxins with virulence potential emerge. The results obtained from this study corroborate previous findings that indicate that this diversity and distribution of AB₅ toxins in the *Salmonella* genus likely holds important biological relevance and thus, requires a more in-depth analysis. Considering the negative impact of *Salmonella* infections on human health and the rise in multi-drug resistant strains, elucidating the molecular mechanisms of AB₅ toxin evolution and biology may inspire the development of tools and control strategies needed to alleviate the burden of salmonellosis worldwide. In addition to this, many studies aimed at understanding the molecular factors underlying *Salmonella* pathogenesis so far have been largely focused on a narrow range of serovars such as *S. Typhimurium* and *S. Typhi* as a result of their frequent association with human disease. However, with increasing reports of infections caused by other *Salmonella* strains, including many that encode AB₅ toxins, it is necessary to redirect and expand our focus to a wider range of strains and serovars beyond the historically used model strains, since they too have the potential to cause severe disease and may have unique aspects to their pathogenesis.

Supplementary Data and Figures (Chapter 2)

Table S2.1. Percent query coverage matrix between the identified groups of *artAB* and *pltC*-encoding *Salmonella* phages.

		ArtAB phages										PltC phages							
		Percent Query coverage ^{a,b}																	
PHAGE GROUP		1	2	3	4	5	6	7	8	9	10	11	A	B	C	D	E	F	G
ArtAB phages	1	100	78	27	21	4	5	12	54	68	6	6	6	6	50	35	52	3	32
	2	69	100	43	35	4	4	11	43	50	5	0	6	6	43	30	46	3	28
	3	26	47	100	40	4	4	4	5	5	5	0	5	5	6	6	6	2	4
	4	19	36	38	100	3	5	5	5	5	46	1	46	46	5	3	5	2	4
	5	4	5	4	4	100	3	8	1	2	2	7	28	4	23	22	25	1	12
	6	5	6	4	6	3	100	47	32	18	17	18	5	5	6	7	5	1	3
	7	10	11	4	4	6	37	100	46	21	23	51	4	4	13	11	7	0	9
	8	46	41	4	4	1	25	45	100	60	18	16	5	5	36	24	40	0	22
	9	59	49	5	5	1	14	21	62	100	15	15	5	5	43	28	44	1	26
	10	6	6	5	47	2	14	24	20	16	100	10	48	48	5	3	4	0	3
	11	5	0	0	1	5	11	44	14	13	8	100	0	0	7	2	2	0	2
PltC phages	A	5	6	5	44	22	4	4	5	5	44	0	100	62	28	20	32	9	24
	B	6	6	5	50	4	4	4	5	5	50	0	70	100	18	11	23	10	19
	C	34	33	4	3	14	3	10	29	34	4	7	22	13	100	64	61	6	30
	D	25	24	5	2	14	4	9	20	23	2	2	16	8	66	100	47	3	45
	E	46	45	5	5	20	4	7	42	45	4	5	32	21	78	58	100	11	51
	F	22	22	18	18	7	5	5	5	14	5	0	66	66	63	34	84	100	66
	G	28	27	3	4	9	3	9	24	26	3	2	25	17	38	56	51	9	100

^a: Percent query coverage when doing pairwise DNA sequence alignments between the representative members of the two phage groups being compared

^b: The lighter shaded region shows values obtained from using the phage group from the row (along the side) as the query sequence. The darker shaded region shows values obtained from using the phage group from the column (along the top) as the query sequence. These values, although similar, are not equivalent because of size differences amongst the phage being compared.

A)

```
1a 1- -----MIKKVILFLAFFSGYASAVDFVYRVDSRPPDVI FRDGFNSHGNNRNLQQHIRGDCSAGSRDSNYIATTS DINETYNIAR
1b 1- -----MIKKVILFLAFFSGYASAVDFVYRVDSRPPDVI FRDGFSSHGNNRNLQQHIRGDCSAGSRDSNYIATTS DINETYNIAR
1c 1- -----MIKKAILFLMFFSGCASAVDFVYRVDSRPPDVI FRDGFSGHGNNRNLQQHIRGDCSAGSRDSNYIATTS DINETYSIAA
1d 1- -----MIKKTILFLMFFSGCASAVDFVYRVDSRPPDVI FRDGFSGHGNNRNLQQHIRGDCSAGSRDSNYIATTS DINETYRIAT
2a 1- MTGYSRFLRLGLVYLMFAYSPFSSAVDFVYRVDSRPPDVI FRDGFSSHGNNRNLQQHIRGDCSAGSRDSNYIATTS DINETYNIAR
2b 1- MTGYSRFLRLGLVYLMFAYSPFSSAVDFVYRVDSRPPDVI FRDGFSAHGNNRSLQQHIRGDCSAGSRDSNYIATTS DINETYNIAR
2c 1- -MSYSFLLRPGVCLLFLVYSSFSASVDFVYRVDSRPPDVI FRDGFSAHGNNRSLQQHIRGDCSAGSRDSNYIATTS DLNEALNTAR
      * *****
1a 81- VVYSRTTFSGRLRYRIRADNSFYSLLPVSVAIESRGIQFSHFERVMRLQSEYVAVNSIPIENIQEAVELVYDRNTSQVRDGSST
1b 81- VVYSRTTFSGRLRYRIRADNSFYSLLPVSVAIESRGIQFSHFERVMRLQSEYVAVNSIPIENIQEAVELVYDRNTSQVRDGSST
1c 81- VVYSNAAFSGRLRYRIRADNSFYSLLAPSVDIIESRGIQFSYFERVMRLQSEYVAVNSIPIENIQEAVELVYDRNTSQVRDGPST
1d 81- VVYSNAAFSGRLRYRIRADNSFYSLLAPSVDIIESRGIQFSYFERVMRLQSEYVAVNSIPIENIQEAVELVYDRNTSQVRDGPST
2a 87- VVYSRATFSGRLRYRIRADNSFYSLLPVSVAIESRGIQFSHFERVMRLQSEYVAVNSIPIENIQEAVELVYDRNTSQVRDGPST
2b 87- VVYSSTFSGRLRYRIRADNSFYSLLPVSVAIESRGIQFSHFERVMRLQSEYVAVNSIPIENIQEAVELVYDRNTSQVRDGPST
2c 86- VVYSSTFSGRLRYRIRADNTFYSLEPSVAYLESHDIQFNHFERAMRLQSEYVAVSSIPIENIQEAVELVYDRNTSHVREGPST
      **** *****
1a 167- SNSRYLRVSTQSNPGVIFNLFVVPQVSTRERISAFGLTISACFSMRGVRDDARSNY-NYEMEFYDARGVLTPELLD--
1b 167- SNSRYLRVSTQSNPGVIFNLFVVPQVSTRERISAFGLTISACFSMRGVRDDARSNY-NYEMEFYDARGVLTPELLN--
1c 167- SNSRYLRVSTQSNPGVIFNLFVVPQLSTRERISAFGLTISACFSMRGVRDDDEHLKF-NYDVEFYDARGVLTPELLN--
1d 167- SNSRYLRVSTQSNPGVIFNLFVVPQLSTRERISAFGLTISACFSMRGVRDDENLKF-NYDVEFYDARGVLTPELLN--
2a 173- SNSRYLRVSTQSNPGVIFNLFVVPQVSTRERISAFGLTISACFSMRGVRDEARSNY-NYEMEFYDARGVLTPELLK--
2b 173- SNARYLRVSTQSNPGVIFNLFVVPQVSTRERISAFGLTISACFSMRGVRDDARSNY-NYEMEFYDARGVLTPELLN--
2c 172- SNPHYLRVSTVSNPGVIFNLFVVPQLSTRERISAFGLTISACFSMRGVNHPDSRENGVSPDFMFFDARPLIEQIINYR
      ** ***** ** *****
```

B)

```
1a 1- --MKNKLVLAFLASLSSVCYANMAD----YNTYQSNVQINNLSYGVYRSGDKESQFFCVGLKRGSQVNVHTICKIDVFG--
1b 1- --MKNKLVLAFLASLSSVCYANMAD----YNTYQSNVQINNLSHGVIKSGGKDSQFFCIGLNSESQIPNANTMCKMDVFG--
1c 1- --MKNKLVLAFLASLSSVCYANMAG----YNKYVSNVQINNLSYGVYTSAGKQTFQFCVGLKRGSQVNVHTMCKIDVFG--
1d 1- --MKNKLVLAFLASLSSVCYANMAG----YNKYVSNVQINNLSYGVYTSAGKQTFQFCVGLKRGSQVNVHTMCKIDVFG--
2a 1- --MKKIFFAFVLMAGASNVYATVNSWYLDTKK-YENVKITNIFYAPYLH----SPRICAFFTASS-GGSNVTGCAVADNGYY
2b 1- --MKKIFFAFVLMAGASNVYATVNSWYLDTKK-YENVKITNIFYAPYLH----SPRICAFFTASS-GGSNVTGCAVADNGYY
2c 1- --MKRFFVFTLVMVAGASNVYASVNRWYLDTKK-YENVKITNIFYAPYLH----SPRICAFFTASS-GGSNVTGCAVADNDYY
      ** ***** ** * * * *
1a 77- ----THKQGFNDMLATARYYYATGEDVRIYKENVWDRNFTAAFSGNELIAITTCSSDYCMGPTLPN--
1b 77- ----THKQGFNDMLATARYYYTGEKVRIYKENVWADRNFTAAGFSGNELIAITTCSSDYCMGPTLPN--
1c 77- ----THKQGFNDMLATARYYYATGESVRYVYMDVWTDTRDFANAFSNKELISITTCSSASNYCMGPT----
1d 77- ----NHKQGFNDMLATARYYYATGEEVRLYYIDNVWSDSDFGAFSNKELISITTCSSASDYCMGPTVFN--
2a 82- QKNAVQTSPPMEIFDVTVKYFYTTGKISVYIRINA--FSHFDSVVSQNEIVAIGTCN--QWCFGEIIK--
2b 82- LKNEAQTSPFMEIFDVTVKYFYTTGKISVYIRINA--FPNFDSSLKNEIVAIGTCN--GWCFGETIK--
2c 82- QKNTAQTSPFMEIFDVTVKYFYTTGENISVYIKLNA--FPEFDTVSKHEIVAIGTCN--GWCFGETIK--
      * * * * * * * * * * * *
```

Figure S2.1. Amino acid sequence alignment of the subunits of different ArtAB toxin subtypes. Protein sequence alignments for representative members of the 7 different ArtAB toxin subtypes (see Supplemental Data File 1) were performed using Clustal Omega for **(A)** ArtA and **(B)** ArtB. Asterisks (*) denote positions in the alignment where there is complete conservation of amino acid residues among all subtypes. Due to the divergent nature of the type 1 and type 2 B ArtB sequences, two additional homologs from this toxin family (*S. Typhi* PltB and *E. coli* SubB) were included as outgroups to improve the alignment, but are not shown above.

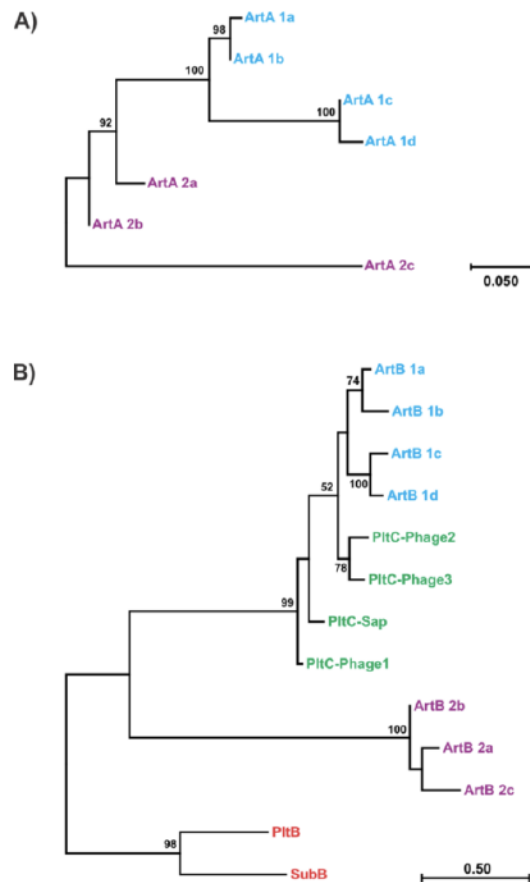


Figure S2.2. Phylogenetic trees depicting the relationships between the amino acid sequences encoded by different *Salmonella artAB*-like genetic elements. Amino acid sequence alignments for the representative members for each the seven ArtAB toxin subtypes (For A subunit alignments (**A**) and for B subunit alignments (**B**)) and the PltC groups (**B**) were used to generate phylogenetic trees using the MEGA (Molecular Evolutionary Genetics Analysis) V11 software using the maximum likelihood method and a WAG +G +I substitution model. A bootstrap method with 500 total replicates was used and the numbers at the nodes represent the support values. For the B subunit tree (B), two other members of the pertussis family of B subunits were included as outgroups; PltB (*S. Typhi*, strain TY2) and SubB (*E. coli*, strain 98NK2). The different ArtAB types and PltC groups are colour-coded for visual clarity.



	Percent Identity
Javiana vs. Typhi	97.5%
DT104 vs. Javiana	88.2%
Typhi vs. DT104	88.1%

Figure S2.3. DNA sequence alignment of the *S. Typhimurium* DT104 artAB locus and the plfC loci of *S. Typhi* TY2 and *S. Javiana* CFSAN001070. The sequences of the artA gene (DT104) or pseudogenes (Typhi, Javiana) are shown in blue, the plfC and artB sequences are shown in green and the intergenic sequences are shown in black. The red triangle shows the single base deletion in the plfC loci that results in a premature stop codon (red) in the A subunit pseudogene. The 359bp deletion in the Javiana and Typhi sequences is shown using red dashes. The inset shows the percent identity of each strain relative to the others (excluding the 359bp deletion). Alignments performed using the Clustal Omega alignment tool (European Bioinformatics Institute).

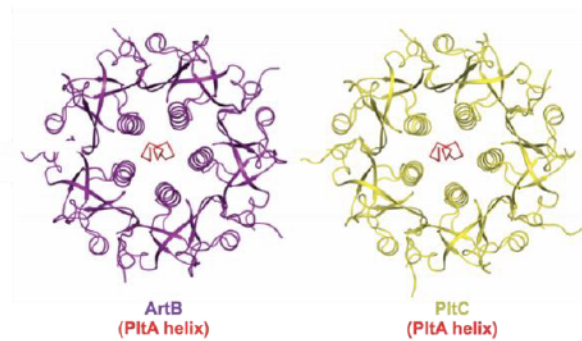


Figure S2.4. PltC and ArtB have similar central pores capable of accommodating the PltA C-terminal α -helix. Top-down views of the ribbon diagram structures of *S. Typhimurium* DT104 ArtB (PDB ID: 5WHU) and *S. Typhi* PltC (PDB ID: 7EE6), showing the positioning of the PltA helix (stick diagram) in the central pore. The PltA helix shown in the PltC structure is based on its position in the holotoxin structure, which was used to orient (model) this helix within the analogous ArtB pentamer structure.

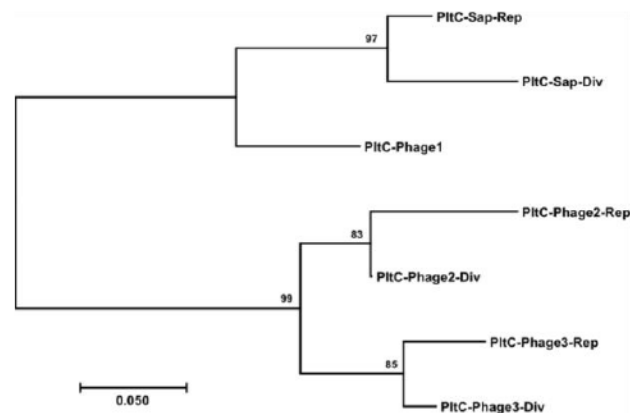


Figure S2.5. Phylogenetic trees depicting the relationships between the amino acid sequences of the various PltC groups identified in this study. Amino acid sequence alignments were generated for the representative members for each of the four PltC groups identified (“Rep”) as well as the member of each of these groups with the lowest % sequence identity compared to the representative member (most divergent member; “Div”); only one Phage1 sequence is used since this group is comprised of a single member. This alignment was used to generate phylogenetic trees using the MEGA (Molecular Evolutionary Genetics Analysis) V11 software using the maximum likelihood method and a WAG +G +I substitution model. A bootstrap method with 500 total replicates was used and the numbers at the nodes represent the support values. Accession numbers for the genomes for each of the PltC sequences used are as follows: Sap Rep (AE014613.1), Sap Div (CP082381.1), Phage1 Rep (CP054715.1), Phage2 Rep (CP019181.1), Phage2 Div (CP042441.1), Phage3 Rep (CP034697.1), Phage3 Div (CP014996.1).

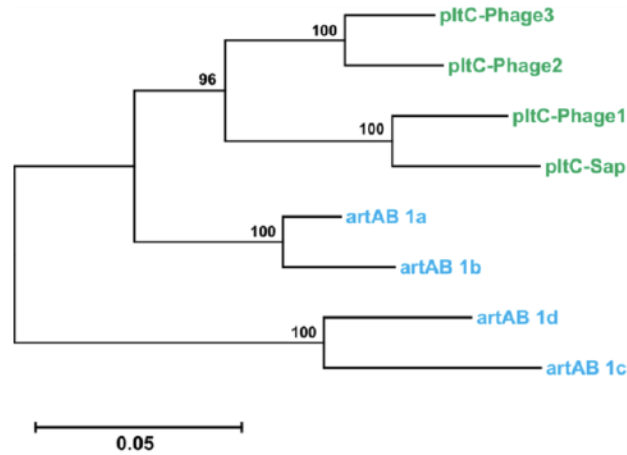


Figure S2.6. Phylogenetic trees depicting the relationships between the DNA sequences of the various *artAB* type 1 and *pltC* genetic elements identified in this study. DNA sequence alignments for the representative members for each the seven *artAB* toxin subtypes and each of the *pltC* groups were used to generate phylogenetic trees using the MEGA (Molecular Evolutionary Genetics Analysis) V11 software using the maximum likelihood method and a Tamura-3 +G +I substitution model. A bootstrap method with 1000 total replicates was used and the numbers at the nodes represent the support values. The distinguishing 359 bp segment that is present in *artAB* but absent from *pltC* was removed for the purposes of this analysis. The different *artAB* types and *pltC* groups are colour-coded for visual clarity.

100% conserved glycan-binding residues (not highlighted in main figs)					Variable glycan-binding residues (not highlighted in main figs)					
	76	107	110	29	103	46	50	75	27	131
ArtB-1a	G	V	D	Y	Y	G	S	F	N	S
ArtB-1b	G	V	D	Y	Y	G	S	F	N	I
ArtB-1c	G	V	D	Y	Y	G	T	F	N	S
ArtB-1d	G	V	D	Y	Y	A	T	F	N	S
PltC-sap	G	V	D	Y	Y	G	T	Y	D	S
PltC-phage1	G	V	D	Y	Y	D	T	Y	D	S
PltC-phage2	G	V	D	Y	Y	G	T	F	D	P
PltC-phage3	G	V	D	Y	Y	G	T	F	D	S
	S45 site			S31 site		S45 site			S31 site	

Figure S2.7. Conservation of glycan-binding residues amongst the different ArtB type 1 subtypes and PltC groups. Multiple sequence alignments of the various ArtB type 1 subtypes and PltC groups. The conservation of selected amino acids previously determined to contact the glycan in the basal (S45) or lateral (S31) binding sites in the glycan-bound structures of *S. Typhimurium* ArtB (PBD: 5WHU) and *S. Typhi* PltC (PDB: 7EE4, 7EE5) is shown for each PltC group and ArtB type 1 subtype. Bold numbers denote amino acid positions of glycan-binding amino acid residues.

Chapter 3: Identification and characterization of two novel putative AB₅ toxins identified in *Salmonella*

Preface

This chapter covers the majority of the efforts from my graduate research and is composed primarily of experiments independently conducted by me. However, other members of the Fowler lab also contributed to some of the work presented here:

- The discovery and initial analysis of the two novel AB₅ toxins introduced here (RIP-TT and RIP-HLT) was made by Dr. Casey Fowler prior to my arrival in the lab.
- Molecular cloning of a few plasmids used in this study was completed by undergraduate researchers in the Fowler lab. Specifically, the cloning of the plasmids encoding the RIP-HLT R192A catalytic mutant, WT Stx2a and the synthetic hybrid Stx2a A/RIP-HLT B toxins was done by Eric Schultz and Gillian Cameron.

3.1 Introduction

Bacterial AB₅ toxins constitute important virulence factors in several human and animal pathogens, many of which cause severe diseases. Despite obvious differences in enzymatic A activities and binding properties, most AB₅ toxins share structural and functional similarities in one or both subunits to other AB₅ toxins, indicating that these toxins are connected and likely evolutionarily related. For example, the ADP-ribosylating toxins which include Ptx, Ctx, LT and ArtAB share a generally conserved enzymatic activity defined by the modification of host cell G proteins via the transfer of an ADP-ribose moiety to specific host cell proteins, a process which is mediated by their A subunits (230). Shiga toxins (Stx), however, have no significant sequence similarities in either their A or B subunits to other characterized families of AB₅ toxins and the enzymatic RIP activity of the Stx A subunit has not been previously associated with any other characterized AB₅ toxin. The evolutionary connection of the Shiga family of toxins to other AB₅ toxin families, if such a connection exists, is currently unknown. Considering the role of Stx in severe human and animal diseases, efforts aimed at clarifying the evolution and biology of these toxins could have useful therapeutic implications that would help alleviate the current burden associated with STEC strains worldwide.

Based on the cumulative findings from our previous study (Chapter 2) on the diversity and distribution of AB₅ genetic elements in *Salmonella* and the inherent flexibility exhibited by AB₅ toxins, we extended our use of bioinformatic tools to investigate other AB₅-type toxins that may be encoded by *Salmonella*. Our lab (Dr. Fowler) uncovered two novel putative AB₅ toxins encoded by a variety of *Salmonella* strains, both of which possess Stx-like A subunit genes and are thus expected to encode ribosome inactivating protein (RIP) A subunits with a similar intoxication mechanism as Shiga toxins. The first putative toxin, which was designated “RIP-

TT”, was found on a locus encoding an *artB/pltC* homolog next to the *rip* gene (Figure 3.1). The second identified toxin, designated “RIP-HLT”, was mapped to a locus in which the *rip* gene is adjacent to a homolog of the B subunit of type II heat-labile toxins (LT-II) (Figure 3.1). These genetic arrangements suggested an association between Stx-like A subunits and B subunits from very distant AB₅ toxin families. This would suggest that the A-B interface of AB₅ toxins exhibits a remarkable amount of flexibility and would have substantial implications for understanding how the Shiga family of toxins could be evolutionarily connected to other AB₅ toxin families.

Ribosome inactivating proteins like Stx are highly potent protein toxins which are able to induce substantial cytotoxicity at relatively low concentrations and as a result of this, the Stx family of toxins are one of the most well-studied bacterial AB₅ toxins. Considering the biological and medical relevance of Stxs and LT in human health, as well as the suggested role of AB₅ toxin genetic elements in the emergence of virulent bacterial strains that have been linked to severe disease, characterizing these unusual toxins might provide us with some useful information needed to understand the complexities often associated with AB₅ toxin evolution and provide insight into the unique biology of Stx. This chapter of my thesis aims to provide useful insights that might contribute to our overall understanding of AB₅ toxin evolution, biology, and cellular activity.

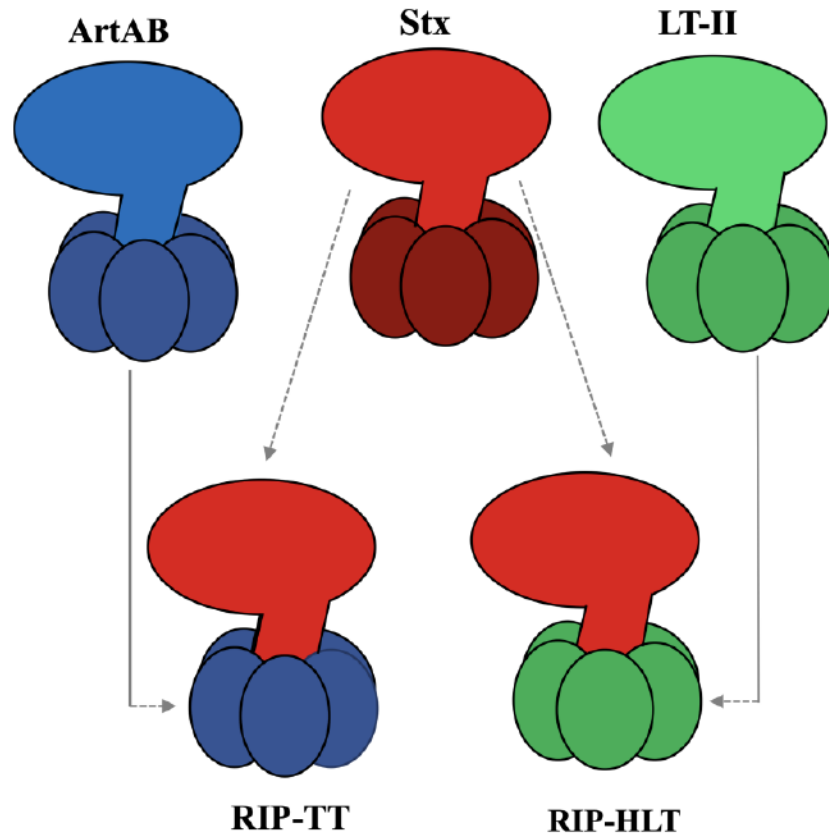


Figure 3.1. Schematic representation of the predicted architectures of two novel AB₅ toxins identified in *Salmonella* and their relationships to other known AB₅ toxins. Two putative AB₅-type toxins with unique A and B subunit combinations have been identified in *Salmonella*. The first toxin, dubbed “RIP-TT” represents a Stx-like A subunit (which is a RIP enzyme) in complex with an ArtB/PltC-like B subunit. The second toxin, dubbed “RIP-HLT” also has a Stx-like A subunit, but in a complex with a LT type II-like B subunit.

3.2 Materials and Methods

3.2.1 Identification and analysis of putative AB₅ toxins in *Salmonella*

3.2.1.1 Identification of the RIP-TT and RIP-HLT toxins in *Salmonella*

The RIP-TT and RIP-HLT toxins were discovered by Dr. Casey during a screening of the Nation Center for Biotechnology Information (NCBI) database to identify other putative AB₅ genetic elements present within the *Salmonella* genus. Dr. Fowler identified genomic sequences with striking similarities to well-characterized AB₅ toxin subunits sequences.

3.2.1.2 Analysis of the evolution, diversity and distribution of RIP-TT and RIP-HLT within the *Salmonella* genus

All *Salmonella* genomes within the NCBI nonredundant protein sequence database that encode a *rip*-like A subunit gene adjacent to either an *artB/pltC*-like B subunit gene or an *lt-II*-like B subunit gene were identified using BLASTp searches using the full-length *Salmonella enterica* subsp. *enterica* serovar Stanleyville RSEI RIP protein sequence. These searches were done in September 2021 and genomes containing both A and B protein sequences for both RIP-TT and RIP-HLT were compiled (>100 genomes for RIP-TT and 2 genomes for RIP-HLT). Multiple sequence alignments on A and B protein sequences from RIP-TT, RIP-HLT and related toxins were done using Clustal Omega sequence alignment program (EMBL-EBI) with the same default parameters described in 2.2.1. Phylogenetic trees were constructed using compiled protein sequences downloaded from the NCBI database and imported into the MEGA (Molecular Evolutionary Genetics Analysis) X software program (version 10.2.1) (213).

3.2.2 Bacterial strains, plasmids, and growth conditions

All bacterial strains and plasmids used in this study are listed in Table 3.2.1 and all reagents are listed in Table 3.2.2 All bacterial strains and plasmids were stocked by resuspension in lysogeny broth (LB) supplemented with 15% glycerol and stored at -80°C. *E. coli* strains BL21(DE3) and DH5 α were routinely cultured in LB (10g/L tryptone; 5g/L yeast extract and 5g/L Sodium chloride (NaCl)) at 37°C in a rotating incubator (VWR Scientific, Canada). Bacterial cultures were supplemented with 50 μ g/ml ampicillin when required.

Table 3.2.1. List of bacterial strains, plasmids and mammalian cells used in this study.

Bacterial strains, plasmids, and mammalian cells	Source	Description/Use
Strains		
<i>E. coli</i> DH5 α	Fowler lab	Molecular cloning of plasmid collection
<i>E. coli</i> BL21(DE3)	Fowler lab	Used in protein purification
Plasmids		
pET-22b (+)	Novagene	Parental vector used to design and overexpress plasmids
pET22-RIP-TT wild type	Fowler lab	Plasmid encoding wild type RIP-TT
pET22-RIP-TT B	Fowler lab	Plasmid encoding only the B subunit of RIP-TT
pET22-RIP-TT (R192A)	Fowler lab	Plasmid encoding RIP-TT catalytic mutant
pET22-RIP-TT (S31A/S45A)	Fowler lab	Plasmid encoding RIP-TT double binding mutant
pET22-RIP-HLT wild type	Fowler lab	Plasmid encoding wild type RIP-HLT
pET22-RIP-HLT B	Fowler lab	Plasmid encoding only the B subunit of RIP-HLT
pET22-RIP-HLT (R192A)	Fowler lab	Plasmid encoding RIP-HLT catalytic mutant
pET22-RIP-HLT (T36I/T37I)	Fowler lab	Plasmid encoding RIP-HLT double binding mutant
pET22-Stx2a	Fowler lab	Plasmid encoding the wild type <i>E. coli</i> Stx2a
pET22-Stx2a A/RIP-TT B	Fowler lab	Plasmid encoding hybrid Stx2a A/RIP-TT B
pEt22-Stx2a A/RIP-HLT B	Fowler lab	Plasmid encoding hybrid Stx2a A/RIP-HLT B
Mammalian cells		
HeLa cells		Used in cell culture /cell viability MTT assays

Table 3.2.2. List of reagents used in this study.

Reagent/Resource	Source	Use
Reagent		
Dulbecco's Modified Eagle Medium (DMEM)	Gibco	Cell culture
Foetal Bovine Serum (FBS)	Gibco	Cell culture
Phosphate Buffered Saline (PBS)	Gibco	Cell culture
Trypsin/Ethylenediamine tetraacetic acid (EDTA)	Gibco	Cell culture
Hank's Balanced Salt Solution (HBSS)	Gibco	Cell culture
3-(4,5-dimethylthiazol-2-yl)-2,5-diphenyl-2H-tetrazolium bromide (MTT)	EMD Millipore	Cell viability assays
Methanol	Fisher Chemicals	Coomassie staining
Glacial acetic acid	Fisher Chemicals	Coomassie staining
10% Sodium dodecyl Sulphate (SDS)	Fisher Bioreagents	Coomassie staining
NaCl		Coomassie staining
2-Mercaptaethanol		Coomassie staining
40% Acrylamide Bis-Acrylamide	Fisher Bioreagents	Coomassie staining
N, N',N',N'-Tetramethyl-ethylenediamine (TEMED)	Fisher Bioreagents	Coomassie staining
Ammonium Persulphate (APS)	Fisher Bioreagents	Coomassie staining
Bromophenol blue	Fisher Bioreagents	Protein purification
Agarose		Gel electrophoresis
Glycerol (99%)	Fisher Bioreagents	Preparing competent cells, bacterial strains, and plasmid stocks
Dimethyl sulfoxide (DMSO)	Fisher Bioreagents	Cell viability MTT assays
Isopropanol	Fisher Bioreagents	Coomassie staining
α -Toluenesulfonyl fluoride (PMSF)	Fisher Scientific	Protein purification
Isopropyl β - d-1-thiogalactopyranoside (IPTG)	Fisher Bioreagents	Protein purification
Deoxyribonuclease I (DNase), bovine pancreas	Fisher Scientific	Protein purification
Lysozyme	Bioshop	Protein purification
Ethidium Bromide	Fisher Scientific	Gel electrophoresis

3.2.3 Plasmid design

3.2.3.1 Insert amplification of A and B subunit sequences

All primers used in this study and are listed in Table 3.2.3. The inserts were amplified by polymerase chain reaction (PCR) from previously constructed plasmids encoding one or both toxin subunits and from synthetic DNA gBlocks (Integrated DNA Technologies, Canada). A polyhistidine (His₆) tag sequence was cloned into and attached to the C-terminal of all B subunits. All RIP-TT and RIP-HLT toxins including mutants and synthetic hybrid Stx2a A/RIP-TT B and Stx2A/RIP-HLT B toxins were amplified via cross-over PCR in two separate rounds of amplification. In the first round, the desired upstream and downstream sequences were separately amplified using primers with built-in overlapping sequences that allowed the ligation of the resulting DNA fragments in a second round of amplification. PCR products were purified using the QIAquick PCR purification kit according to the manufacturer's instructions (Qiagen, Germany) or run on a 1% agarose gel w/v in TAE buffer (0.4 M Tris, pH 8.4, 0.01 M EDTA, 0.2 M Glacial Acetic Acid) containing a 1:6 dilution of 10 mg/ml UltraPure™ ethidium bromide (Fisher Scientific, USA, cat. no. 15585011) and desired bands excised and purified using the GeneJET gel extraction kit (ThermoFisher Scientific, Lithuania, cat. no. K0691) according to the manufacturer's instructions.

3.2.3.2 Restriction enzyme cloning

The pET22b (+) overexpression vector which contains a T7 promoter was used to clone all toxins used in this study and all constructs were designed by restriction enzyme cloning. Purified plasmid vectors and inserts were digested with the corresponding restriction enzymes indicated in Table 3.2.4. The digested pET22b (+) vector was ligated in a 1:1 ratio with each

insert using the T4 DNA ligase (New England Biolabs, Canada, cat. no. M0202L) and incubated overnight at 4°C. Ligated plasmid DNA was transformed into electrocompetent *E. coli* DH5α via electroporation and positive clones were identified by colony PCR using primers that bound sequences located ~ 300bp upstream and downstream of the DNA insertion site or by restriction digests with the same enzymes used in cloning. Identified positive transformants were confirmed by sequencing.

Table 3.2.3. Primers used in this study.

Primer name	Primer sequence (5' to 3')	Use
pET22-US-For	GCAAGGAATGGTGCATGCAAG	PCR amplification of vector plasmid and sequencing
pET22-DS-Rev	CCGGATATAGTTCCTCCTTTCAG	PCR amplification of vector plasmid and sequencing
CF-A39-pET22-For	GTAGAGGATCGAGATCTCGATCC	Sequencing
CF-A40-pET22-Rev	GCTAGTTATTGCTCAGCGGTG	Sequencing
RIP-TT-Bsub+350-For	CGACCCCGATTTCAAATGTGG	PCR amplification of RIP-TT B
RIP-TT-Bsub-S31A-DS-For	GAGTATGGCTGATTATAATAATTA TACGGCTGAAGTTCATATTAAGA ATCTGTCCTATG	PCR amplification of RIP-TT S31A binding mutant
RIP-TT-Bsub-S31A-US-Rev	CATAGGACAGATTCTTAATATGA ACTTCAGCCGTATAATTATTATAA TCAGCCATACTC	PCR amplification of RIP-TT S31A binding mutant
RIP-TT-Bsub-S45A-DS-For	GAATCTGTCCTATGGCGTGATAA AGCAGGGGAGAAGGAGACTCAG	PCR amplification of RIP-TT S45A binding mutant
RIP-TT-Bsub-S45A-US-Rev	CTGAGTCTCCTTCTCCCCTGCTTT ATACACGCCATAGGACAGATTC	PCR amplification of RIP-TT S45A binding mutant
RIP-TT-Bsub-S31A-DS-For	GAGTATGGCTGATTATAATTATAC GGCTGAAGTTCATATTAAGAATCT TATTAAGAATCTGTCCTATG	PCR amplification of RIP-TT S31A binding mutant
RIP-TT-Bsub-S45A-US-Rev	CTGAGTCTCCTTCTCCCCTGCTTT ATACACGCCATAGGACAGATTC	PCR amplification of RIP-TT S31A binding mutant
RHLT-Fix-Us-Rev	GGCGTCTTCCCCTGGGACTGTCT GGAGAAAATTACGACTTAGTTGA C	PCR amplification of RIP-HLT WT
RHLT-Fix-DS-For	GTCAACTAAGTCGTAATTTTCTCC AGACAGTCCCAGGGGAAGAACGC C	PCR amplification of RIP-HLT WT
RIP-HLT-Bsub-T13I-4-Mut-D	GATTTTGAAGCTTCATGTAGTGCA ATCATCGCTGTCATGGAAAAA TATCAA	PCR amplification of RIP-HLT T36I/T37I binding mutant
RIP-HLT-Bsub-T13I-4-Mut-U	TTGATATTTTCCATGCAGACGCG ATGATTGCACTACATGAAGCTTCA AAATC	PCR amplification of RIP-HLT T36I/T37I binding mutant
RIP-TT-StxA2-DS-For	GATCCGAGAAGGAGATTATCAA TGAAGTGATATTAATTTAAATGGG TACTG	PCR amplification of hybrid Stx2a A/RIP-TT B
RIP-TT-StxA2-US-Rev	CAGTACCCATTTAAATAAACACTT CATTGAATTATCTCCTTCTAGCCG GATC	PCR amplification of hybrid Stx2a A/RIP-TT B
pET22-StxA2-Ds-Rev	ATGATGCGGATCCTTATTTACCCG TTGTATATAAAAACCTGTGAC	PCR amplification of hybrid Stx2a A/RIP-TT B

Table 3.2.4. Restriction enzymes used in cloning the collection of plasmids used in this study.

Plasmid	Restriction enzymes	Source
pET22-RIP-TT wild type	NdeI and BamHI	New England Biolabs
pET22-RIP-TT B	NdeI and BamHI	New England Biolabs
pET22-RIP-TT (R192A)	NdeI and BamHI	New England Biolabs
pET22-RIP-TT (S31A/S45A)	NdeI and BamHI	New England Biolabs
pET22-RIP-HLT wild type	XbaI and XhoI	New England Biolabs
pET22-RIP-HLT B	XbaI and XhoI	New England Biolabs
pET22-RIP-HLT (R192A)	XbaI and XhoI	New England Biolabs
pET22-RIP-HLT (T36I/T37I)	XbaI and XhoI	New England Biolabs
pET22-Stx2a wild type	EcoRI and XhoI	New England Biolabs
pET22-Stx2a A/RIP-TT B	NdeI and BamHI	New England Biolabs
pEt22-Stx2a A/RIP-HLT B	NdeI and BamHI	New England Biolabs

3.2.4 Purification of His₆-tagged proteins

3.2.4.1 Growth and overexpression of RIP-TT, RIP-HLT and related toxins

The pET22b (+) plasmids encoding all versions of the RIP-TT and RIP-HLT proteins as well as the Stx2a holotoxin were transformed into *E. coli* BL21 (DE3) following confirmation of constructs by sequencing. Transformed bacterial cells were grown overnight in 5 ml of LB supplemented with 5 µl ampicillin. The next day, bacterial cultures were back diluted 1: 40 in 500 ml of fresh LB supplemented with 500 µl ampicillin and grown in a shaking incubator at a Revolutions per minute (RPM) of 200 at 37°C till an optical density (OD₆₀₀) of ~0.8 was reached. Protein expression was induced by the addition of Isopropyl β- d-1-thiogalactopyranoside (IPTG) (0.2 mM for WT RIP-TT, RIP-TT R192A, WT RIP-HLT, RIP-HLT R192A, synthetic hybrid Stx2a A/RIP-TT B and Stx2a A/RIP-HLT B toxins and 1 mM

for WT Stx2a, RIP-TT S31A/S45A and RIP-HLT T36I/T37I). Cultures were incubated overnight at room temperature in a shaking incubator.

3.2.4.2 Sample preparation and purification of His₆-tagged recombinant proteins

Bacterial cultures were centrifuged at 4255 RPM for 18 minutes at room temperature and cell pellets resuspended in 10 ml of lysis buffer (Tris, pH 8.0; NaCl, DNase; lysozyme and 99% α -Toluenesulfonyl fluoride (Fisher Scientific, Canada, cat. no. B22146.14). Cells were lysed using the Emulsiflex-B15 high pressure homogenizer (Avestin) in four to six rounds of homogenizations or until sample was clear. The obtained whole cell lysates were then centrifuged at 20,000 x g for 40 minutes at -4°C and the supernatant was collected.

All proteins used in this study were purified from *E. coli* BL21 (DE3) using a Nickel (Ni) resin gravity column (New England Biolabs, USA, cat. no. S1428S) according to the manufacturer's instructions. Briefly, 6 ml of resin was added to empty gravity columns and the storage buffer was allowed to flow-through once the resin settled. 8 ml of binding buffer (20 mM Tris pH 8.0, 150 mM NaCl) was added to columns to equilibrate the resin (x 3). Fractions of the clarified lysate were added periodically to the equilibrated column and columns were washed (x 3) with 8 ml of wash buffer (lysis buffer + 20 mM imidazole pH 8.0). Finally, the His₆-tagged proteins were eluted in 250 μ l (x 4) of elution buffer (wash buffer + 300 mM imidazole pH 8.0). Concentrations of purified elutions were determined using the Pierce™ Bradford protein assay kit containing 2 mg/ml of Bovine Serum Albumin standard (ThermoFisher Scientific, USA cat. no. 23200), according to the manufacturer's instructions and the absorbance values were determined using a Bio-Rad micro-plate reader.

3.2.5 Sodium Dodecyl Sulphate-Polyacrylamide Gel Electrophoresis (SDS-PAGE)

analysis of purified toxins

To evaluate interactions between the B-His₆ subunits and their corresponding A subunits for all purified holotoxins, separate fractions of products from multiple stages of the purification process were run on an SDS-PAGE gel. Purified toxin elutions were diluted 1:1 v/v in 2 x concentrated SDS sample buffer (4% SDS, 20% glycerol, 5% 2-mercapthanol, 0.02% bromophenol blue and 62.5 mM Tris, pH 6.8) and heated in a heating block for 5 minutes at 96°C. Resolving solution was prepared with 12% acrylamide bis-acrylamide while the stacking gel solution was prepared with 5% acrylamide bis-acrylamide. 30 µl of each sample was loaded alongside 5 µl of a 100 kDa protein ladder (Bio-Rad, Canada). Electrophoresis was done using a Powerpac Basic machine (Bio-Rad) and run at 100V for 30 min, then 150V for 1 hour. To evaluate subunit interaction, Coomassie staining was done as previously described (231,232). Briefly the run gels were immersed in 5-10 ml of Coomassie staining solution (50% methanol, 10% glacial acetic acid, 40% ddH₂O) supplemented with 12 ml of 10% Pierce™ Coomassie brilliant blue dye (ThermoScientific USA, cat. no. 20278) and incubated on a rolling platform for 30 minutes to 1 hour at RT. Gels were then destained 2 x by submerging them in 5 ml of destain solution (50% ddH₂O, 40% methanol and 10% glacial acetic acid) for 10 to 20 min. The gels were incubated in 10 ml of destain solution overnight and visualized using Bio-Rad GelDoc Go Gel imaging system.

3.2.6 Cell viability assays

All cell culture assays were performed in a class II biological safety cabinet (Baker SterilGARD, USA). To evaluate the cytotoxicity of RIP-TT and RIP-HLT as well as other toxins used in this study, an MTT (3-(4,5-dimethylthiazol-2-yl)-2,5-diphenyl-2H-tetrazolium bromide) HeLa cell viability assay was performed as previously described (233). Briefly, HeLa cells were seeded in 96-well plates (Corning) at a cell density of 1×10^4 cells/ml in Dulbecco's Modified Eagle Medium (DMEM) supplemented with 10% Foetal Bovine Serum (FBS) (Gibco™ cat. no. 11995065), and 50 µg/ml gentamicin and incubated overnight at 37°C and 5% CO₂. The following day, 10- or 4-fold serial dilutions of purified toxins diluted in Hanks Balanced Salt Solution (HBSS) (Gibco™ cat. no. 14170112) were added to wells in triplicate and incubated for 1 hour at 37°C and 5% CO₂. The media was then replaced with fresh pre-warmed DMEM + 10% FBS (100 µl/well) and cells were left to grow and recover. An MTT assay was performed 72 hours post intoxication by adding 10 µl of a 12 mM MTT solution made up of the MTT reagent (MilliporeSigma, Canada, cat. no. CT01-5) diluted in Phosphate Buffered Saline (PBS) (Gibco™ cat. no. 10010031) to each well and re-incubated for 2 hours at 37 °C and 5% CO₂. The media was discarded and 100 µl of dimethyl sulfoxide (DMSO) (Fisher BioReagents™, Canada, cat. no. BP231-100) was added to each well to solubilize the formazan crystal precipitates. The plate was then incubated for 30 minutes at RT, protected from light. All data points were done in triplicate and absorbance A₅₇₀ values corresponding to the amount of viable and metabolically active cells were obtained using a Bio-Rad microplate reader. To obtain normalized absorbance values, the average blank absorbance value of blank control wells (no cells) was subtracted from the absorbance values for wells containing cells treated with each toxin dilution (toxin-treated cells) and wells containing cells that were

mock-treated with toxin (unintoxicated cells). The percentage of viable cells was calculated using the formula: Average absorbance of toxin-treated sample/Average absorbance of mock-treated controls x100. Percent cell viability values were plotted against toxin concentrations in a Microsoft excel line graph.

3.3 Results

3.3.1 The *rip-tt* genomic locus exhibits significant similarity to the *artAB* genomic locus

The *rip-tt* locus was initially identified by Dr. Fowler through a comprehensive genomic analysis of AB₅ toxins in the *Salmonella* genus. We first set out to dissect the genomic locus that encodes this unique toxin. *S. enterica* subspecies *enterica* serovar Stanleyville RSE1 strain (Accession no: CP034723.1) was arbitrarily selected as a reference strain for analysis of the *rip-tt* genomic locus. In this strain, the genes encoding the RIP A subunit and the ArtB/PltC-like B subunit are located downstream of genetic elements with striking sequence similarities to the structural genes that encode the ArtAB toxin (*artA* and *artB*), with the primary distinction being that the *artA* gene in the *rip-tt* locus is a pseudogene. To investigate the possible evolutionary relationship between RIP-TT and ArtAB, we used the well-characterized *S. Typhimurium* DT104 *artAB* locus (Accession no: CQB84322.1). Comparison of the *S. Stanleyville* RSE1 *rip-tt* locus and the *S. Typhimurium* DT104 *artAB* locus revealed that most of the genes found in the *artAB* locus are also found in the *rip-tt* locus (Figure 3.3.1A). In addition to the *artA* and *artB* genes, both loci harbour an assortment of prophage-related genetic elements including a gene that encodes a putative antiterminator and multiple genes that encode holins, proteins that are found in diverse phages and play a key role in the expression and secretion of the ArtAB toxin, and endolysins, which play crucial roles in bacterial cell lysis (Figure 3.3.1A) (220). Located immediately downstream of the *rip*-like A subunit gene in the *rip-tt* locus but not in the *artAB* locus is a pseudogene, the functional version of which is predicted to encode a CopG transcriptional regulator. This is followed by a short DNA sequence that encodes a putative type II toxin-antitoxin, proteins that are ubiquitously found in several bacterial chromosomes and

mobile genetic elements and contribute to bacterial virulence, antimicrobial resistance, and phage replication (234).

A closer inspection of the DNA sequence of the *S. Stanleyville* RSE1 RIP-TT *artA* pseudogene revealed that the two main differences between this gene and the functional *artA* gene encoded by *S. Typhimurium* DT104 are that the *artA* pseudogene in the *rip-tt* locus: (i) has a 58 bp deletion located 205 bp into the N-terminal of the ArtA sequence (Supplementary Figure S3.1), and (ii) has a frameshift mutation that results in a premature stop codon near the beginning of the gene. The similarities in the nature and organization of genes in the *rip-tt* and *artAB* loci suggests that the RIP-TT toxin likely evolved from an ArtAB-like precursor following horizontal gene transfer of phage-encoded *artAB* genetic elements in *Salmonella*. However, the *artA* gene, which is non-functional has now been replaced by a divergent *rip*-like gene that serves as the A subunit in a functionally different AB₅ complex.

3.3.2 The RIP-TT toxin is widely distributed in the *Salmonella* genus

To evaluate the distribution of the RIP-TT toxin in *Salmonella*, we mined the NCBI non-redundant (nr) protein database for the presence of the RIP-TT A and B subunit genes and identified 103 *Salmonella* strains that encode the *rip*-like gene adjacent to an *artB* homolog (Supplementary Table S3.1). 102 of the 103 strains belong to the *S. enterica* species with 42 of these reported to be isolated from humans and the rest from a variety of animal and food sources or the source was not identified and only one *S. bongori* strain (PNUSAS088562) from an unidentified source was found (Supplementary Table S3.1). Many of the *S. enterica* strains also belong to the subspecies *enterica*, with only a few strains from other subspecies, including *indica*, *arizonae* and *diarizonae*. The *S. enterica* subsp. *enterica* strains were from a variety of

NTS serovars including Stanleyville, Wagenia, Kouka, Macclesfield, Kambole, Typhimurium and several others. The most common serovar reported was Kambole with 13 total strains of which 11 were reported to be isolated from humans. The amino acid sequences of the A and B subunits in all 103 strains were nearly identical (> 94% and > 91% respectively). Our collective findings reveal that the RIP-TT toxin is widespread in *S. enterica*, and that the structure of this locus is relatively well conserved regardless of what serovars they are found in.

3.3.3 Identification, analysis, and distribution of the *rip-hlt* genomic locus

In contrast to the broad distribution of the *rip-tt* locus, the *rip-hlt* locus was only identified in two *Salmonella* strains, *S. enterica* subsp. *enterica* str. 431409 (Accession no: ECC9924939) and *S. enterica* subsp. *enterica* serovar Paratyphi B var. L(+) tartrate + (Java) str. FNE0063 (Accession no: EDP8718245), which were respectively isolated from human and food sources. The composition and arrangement of genes in the *rip-hlt* locus is identical in both *Salmonella* genomes and we selected the *S. enterica* str. 431409 for further analysis. In this locus, the RIP-like A subunit gene is located upstream of a putative *It-II*-like B subunit gene and downstream of a TnR family transposase pseudogene (Figure 3.3.1B), suggesting that this toxin locus might have been horizontally acquired via transposition. Immediately upstream of the TnR family transposase pseudogene is another gene that encodes a putative recombinase protein, an agent of bacterial genome manipulation and homologous recombination (235) and other genetic elements found such as a MerR transcriptional regulator pseudogene and a gene that encodes a putative N-acetyltransferase (Figure 3.3.1B). Together, these observations hint at the probability that the evolution of the RIP-HLT toxin was mediated by mobile genetic (transposable) elements, which resulted in adjacent heterologous genes that encode a unique

putative AB₅ toxin. While the *rip-hlt* locus is found in fully sequenced *Salmonella* genomes, the genes encoding the A and B subunits of the toxin are found near the end of a contiguous genomic region (contig) that consists of overlapping sequences and as a result, the genes downstream of the *lt-II*-like B subunit gene are yet to be identified.

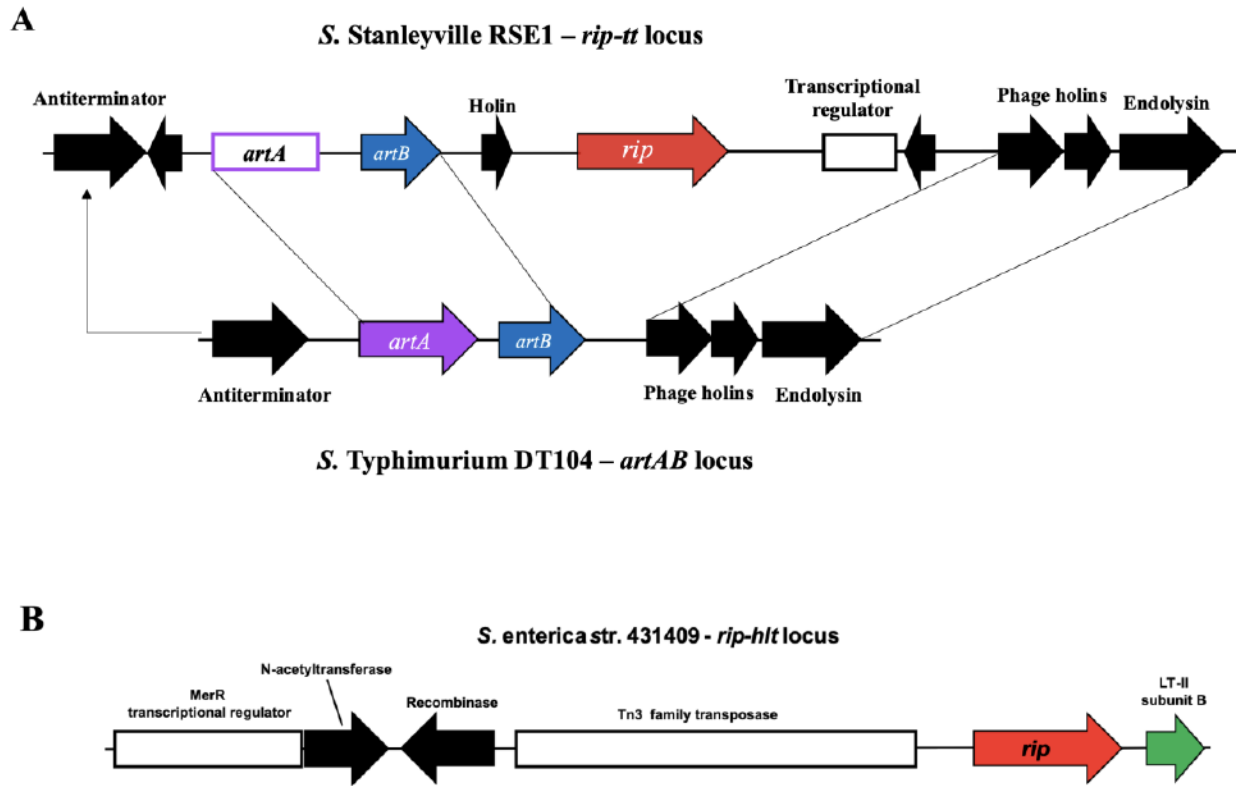


Figure 3.3.1. Genomic loci encoding the putative RIP-TT and RIP-HLT hybrid toxins. (A) Comparison of the *S. Stanleyville* RSE1 *rip-tt* locus (Accession no: CP034723) and the *S. Typhimurium* DT104 *artAB* locus (Accession no: CCW75371.1). Straight and elbow connectors indicate homologous regions and genes shared by both loci. **(B)** *S. enterica* strain 431409 *rip-hlt* locus (Accession no: ECC9924938.1) showing the *rip*-like A subunit gene immediately upstream of a gene that encodes a putative LT-II-like B subunit. The A and B subunit genes are situated at the end of a contiguous region of the *S. enterica* 431409 genome and putative genes located downstream of *lt-II* B are yet to be identified. The genes encoding the A and B subunits of RIP-TT, RIP-HLT and ArtAB are depicted using coloured arrows. Intact genes are indicated by black arrows and white boxes represent pseudogenes. Both the *rip-tt* and *rip-hlt* genomic loci were initially identified by Dr. Fowler prior to my arrival in the lab.

3.3.4 Phylogenetic and comparative sequence analyses of the RIP-TT and RIP-HLT toxins

Although the A subunits of both the RIP-TT and RIP-HLT toxins share significant sequence similarity to RIPs like Stx, they are predicted to associate with very different B subunits, suggesting that some extent of structural divergence may have occurred to allow these subunits to interact with very different binding pentamers. To better understand the evolutionary relationships and extent of sequence divergence between these A subunits, we performed a multiple sequence alignment and compared the unprocessed RIP-TT and RIP-HLT A subunit protein sequences to those of Stx1a (*E. coli* O157: H7 str. Sakai, Accession no: NP_3110010) and Stx2a (*E. coli* O157: H7 str. Sakai, Accession no: NP_309232.1). We also included the first 320 N-terminal amino acid residues from a similar RIP-like A subunit identified in *Aeromonas salmonicida* (str. CIP 104001; Accession no: NKWK01000225), a pathogen of aquatic animals which causes systemic disease in Salmonids but is rarely associated with human disease (236). We chose to include this protein sequence since BLAST identified this putative protein as the strongest hit for our RIP-TT and RIP-HLT A subunits outside of the *Salmonella* lineage. The *rip* gene in *A. salmonicida* is encoded on a locus that does not appear to contain any other AB₅ genetic elements and thus this RIP sequence is not predicted to be an AB₅-type toxin subunit and the RIP enzyme probably utilizes alternative uncharacterized delivery mechanisms to enter cells and reach its target. We found that the RIP-TT and RIP-HLT A subunits were ~70% identical to one another, ~45% identical to the *A. salmonicida* RIP sequence, and ~ 33% identical to the RIP A subunits of both Stx1a and Stx2a at the amino acid sequence level. Our sequence alignment results also revealed conservation of several of the key amino acid residues postulated to be required for the N-glycosidase activity of characterized RIPs such as Tyr99, Tyr136, Glu189, Arg192 and Trp225 (Figure 3.3.2A) (237–240). We identified one amino acid,

Asn97, predicted to be important in the Stx RIP activity (237) that was not conserved in the *A. salmonicida* RIP sequence but was present in the RIP-TT and RIP-HLT A subunit sequences.

Due to the significant structural and functional variation in the B subunits of Stx family toxins and the RIP-TT and RIP-HLT toxins, we predicted that the RIP A2 C-terminal α -helical structure which mediates interactions with the amino acids that line the pore of the B pentamer and serve a crucial role in the integrity of the AB₅ complex (182) would be highly variable amongst these different RIP proteins. In the complete Stx1a A protein sequence, this C-terminal α -helical structure is composed of 15 amino acids, while the Stx2a C-terminal helix includes 20 amino acids (Figure 3.3.2A) and extends through the pore of the B pentamer. This extended loop is a distinguishing structural feature between the two Stx types and has been shown to have important functional and biological implications (83,241,242). In comparison to the Stx C-terminal sequences, both the RIP-TT and RIP-HLT putative A2 C-terminal sequences were found to be significantly shorter. This is interesting given that the C-terminal alpha helices of the A subunits commonly associated with the characterized homologs of their cognate B subunits (i.e., ArtA and the LT-II A subunit) are also notably shorter than those of Stx (125,147). As predicted, we observed no significant sequence conservation in the C-terminal helices of all five A subunit protein sequences including the *A. salmonicida* RIP (Figure 3.3.2A). This finding indicates that despite the similarities in their A subunits, the individual toxins have presumably evolved to adapt to the architecture of their respective B pentamers to form stable AB₅ complexes that may differentially bind and target different cell types.

To predict possible evolutionary relationships between these different A subunit sequences, a maximum likelihood phylogenetic tree was constructed using the same five RIP protein sequences described above (Figure 3.3.2B). As expected, we observed clustering of the Stx1

and Stx2 A subunit sequence branches indicating that both sequences likely originate from a common ancestor and as such, are more closely related. Similarly, the RIP-TT and RIP-HLT A subunit sequences appeared to be closely related to each other but evolutionarily distant from those of Stx. Interestingly, the RIP-TT and RIP-HLT A subunit sequences were predicted to share a more recent common ancestor with the *A. salmonicida* RIP than with the Stx1/Stx2 A subunit sequences. Overall, our phylogenetic analysis indicates that the Stx1a, Stx2a, RIP-TT and RIP-HLT A subunits may have evolved from a common ancestor also shared by the RIP of *A. salmonicida*, but the Stx A subunits have evidently undergone substantial modifications that allow stable interactions with very different B subunits in a highly potent AB₅ toxin complex.

A

```

Stx1a      84- GRFNNLRLLIVERNNLVVIGFVNRNNVFFRFADEFSHVFFGDTA---VLSGSSVYTLQRVAGISRTGMQINRHSLTETS YLDLMSHS
Stx2a      84- ARFDHLRLIIEQNLVVAGFVNTAINTFYRPSDFTHISVGGVTT---VEMTDDSSVYTLQVVAALERSGMQISRHSLVSSYLALMEFS
A. salmonicida 85- DELSIVRPFVLSFDLVLTGFIY--NNVYHYTDQSTITVSPHARSQSINLSSN YLSMERAQVDRIGLEISNENLISDMFALTNIIE
RIP-TT     83- ETISVVRPFVLSQNLVLTGFIY--NRVYHFRDEANITVCFDFADSTRAIKLASN YDLQVWGLSRQGLVLSNNLNLSGLITLMSIN
RIP-HLT    83- ETYSVVRPFVMSQNLVLTGFIY--NRVYHFRNEDTITVCFELVDGMEIMNLES YFALQKADLRSQGLEPSPGNLNSGLISLNTNIA
          :*:::.. :**::** :...*::: : : : : : : : : : : : : : : : : : : : : : : : : : : : : : : : : : : : :
          : : : : : : : : : : : : : : : : : : : : : : : : : : : : : : : : : : : : : : : : : : : : : : : : :

Stx1a      169- QTELQSVARAMLRFVTVIAEALRFQIQGFRPTLDDLS--GRSYWHEAEVDLELNHGRLSVLEF--YHQDSVVRVGRISFGSIN
Stx2a      169- GNITMDASRAVLRFTVIAEALRFQIQREFRQALSET--APVYIMTFGDVLELNHGRISNVLEF--YRGEQVVRVGRISFNNIS
A. salmonicida 171- SSRHYANLAVALMRYATVISKATRFQIQGNIRVIFGSH--SKTYNISESDYLNLRKRLSNLFLMTQVWQEMIDAGNVRDTGNH
RIP-TT     169- DQSVYRACACTLLRFARVIDEALRFQIQNVRTIFDLRFVWVYLSGSDIEIENSWEQLSQNFIRHTYDGGQAIRVGAIFLQNNH
RIP-HLT    170- PESITRSHAGAMLAFARVIDEALRFQIQNLRPIEDLRFVWVYLSGSDIEIENSWEQLSNFLQVTPGEERIRVQGVFLQNNH
          * : : : : : : * * * * * * * * * * * * * * * * * * * * * * * * * * * * * * * * * * * * * * * * * * *
          * : : : : : : * * * * * * * * * * * * * * * * * * * * * * * * * * * * * * * * * * * * * * * * * * *

Stx1a      254- AILGVALIINLHHASKVARAGASDEFPSPAD-GVVRGI-----THNKIWDSSYLGATIMRRTISS
Stx2a      253- AILGTVAVILNHQGARSURAVNERSQPEQIT-GQRFVI-----KINNTLWESNTAAFLMRKRSQFLYTTCK
A. salmonicida 257- SILSALGLLLYHSSPFRSFAQ-NHTTCTASGRGNLRFPLIKIKYHNAQCIVN SNTYASLEKQ
RIP-TT     257- AILALAMLYKSSST-GNMSYS---EGYEAHSKSYVVM-----GVVWDKTLFFI
RIP-HLT    258- AILSALALLLYAPNPTSKSILS---EGYEAHTGKSYVVM-----GVVWDKTLFNTIK
          :**::: : : : : : : : : : : : : : : : : : : : : : : : : : : : : : : : : : : : : : : : : : : : : : : :
  
```

B

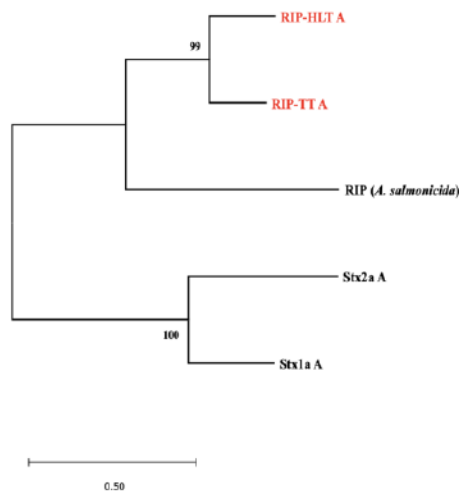


Figure 3.3.2. Sequence alignment and phylogenetic analysis of the amino acid sequences of RIP A subunits from different bacterial species. (A) Protein sequence alignments for the RIP sequences of RIP-TT, RIP-HLT, Stx1a, Stx2a and *A. salmonicida* (from ~ aa 83 of the N-terminal sequence to the end of the A2 peptide sequence) showing conservation of several putative amino acid residues essential in the enzymatic activity of Stx and similar RIPs (residues coloured in red). Conserved residues in yellow represent the cysteine residues that form a disulphide bond between the A1 and A2 peptide sequences. Blue coloured residues are the amino acid residues that make up the A2 C-terminal sequence that inserts into the pore of the B pentamer and is variable among all sequences. Alignment was done using the ClustalW Omega alignment tool (European Bioinformatics Institute). Asterisks (*) denote positions of total conservation of amino acids and colons (:) indicate positions of partial conservation. (B) Phylogenetic trees inferring the relationships between the same amino acid sequences in panel A, constructed with the MEGA (Molecular Evolutionary Genetics Analysis) X software using the maximum-likelihood method and the WAG + I + G substitution model with a total of 100 bootstrap replicates. Numbers at the nodes represent branch support values.

In our previous study, we highlighted the strong genetic evidence that the typhoid toxin PltC subunit evolved from an ArtB-like precursor. We predicted that the RIP-TT B subunit likely exhibits structural and functional homology to both ArtB and PltC. Sequence comparisons between all three B subunits (*S. Typhimurium* DT104 ArtB, *S. Stanleyville* RSE1 RIP-TT B and *S. Typhi* Ty2 PltC, Accession no: LR590082) revealed that the RIP-TT B subunit is equally divergent (~70% amino acid sequence identity) from both ArtB and PltC. We also performed a multiple sequence alignment on representative B subunits from the seven ArtAB subtypes and four PltC groups described in Chapter 2 of this thesis as well as PltB from *S. Typhi* CT18 (Accession no: AC0719). Our results showed that the RIP-TT B subunit exhibits high protein sequence similarities (> 65%) to all type 1 ArtAB subtypes and PltC groups and considerably less sequence similarity ($\leq 30\%$) to all type 2 ArtAB subtypes and the *S. Typhi* PltB sequence. Our multiple sequence alignments also revealed conservation of key residues required for

efficient binding to glycans between the RIP-TT B, type 1 ArtB and PltC B subunit sequences (Figure 3.3.3A). Of particular note was the conservation of both critical serine residues at the lateral (Ser31) and basal (Ser45) binding sites in RIP-TT B, a feature that is absent in type 2 ArtB sequences. The presence of the Ser45 residue in RIP-TT B which has been found to be important in the binding of ArtB and PltC to Neu5Gc glycans but is absent in PltB which is unable to bind the same glycan (70,147), indicates that the RIP-TT B subunit might also utilize two binding pockets to target an array of cell types similar to ArtB and PltC. Tyr103 in ArtB, which is postulated to form a critical hydrogen bond with the extra hydroxyl group of Neu5Gc (70,150), is also conserved in the RIP-TT B subunit sequence. Several of the other amino acids in ArtB such as Asn27, Tyr29 and Arg59 which form direct hydrogen bonds with Neu5Ac and Gly46, Lys79, Tyr109, Val107 and Asp110 which interact with the terminal galactose moieties in Neu5Ac are also conserved in RIP-TT B (Supplementary Figure S3.2). A phylogenetic tree of all 13 sequences used in the sequence alignments above was constructed to uncover a possible evolutionary pathway for the emergence of the RIP-TT B subunit. Consistent with the sequence conservation and similarities highlighted above, our phylogenetic tree hypothesized a closer evolutionary relationship between type 1 ArtB/PltC and RIP-TT B relative to type 2 ArtB and PltB based on the recent ancestor from which they are predicted to originate from (Figure 3.3.3C). Collectively these results suggest that RIP-TT may target cells expressing both Neu5Ac and Neu5Gc glycans and similar to the evolutionary adaptation of PltC, specific amino acid modifications in the RIP-TT B subunit likely occurred to mediate interactions with a RIP-like A subunit.

Phylogenetic and sequence analysis of the RIP-HLT B subunit included sequence comparisons between RIP-HLT B and representative members from the Ctx/LT family of AB₅

including the *V. cholerae* Ctx B (Accession no: WP_000593519.1), *E. coli* LT-I B (Accession no: WP_086200689.1), *E. coli* LT-IIa B (Accession no: WP_000095643.1), *E. coli* LT-IIb B (Accession no: GDL79131.1) and *E. coli* LT-IIc B (Accession no: UYK53806.1). Our analyses revealed that the RIP-HLT B subunit shares greater sequence similarity to the LT-II B subunits (~ 40%) compared to the Ctx/LT-I B subunits (<18%). We also performed a multiple sequence alignment of the same B subunits above, to examine the conservation of putative key binding residues. The predominant amino acids previously shown to be required for efficient LT-II binding to GD1a and GD1b gangliosides are two threonine residues located at position 36 (Thr36) and 37 (Thr37) in the unprocessed B subunit sequence (243,244), and both residues were found to be conserved in the RIP-HLT B subunit sequence (Figure 3.3.3C). In the Ctx and LT-I B subunits, the primary amino acid residue suggested to be required for GM1 binding is Gly54 (245,246), which is absent in the LT- II and RIP-HLT B subunit sequences and likely accounts for the low avidity binding of LT-II to GM1 gangliosides. Interestingly, we found that the amino acid residues that are reported to mediate LT-II binding to toll-like receptors (Met96, Ala97, Leu100 and Ser74) (247) were mostly conserved in the RIP-HLT B subunit sequence (Figure 3.3.3B). A phylogenetic tree was also constructed using the same B subunit sequences of representatives from RIP-HLT, Ctx, LT-I, LT-IIa, LT-IIb and LT-IIc to infer possible evolutionary relationships between these subunits (Figure 3.3.3D). Consistent with previous findings, there was an obvious clustering of the LT-II sequences which was separate from the Ctx/LT-I B subunit sequences. Despite the low bootstrap support value indicated on our phylogenetic tree for RIP-HLT branching, our previous results support the possibility that the RIP-HLT toxin shares a common ancestor with the LT-IIa B subunit sequences and is more

closely related to LT-II B compared to Ctx B and LT-I B which were predicted to be more distantly related to all other toxin sequences implicated in this analysis.

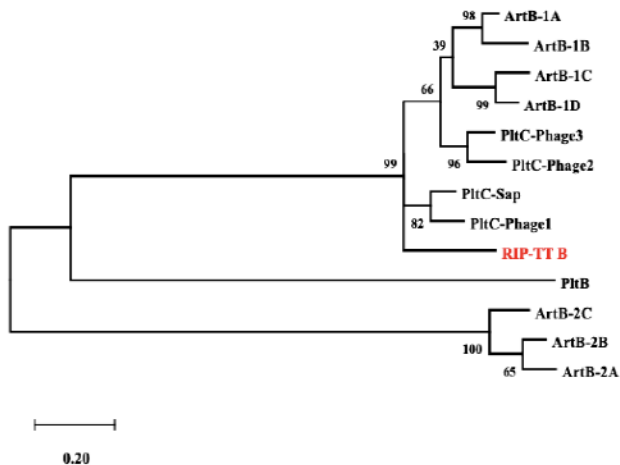
A

	← S31	S45 →	
	Lateral binding site		Basal binding site
ArtB-1A	NMADYNTYQSNVQINNLSYGVYRS	GGDKESQFPCVGLKRGS	
ArtB-1B	NMADYNTYQSNVQINNLSHGVIK	SGGKDSQFPCIGLNNES	
ArtB-1C	DMAGYNKYVSNVQINNLSYGVYT	SGGKQTQFPCVGLKRGS	
ArtB-1D	NMAGYNKYVSNVQINNLSYGVYT	SAGKQTQFLCVGLKRGS	
ArtB-2A	YLKDTTKY-ENVRITNVFYAPYLHSPRICAYFTAS	-----	
ArtB-2B	YLKDTTKY-ENVKITNIFYAPYLHSPRICAFFTAS	-----	
ArtB-2C	YLKDTVKY-ENVKVTNVFYAPYLHSPRICAFFTTS	-----	
PltC-Sap	AMADYDTYVSNVQINNLSYGVYT	SGGKETQFPCIGLKHGS	
PltC-Phage1	GMADYDTYVSNVQINNLSYGVIK	DDKETQFPCIGLKRGS	
PltC-Phage2	GMADYDKYISNAQINNMSYGVYT	SGGKETQFPCIGLKRGS	
PltC-Phage3	GMADYDKYISNAQINNLSYGVYTT	GGKETQYFCIGVKRGS	
RIP-TT	SMADYNNYTS	EVHIKNLSYGVIKSGEKETQFPCIELKRGS	
PltB	TGDNTNAYYS	DEVISELHVQG----IDTSPYFCIKTVKAN	

B

Ctx	1-	-----MIKLLK---FGVFFTVLLSSAYAHGTPQNIITDLCAEYHNTQIHTLNDKIFSYTESL
LT-I	1-	-----MNVK---CYVLFALLSLYVHGAPQITELCSEYRNTQIYITINDKILSYTESM
RIP-HLT	1-	-----MVKKIIIPMILSANMLLGSAPAAAENGDFEASCSATTASAWKNIKI--DKVFSDI
LT-IIa	1-	----MSSKKIIGAFVLMGTGI-LSGQVYAGVSEHFRNICNQTADIVAGVQL--KKYIADV
LT-IIb	1-	MKIKMNFKKSIALLFIALNI-ASLPTYAGVSKTFKDKCASTTAKLVQSVQL--VNISSDV
LT-IIc	1-	----MNFKKSIALLFIALNI-ASLPTYAGVSKTFKDKCASTTAKLVQSVQL--VNISSDV
		* : : : : * : : *
Ctx	53-	AGKREMAIITFKNGATFQVEVPGSQHIDSQKKAIERMKDTRLRIAYLTEAKVEKLCVWNNK
LT-I	53-	AGKREMVIIITFKSGETFQVEVPGSQHIDSQKKAIERMKDTRLRIAYLLETETKIDKLCVWNNK
RIP-HLT	54-	TQSGSGFYVA-GSGGVW--RVEQSNISYPQN-YLTDEMRRISMAALLTGT-LVNICASTKI
LT-IIa	54-	NTNTRGIYVVSNTGGVW--YIPGGRDYPDN-FLSGEIRKTAMAAILSDT-KVNLCARTSS
LT-IIb	58-	NKDSKGLYVSSSAGKTW--FIPGGQYYPDN-YLSNEMRKIAMAAVLSNV-RVNLCASEAY
LT-IIc	54-	NKDSKGLYVSSSAGKTW--FIPGGQYYPDN-YLSNEMRKIAMAAVLSNV-RVNLCASEAY
		. : * : : . . : : : * : . : *

C



D

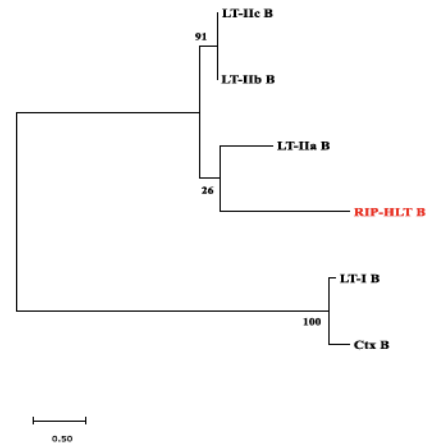
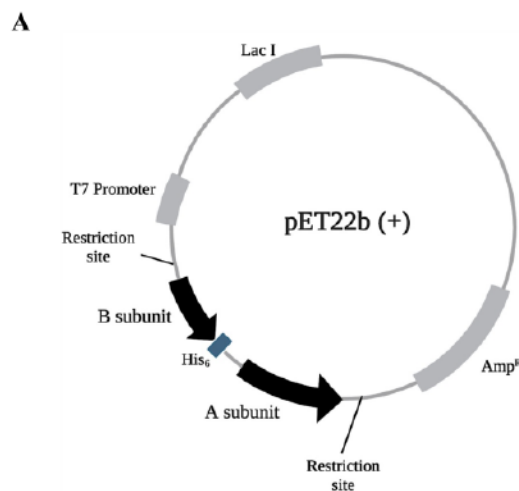


Figure 3.3.3. Sequence alignment and phylogenetic analyses of the B subunit protein sequences of RIP-TT and RIP-HLT. (A) Protein sequence alignment showing a section of the B subunit protein sequences of RIP-TT, representative ArtAB subtypes and PltC groups and PltB, highlighting conservation of critical residues (shown in red) located in the lateral (S31) and basal (S45) binding pockets in RIP-TT B and type 1 ArtAB and PltC groups, which is absent in all representative type 2 ArtB sequences. (B) Protein sequence alignment showing a section of the B subunit protein sequences of RIP-HLT, Ctx, LT-I and LT-II subtypes and highlighting conservation of Thr37 and Thr38, two amino acid residues postulated to be essential for LT-II binding to GD1 gangliosides (shown in red) and partial conservation of the “MA-LS” motif that is suggested to mediate binding of LT-II to toll-like receptors (shown in green). The majority of these binding residues are not found in the Ctx and LT-I B subunits which exhibit a higher affinity for different gangliosides (GM1). (C and D) Phylogenetic trees inferring the relationships between the same amino acid sequences in figures A and B respectively and constructed with the MEGA X software using the maximum-likelihood method and the WAG + I + G substitution model with a total of 100 bootstrap replicates. Numbers at the nodes represent branch support values.

3.3.5 Molecular cloning of a collection of plasmids for heterologous overexpression and analysis of RIP-TT, RIP-HLT and related toxins

Our first approach to understanding the biology of the RIP-TT and RIP-HLT toxins was to confirm interactions between the A and B subunits that would indicate assembly of a functional AB₅-type protein complex capable of intoxicating cells. The genes encoding the A and B subunits of both toxins were cloned separately into the pET22b (+) expression vector with a His₆ tag fused to the C-terminal of the B subunits (Figure 3.3.4A). In addition to wild type (WT) constructs for RIP-TT and RIP-HLT, we also designed recombinant plasmids with modifications in the putative amino acid residues postulated to be important for the enzymatic and binding activities of both toxins. For RIP-TT and RIP-HLT catalytic A subunit mutants, we substituted the arginine at position 192 for alanine (R192A) based on previous studies that have shown that this residue is essential for the N-glycosidase catalytic mechanism of RIPs including

Stx as well as more distantly related RIPs such as ricin (237,239,248). To construct the binding mutant of RIP-TT, we mutated the critical serine residues from both glycan binding pockets, Ser31 and Ser45, to Alanine residues (S31A/S45A), creating a RIP-TT double binding mutant that is expected to be defective in binding to both Neu5Ac and Neu5Gc glycan, based on data from studies performed using ArtB (147). Likewise, we also engineered double binding mutants of RIP-HLT with substitutions in the threonine residues at positions 36 and 37 (T36I/T37I) established to be critical in LT-II binding to gangliosides GD1a and GD1b (243). As a positive control for activity assays (described below), an analogous plasmid encoding Stx2a A and B subunits (from *E. coli* O183:H18 str. 2014C-3338 WT, accession no: CP027452) was also designed. Plasmids encoding only the His₆-tagged B subunits of RIP-TT and RIP-HLT were also constructed as controls to examining A-B interactions. Figure 3.3.4B shows the various combinations of gene sequences cloned into the pET22b (+) vector to make up the collection of plasmids used for further analysis in this study.



B

Plasmid	Description
 	Overexpression of wild type RIP-TT
 	Overexpression of RIP-TT with a point mutation in an essential A subunit catalytic residue
 	Overexpression of RIP-TT with point mutations in two essential B subunit binding residues located in the lateral and basal binding pockets
	Overexpression of RIP-TT B subunit only
 	Overexpression of wild type RIP-HLT
 	Overexpression of RIP-HLT with a point mutation in an essential A subunit catalytic residue
 	Overexpression of the RIP-HLT with point mutations in two essential B subunit binding residues
	Overexpression of RIP-HLT B subunit only
 	Overexpression of hybrid Stx2a A/RIP-TT B
 	Overexpression of hybrid Stx2a A/RIP-HLT B

Figure 3.3.4. Collection of designed plasmids used in the overexpression of RIP-TT, RIP-HLT and related toxins. (A) Schematic representation of the pET22b (+) vector used to clone and overexpress all proteins via induction of the T7 promoter with IPTG. (B) Gene diagrams illustrating the different combinations of toxins cloned and used in this study. All plasmids were designed using restriction enzyme cloning and a His₆ tag was fused to the C-terminal of all B subunits to subsequently purify and evaluate A-B interactions prior to further experiments. The plasmids encoding the RIP-HLT R192A catalytic mutant, WT Stx2a and the synthetic hybrid Stx2a A/RIP-HLT B toxins was done by Eric Schultz and Gillian Cameron.

3.3.6 Purification of RIP-TT, RIP-HLT and related toxins indicates interactions between RIP-like A subunits and homologs of ArtB and LT-II B

To examine the interactions between the A and B subunits for each construct encoding the complete holotoxin, we expressed our recombinant plasmids in *E. coli* BL21(DE3) and induced expression of the toxin genes by adding IPTG once the bacterial cells were in the logarithmic growth phase and toxins were purified using nickel gravity columns. Since our A subunits were not His₆-tagged, they should only be purified using this approach if they form a stable interaction with the co-expressed His₆-tagged B subunit. SDS-PAGE analysis indicated that for both RIP-TT and RIP-HLT, clear bands were present corresponding to the size of both the A subunits and the B subunits, suggesting that both of hybrid toxins were assembling in this recombinant system. (Figure 3.3.5A, B). Specifically, Coomassie staining of the SDS-PAGE gels for each purified holotoxin showed two distinct bands corresponding the expected molecular weights of the individual A and B monomers in the absence of signal sequences (RIP-TT A \cong 32 kDa, RIP-TT B \cong 14 kDa, RIP-HLT A \cong 34 kDa, RIP-HLT B \cong 12 kDa, Stx2a A \cong 32 kDa, Stx2a B \cong 8 kDa) (Figure 3.3.5A,B). Importantly, the ~32-34 kDa band corresponding to the A subunit was absent when we performed analogous purifications using plasmids that

lack the A subunit (B subunit only), as shown in Figure 3.3.5C, D and our results suggest that the A and B subunits of the RIP-TT and RIP-HLT toxins interact, consistent with our prediction that they represent novel AB₅-type toxins. Note that we did not conduct more rigorous biochemical experiments to explore the assembly or composition of these toxins because our lab has collaborated with Gao lab at Shandong University (China), who have solved the structure of both of these toxins to high resolution by X-ray crystallography (unpublished). These structures reveal that both of these toxins are *bona fide* AB₅-type toxins that adopt the canonical architecture wherein a single A subunit sits atop a ring-shaped B subunit homopentamer (data not shown).

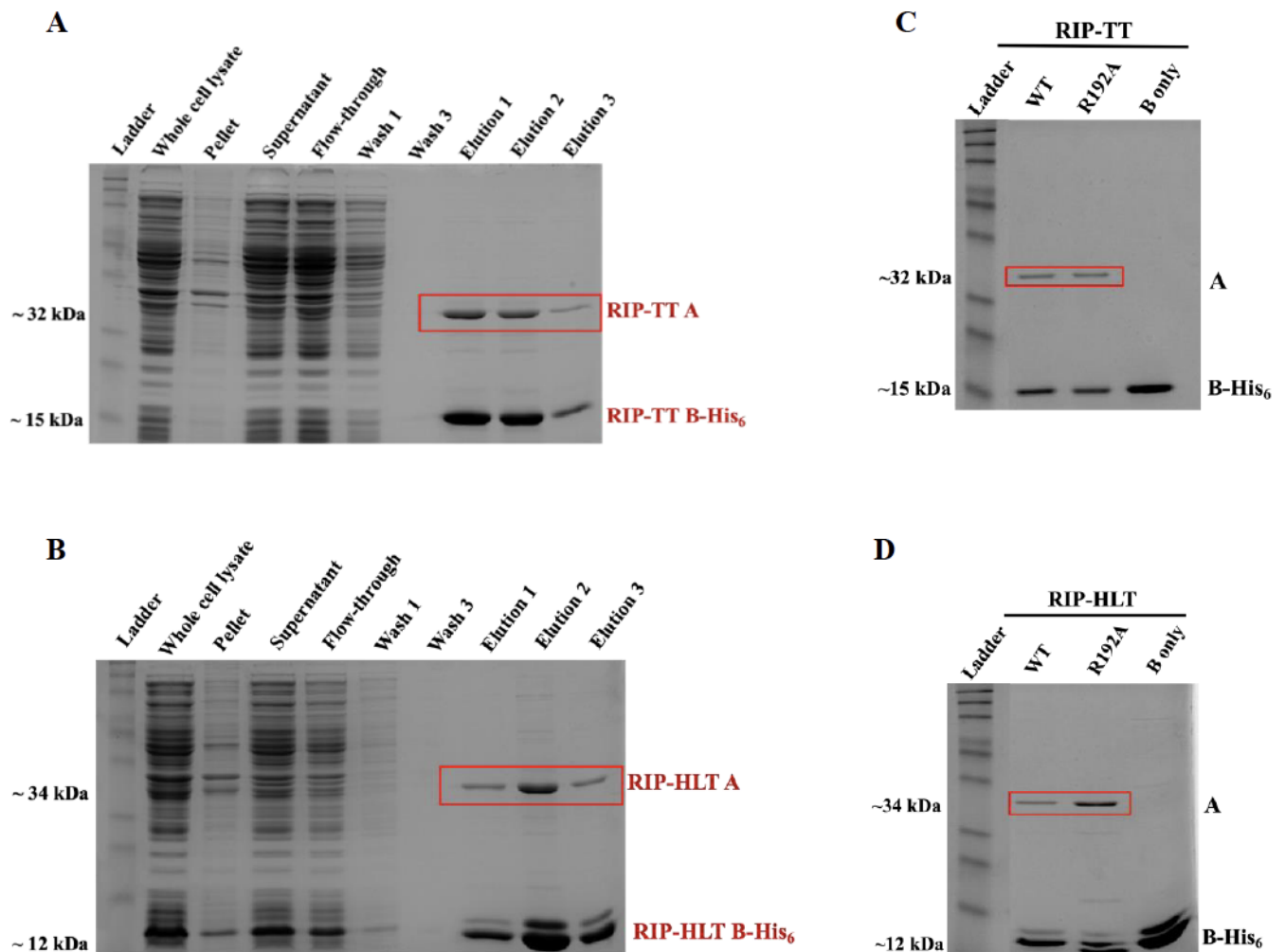


Figure 3.3.5. Analysis and verification of A-B interactions in the RIP-TT and RIP-HLT toxins. Purification and analysis of RIP-TT and RIP-HLT from *E. coli* BL21 (DE3) was done using Nickel Ni resin gravity columns as described in “Materials and Methods”. The His₆ tagged B subunits were analysed by SDS-PAGE with several fractions from the purification of (A) RIP-TT and (B) RIP-HLT. Purified elutions of (C) RIP-TT (WT, R192A, B subunit only) and (D) RIP-HLT(WT, R192A, B only). A-B interactions were confirmed by successful copurification (pull-down) of the A subunits with their respective His₆-tagged B subunits (red boxes).

3.3.7 Cytotoxicity of HeLa cells following intoxication with purified RIP-TT, RIP-HLT and related toxins

Cellular intoxication with lethal concentrations of Stx subtypes, particularly the well-studied Stx1a and Stx2a subtypes has been consistently shown to result in cell death in a variety of mammalian cultured cells (249–252). Given that RIP-TT and RIP-HLT are predicted to exhibit similar RIP activity, we reasoned that these toxins would also be cytotoxic. The cytotoxicity of RIP-TT and RIP-HLT toxins was assessed in HeLa cell lines using an MTT cell viability assay. This colorimetric assay relies on the reduction of the yellow tetrazolium MTT compound to purple formazan crystals by the mitochondrial activity of viable cells and produces a signal proportional to the number of viable cells which we can quantify by taking absorbance readings of the solubilized formazan crystals (233,253). Purified Stx2a holotoxin was used as a positive control based on previous studies that show that Stx2a is capable of inducing cell death in various cell lines including HeLa cells (249). Treatment of HeLa cell monolayers with 10-fold serial dilutions of the WT RIP-TT and RIP-HLT holotoxins induced a significant level of cell death relative to our unintoxicated controls (Figure 3.3.6A). We generated a dose-response curve using various concentrations of WT RIP-TT, WT RIP-HLT and Stx2a plotted against the observed percent cell viability values (Figure 3.3.6A). Our results revealed that, as expected,

Stx2a exhibit very high potency against these cells, eliciting reduced cell viability at very low concentrations (Figure 3.3.6A). Although neither the RIP-TT WT or RIP-HLT WT were found to be as potent as Shiga toxin, both toxins were able to induce significant levels of cytotoxicity in HeLa cells at relatively low concentrations and as such, also represent potent cytotoxins.

Our results so far indicate that both RIP-TT and RIP-HLT exhibit structural and functional similarities to canonical AB₅ toxins. Consistent with the enzymatic and binding activities of AB₅ toxins, we sought to confirm that our observations thus far are in line with the mechanistic pathway of AB₅ toxins which requires the enzymatic activity of the A subunit and the glycan binding ability of the B subunit which delivers the toxins to cells and is needed to elicit cell damage and cell death. To test this, we intoxicated HeLa cell monolayers with different concentrations of purified catalytic and binding mutants of RIP-TT and RIP-HLT alongside the WT version of both proteins and performed a similar MTT assay to assess cellular effects 72 hours after intoxication. For both toxins, we found that the R192A mutation we introduced in their A subunits significantly hindered the enzymatic activity of the RIP proteins. When compared to HeLa cells intoxicated in parallel with the same concentrations of WT RIP-TT and RIP-HLT, the majority of cells treated with the RIP-TT and RIP-HLT R192A catalytic mutants remained viable after 72 hours even at relatively high concentrations of toxin, while those intoxicated with the WT version displayed a marked decline in cell viability (Figure 3.3.6B, C). We performed a similar experiment with the binding mutants of RIP-TT and RIP-HLT (S31A/S45A and T36I/T37I respectively) which also revealed a similar pattern where HeLa cells intoxicated with either binding mutant had no notable decline in cell viability compared to what was observed in the WT versions of RIP-TT and RIP-HLT which was run in parallel (Figure 3.3.6B, C). From these results, it is evident that our catalytic and binding

mutants were unable to induce significant cell death which indicates the requirement for the specific amino acid residues mutated and importantly, strongly suggests that these toxins are working as AB₅ toxins with RIP enzymatic activities.

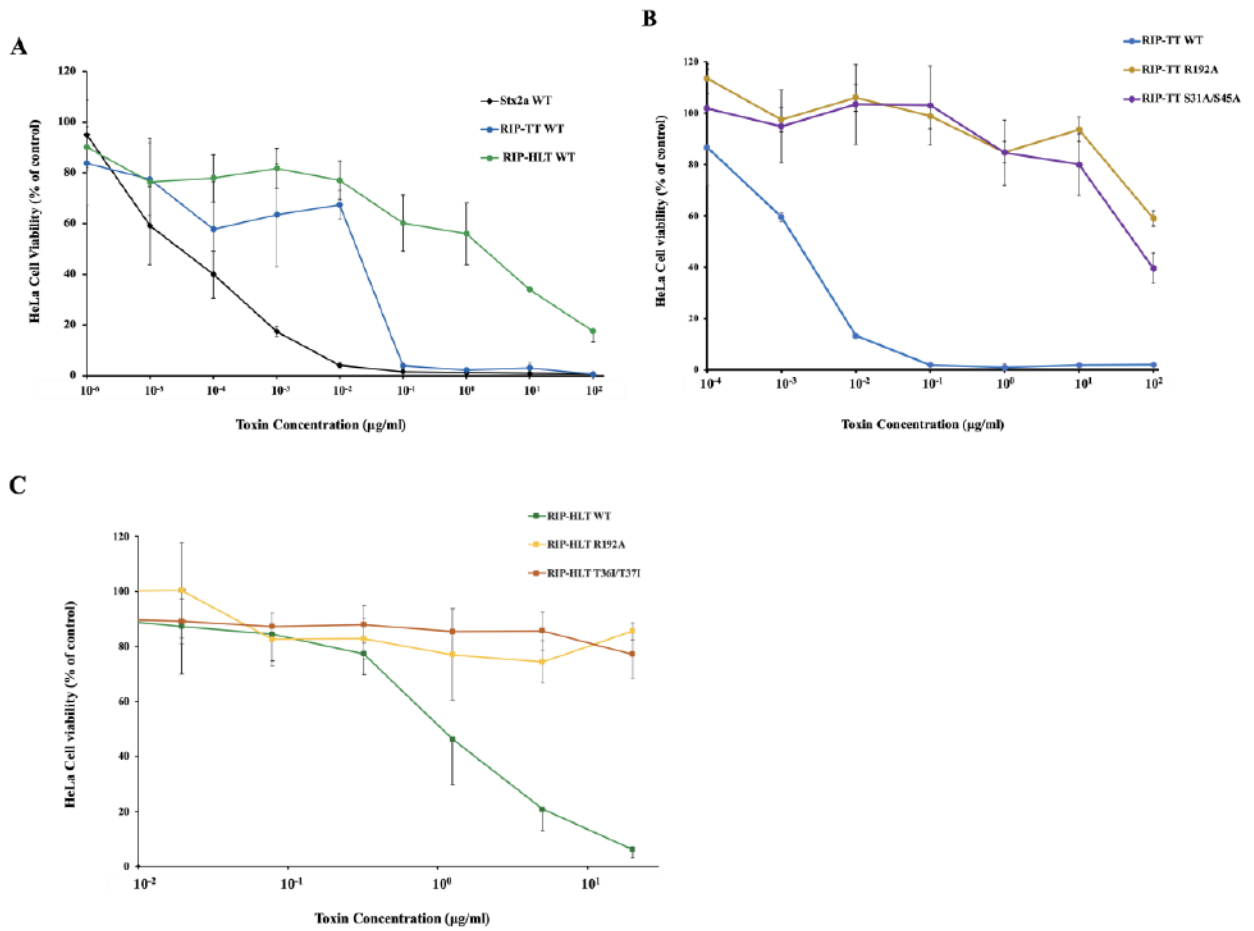


Figure 3.3. 6 The RIP-TT and RIP-HLT toxins induce a dose-dependent cytotoxicity in HeLa cells using an RIP-like mechanism. (A) 10-fold serial dilutions of purified RIP-TT WT, RIP-HLT WT and Stx2a WT (positive control) in HBSS were added to cultured HeLa cells and incubated for 1 hour at 37°C and MTT cell viability assays were performed 72 hours after intoxication to measure the level of cytotoxicity induced by these toxins as described in the Materials and Methods section. Four-fold serial dilutions of (B) purified RIP-TT catalytic mutant (R192A) and RIP-TT binding mutant (S31A/S45A) and (C) purified RIP-HLT catalytic mutant (R192A) and RIP-HLT binding mutant (T36I/T37I) were added to cultured HeLa cells for 1 hour and an MTT cell viability assays were used to determine the percent (%) cell viability at 72 hours after intoxication and compared to the WT versions of both toxins (run in parallel). which is expressed as the percentage of unintoxicated media-only controls. Error bars indicate the standard deviation from the mean for each triplicate dilution. The data shown are the mean normalized cytotoxicity \pm standard deviation (S.D). Starting concentrations for WT RIP-TT, RIP-HLT and Stx2a =100 μ g/ml. Starting concentrations for samples shown in panel (B) =100 μ g/ml and and 20 μ g/ml for (C). For each sample/toxin, two or more independent experiments were performed, and representative dose-response curves generated.

3.3.8 The Stx2a A subunit is able to form a functional toxin complex with the B subunits of both RIP-TT and RIP-HLT

Despite the low sequence similarity between the A subunits of the *Salmonella* RIP-like toxins and the Stx A subunit, our results so far reflected the extent of AB₅ toxin flexibility, and we wondered if subunit switching between these toxin groups would be possible. To investigate this, we engineered recombinant plasmids in which we replaced the A subunits of both RIP-TT and RIP-HLT with the WT Stx2a A subunit, resulting in plasmids encoding the following synthetic hybrid toxins: RIP-TT B(His₆)/Stx2a A and RIP-HLT B(His₆)/Stx2a A. To determine if the Stx2a A subunit was capable of forming a complex with these two B subunits, we expressed and purified these constructs as described above and performed an SDS-PAGE analysis of the purified elutions. Surprisingly, our results showed a distinct band corresponding

to each subunit for both synthetic hybrid toxins, suggesting that the WT Stx2a A subunit could interact with the B subunits of RIP-TT and RIP-HLT in stable AB₅ complex. To explore whether these artificial toxin complexes were active and capable of intoxicating cells, we investigated the cytotoxicity of both toxins using a similar MTT cell viability assay. Our results revealed that, similar to the WT RIP-TT and RIP-HLT toxins, these synthetic hybrid Stx2a A subunit versions were capable of inducing cytotoxicity and elicited a significant decline in cell viability at relatively low concentrations (Figure 3.3.7B). Consistent with what was observed in the WT RIP-TT and RIP-HLT toxins, the RIP-TT B version of the synthetic hybrid Stx2a toxin was more potent than that of RIP-HLT B and neither the Stx2a A/RIP-TT B nor the Stx2a A/RIP-HLT B toxins were as potent as WT Stx2a. These results suggest that the B subunit differences between all three Stx toxins likely impacted the cytotoxicity observed in cultured HeLa cells at 72 hours post intoxication, and that the HeLa cells used are most sensitive to WT Stx2a intoxication and least sensitive to Stx2a A/RIP-HLT B.

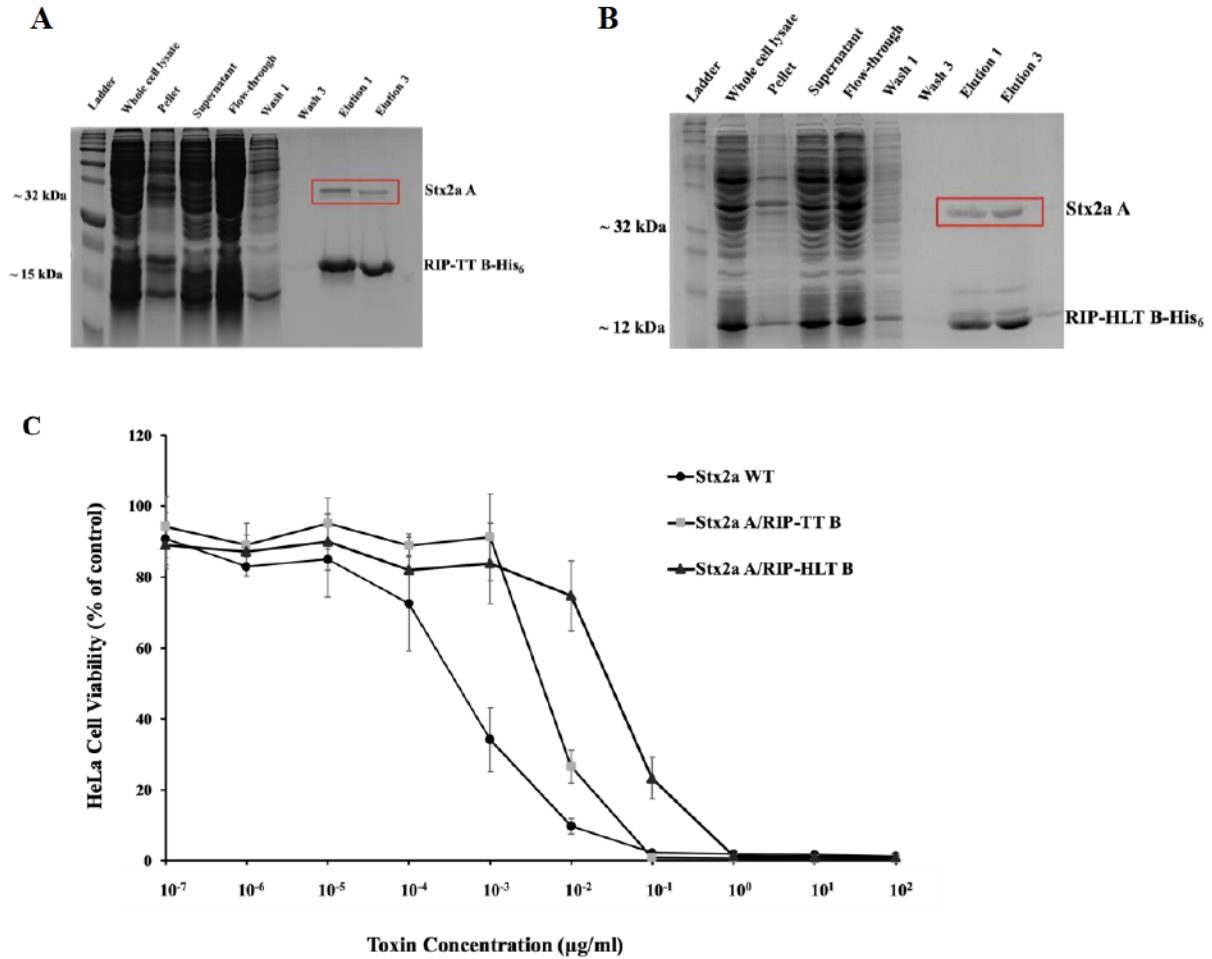


Figure 3.3.7. The Stx2a A subunit is able to form a functional toxin complex with the B subunits of both RIP-TT and RIP-HLT and induce cytotoxicity in HeLa cells. Coomassie staining of SDS-PAGE of multiple fractions from the purification of multiple fractions obtained Protein purification of His₆-tagged RIP-TT B and RIP-HLT B and cellular effects of synthetic hybrid Stx2a A/RIP-TT B and Stx2a A/RIP-HLT-B. SDS-PAGE of several fractions from the purification of (A) Stx2a A/RIP-TT B and (B) Stx2a A/RIP-HLT B showing copurification of the WT Stx2a A subunit and RIP-TT B-His₆ and WT Stx2a A subunit and RIP-HLT B-His₆ in elution fractions, suggesting A-B interactions in both toxins. (C) Dose-response curve obtained from treatment of HeLa cells with 10-fold serial dilutions (starting concentration of 100 μg/ml) of synthetic hybrid Stx2a A/RIP-TT B and Stx2a A/RIP-HLT B for 1 hour after which an MTT cell viability assay was used to quantify the level of cytotoxicity induced both toxins. Error bars indicate the S.D from the mean for each triplicate dilution. Experiment was performed in two or more replicates.

3.4 Discussion

In this study, we identify two novel putative AB₅ toxins in *Salmonella*, RIP-TT and RIP-HLT, which contain Stx-like A subunits, proteins that are well-known for their role in human disease. Sequence analysis revealed that the RIP-TT and RIP-HLT toxins share roughly 70% amino acid sequence similarity in their A subunits but are only ~ 33% identical to the A subunits of Stx1 and Stx2. Despite this relatively low sequence similarity, these toxins were found to induce substantial cytotoxicity in HeLa cells. In addition, the RIP-TT and RIP-HLT A subunits are able to assemble a functional AB₅ complex with distinct B subunits different toxin families. This astounding structural association of an Stx-like A subunit with B subunits with homology to the LT-II B and ArtB in a novel AB₅ complex has not been previously reported or characterized and highlights the structural and functional implications of AB₅ toxin flexibility. Importantly, consistent with common mechanisms of AB₅ toxin evolution, we observed a likely role for horizontal gene transfer in the spread of the prophage-encoded *rip-tt* locus and transposable elements in the emergence of the RIP-HLT toxin in *Salmonella*.

The phylogenetic predictions obtained from analyses of the A subunit protein sequences of RIP-TT, RIP-HLT, Stx1a, Stx2a and the 320 N-terminal RIP sequence from *A. salmonicida* indicates that these subunits might have evolved from a common ancestor. In comparison to the broad distribution of the RIP-TT toxin in *S. enterica* strains, we identified only two *Salmonella* genomes that encode the RIP-HLT toxin, suggesting the presence of factors that likely hinder the distribution of this toxin within the *Salmonella* genus. In contrast to ArtB, *lt-II B*-like subunit genes are not commonly found in *Salmonella* which likely impacts the diversity and distribution of the RIP-HLT toxin. It is also possible likely the RIP-TT toxin evolved from a RIP-HLT-like

precursor following the acquisition of a *rip* gene in *Salmonella* strains already harbouring an *artAB*-like locus.

The significant protein sequence homology between the B subunits of RIP-TT, type 1 ArtAB and PltC groups particularly in respect to the conservation of the putative essential amino acid residues important for glycan binding at the basal and lateral binding pockets indicates that the RIP-TT toxin likely binds both Neu5Ac and Neu5Gc-terminated glycans. In addition, mutations introduced in the serine residues located at both the basal and lateral binding sites of RIP-TT significantly reduced cytotoxicity in HeLa cells suggesting that similar to type 1 ArtAB toxins, these residues play crucial roles in RIP-TT binding and internalization. This finding combined with the exclusive presence of the *rip-tt* locus in nontyphoidal *Salmonella* correlates particularly well with the nature of glycans typically found at the intoxication sites of the *Salmonella* strains that encode this toxin. Phylogenetic analysis coupled with the high sequence conservation of the *rip* gene in all 103 *Salmonella* strains that encode the *rip-tt* locus indicate that these may have recently acquired the RIP toxin. The relatively lower sequence identity (70%) between the A subunit protein sequences of RIP-TT and RIP-HLT suggests that these subunits have most likely adapted in some way to interact with different B subunits, which is also supported by the variations found in their A2 C-terminal sequences. Extending our molecular cloning and protein purification methods to examine possible subunit switching between RIP-TT and RIP-HLT might provide some insight on the extent of functional diversification that exists between the RIP sequence of RIP-TT and RIP-HLT.

Our comparison of the RIP-HLT B subunit sequence to representative members of the Ctx family revealed that the RIP-HLT B subunit is significantly diverged from Ctx and LT-I toxins and more closely related to the LT-II toxins. The binding of Ctx and LT-I to target cells is

partially dependent on a glycine residue at position 54 of the Ctx B and LT-I B subunit sequence, which mediates interactions with GM1 gangliosides and results in a high affinity binding (245). This Gly54 is absent in all LT-II B subunits as well as the RIP-HLT B subunit which have variable amino acids at that position. Instead, functional binding of LT-II is primarily mediated by two threonine residues, Thr36 and Thr37 in the B polypeptide (243,244), both of which are conserved in the RIP-HLT B sequence. Single amino acid substitutions in both residues were also shown to substantially inhibit RIP-HLT mediated cytotoxicity of HeLa cells. Variations in binding preferences between Ctx/LT-I and LT-II are suggested to account for the individual toxin potencies and level of cytotoxicity induced by following intoxication. Despite this, the B subunits of Ctx, LT-I and LT-II toxins are predicted to specifically bind the same terminal sugar sequence- GalB1-3Gal NAcB1-4(Neu5Aca2-3) Gal on GM1 and GD1b gangliosides (120). In addition, LT-II B also binds the Neu5Ac glycans that decorate the GD1b and GD2 receptors on epithelial cells, presumably in a manner that does not disturb its binding to the GalB1-3Gal terminal sequence. As a result of the structural similarities between LT-II B and RIP-HLT B, it is expected that the RIP-HLT toxin would target gangliosides in a somewhat similar manner to the LT-II toxins, and these binding similarities might also influence the level of cytotoxicity induced by this toxin. However, a more in-depth analysis of the specific receptors utilized by RIP-HLT to induce toxin uptake is necessary to provide a better understanding of the underlying mechanistic details that dictate toxin potency and cytotoxicity.

The use of nickel columns for purification of the WT, catalytic and binding mutants of RIP-TT and RIP-HLT as well as the WT and hybrid Stx2a toxins (Stx2a A/RIP-TT B, Stx2a A/RIP-HLT B) was found to be a useful and effective first-line assessment for investigating the biology and cellular activity of these novel toxins. Expression and purification of both RIP-TT and RIP-

HLT resulted in the production of relatively high concentrations of both toxins and confirmed that the A and B subunits were capable of forming functional AB₅-type complexes. The low molecular weight of individual B monomers identified in our SDS-PAGE Coomassie stained gels for both toxins also correlated particularly well with the predicted AB₅ architecture of RIP-TT and RIP-HLT, which was also confirmed by structural data (unpublished) provided by our collaborators. The requirement for fairly high concentrations of RIP-TT and RIP-HLT was important to investigate the effects of both toxins in mammalian cells. As these toxins have not been previously characterized, it is possible that cytotoxicity is only observed at certain concentrations and thus, intoxication with sub-optimal toxin concentrations would present a challenge in our cytotoxicity assays. The remarkable flexibility of AB₅ toxins was also emphasized in the successful copurification of two hybrid toxins, one with the WT *E. coli* Stx2a A subunit together with RIP-TT B-His₆ and the other with the WT *E. coli* Stx2a A subunit and RIP-HLT B-His₆.

Cellular intoxication of HeLa cells with WT RIP-TT and RIP-HLT induced a dose-dependent cytotoxicity indicating that HeLa cells are sensitive to the effects of both toxins and the synthetic hybrid Stx2a toxins which had either the RIP-TT B subunit or the RIP-HLT B subunit exhibited a similar pattern of cytotoxicity to the WT RIP-TT and RIP-HLT toxins. Importantly, our results indicate that despite the relatively low sequence similarities between the A subunits of WT Stx2a and RIP-TT/RIP-HLT, there is a remarkable flexibility of the C-terminal sequences that allows stable interactions with very different B subunits and this structural feature can likely be exploited and used in medicine.

The level of cytotoxicity induced by AB₅ toxins is highly dependent on the enzymatic activity of the A subunit as well as the ability of the respective B pentamers to bind functional

receptors present on host cell plasma membrane and as observed, disruption in one activity (enzymatic or binding) significantly interferes with the cellular activity of the toxins (62,154). Sensitivity of eukaryotic cells to AB₅ toxins also varies by cell type. A multitude of cell types including Vero, Human Renal Tubular Epithelial cells (HRTEC), Caco-2, and HeLa cells have been shown to be sensitive to most AB₅ toxins. Stx-treated cells often exhibit differential susceptibilities and cytotoxic effects. Vero cells lines, which are obtained from kidney epithelial cells are highly sensitive to both Stx1a and Stx2a both *in vitro* and *in vivo* which correlates with the susceptibility of renal epithelial cells and tissues to Stx-induced damage and the frequent development of HUS in STEC infected patients (251,254). In contrast, Chinese Hamster Ovary (CHO) cells which are highly sensitive to the *S. Typhimurium* DT104 ArtAB toxin are less permissive to Stx intoxication with lower levels of cytotoxicity typically observed following Stx treatment in these cell lines, effects which are likely as a result of differences in expression levels of Neu5Ac/Gc glycans and Gb3 to which ArtB and Stx B respectively bind (255,256). Characterizing the nature and abundance of the RIP-TT and RIP-HLT B subunit receptors through glycan array studies and investigating the cytotoxicity elicited by both toxins in multiple cell types is an important area for future research into the biology of these toxins.

The inclusion of the synthetic Stx2a A/RIP-TT B and Stx2a A/RIP-HLT B toxins in this study provided insight regarding the individual contributions of the A and B subunits in cytotoxicity. The similar level of cytotoxicity induced by the WT RIP-TT and the hybrid Stx2a A/RIP-TT B toxin suggests that despite the variations in their A subunits, both toxins target HeLa cells in similar ways and the B subunit likely plays a bigger role in the resulting cellular effects of both toxins which includes receptor binding as well as the mechanism of toxin uptake and intracellular trafficking of the A subunit to its target site. Conversely, the considerable

difference in the level of cytotoxicity induced by the WT RIP-HLT and the hybrid Stx2a A/RIP-HLT B toxin indicates that there are other factors other than the B subunit sequences that contribute to the cellular effects of these toxins, which might range from conserved structural features to flaws in our experimental methods. It is noteworthy to mention that a number of challenges were encountered during the purification and cytotoxic assessment of RIP-HLT and indeed, our results might not be entirely due to the biology or potency of RIP-HLT. However, while glycan binding to cell surface receptors is crucial in AB₅ toxin-mediated cytotoxicity, cellular internalization of the holotoxin does not always lead to productive intoxication or cell death. Studies have shown that although Vero cells express fair amounts of GM1 to which the Ctx B subunit binds, the internalization of the Ctx holotoxin rarely results in cytotoxicity and this might be due to potency of the A subunit in different cell types (257). Similarly, it is possible that the same pattern of toxin internalization holds true for the RIP-TT and RIP-HLT toxins at certain concentrations and more especially for the WT RIP-HLT toxin which was found to be significantly less cytotoxic than RIP-TT despite the observation that HeLa cells treated with the hybrid Stx2a toxin with the RIP-HLT B subunit in place of Stx2 B had a more noticeable decline in cell viability at much lower concentrations. To get a more accurate representation of the cellular effects of RIP-HLT, it may be useful to consider specialized cell lines like the murine Y-1 adrenal cells that have consistently been reported to be sensitive to Ctx , LT-I and LT-II intoxication (258,259).

Other than the enzymatic activities of the A1 subunits, variations in A2 C-terminal sequences within AB₅ toxins from the same family as well as more distantly related AB-type toxins has been repeatedly shown to impact the function and cellular effects of these toxins. In Stx2a, the A2 C-terminal helix extends through the inner pore of the Stx B pentamer to the other

side and occludes one of the binding sites of the Stx2 B pentamer. This structural feature has been proposed to contribute to the higher affinity of Stx1 for Gb3 which has a shorter C-terminal structure that does not obstruct any of the identified Stx binding sites (93). This C-terminal helix extension is also present in Stx2d, one of the more potent Stx2 subtypes often associated with severe disease. Cleavage of the terminal two amino acids in the Stx2d A2 C-terminal helix by intestinal elastase is suggested to influence the level of cytotoxicity and tissue damage associated with the STEC strains that produce this subtype (93,260). In *Pseudomonas aeruginosa*, the arrangement of amino acids in the C-terminal of a secreted AB-type toxin known as exolysin A has been shown to substantially impact cytotoxicity and the Ctx A2 peptide has also been reported to play a crucial role in the cellular effects of this toxin (261). In both RIP-TT and RIP-HLT, the A2 C-terminal helices are relatively truncated and the variations in the amino acids that form this structure and mediate interactions with their respective B subunits indicate that modifications of the C-terminal residues are likely necessary for adaptation to dissimilar B subunits and may influence the activity of these toxins. Thus, the hybrid toxins formed from an association between the extended A2 C-terminal helix of the WT Stx2a and the B pentamer of RIP-TT and RIP-HLT is remarkable especially since the Stx2a A subunit has not been previously shown to form a functional AB₅ complex with either ArtB or LT toxins. A previous study revealed that despite the high structural homology between the Ctx and LT-I holotoxins, variations in the C-terminal region of the A2 peptides played an important role in maintaining the stability of the individual AB₅ complexes and resulted in cytotoxic differences between Ctx and LT-I in T84 cell lines (262,263). Hence, another likely reason for the disparity in HeLa cell cytotoxicity induced by WT Stx2a and all other RIP toxins investigated in this study might also stem from the diversity in their C-terminal sequences and

evaluation of the potential implications of this diversity would be an interesting area of study given its relevance in the overall assembly and functionality of AB-type toxins.

Recently, there has been some compelling evidence that indicates that cellular exposure to sub-optimal toxin concentrations might impact the degree of cytotoxicity observed with some AB₅ toxins (264). A few studies have highlighted that the cytotoxicity observed following Stx intoxication is dependent on the amount of toxin present in the host cytosol which might vary by toxin and cell type (93,233). Previous studies aimed at assessing the cellular effects of Stx in mammalian cells typically utilize various time points and, in many cases, longer cell exposure to toxin results in a much steeper decline in cell viability. This may also vary when investigating the cellular activity of these toxins in the bacterial strains that encode them. While the overall aim of this study was to present a relatively broad understanding of AB₅ toxin flexibility through studies on the evolution and biology of novel *Salmonella* AB₅ toxins, it is evident that several other studies aimed at directly assessing the RIP activity of RIP-TT and RIP-HLT including mechanistic details of ribosomal interaction and protein inhibition are needed. Further investigation into the assembly and secretion of RIP-TT and RIP-HLT in the *Salmonella* strains that encode these toxins is currently underway and we aim to gain a better understanding of the mechanism of regulation, expression and secretion of these toxins which would be useful in further characterization of these remarkable toxins.

Several studies have described the formation of hybrid AB₅ toxin complexes with components from distinct toxin families, some of which are proposed to have relevant implications in the context of human infections. It is probable that the A subunits of AB₅ toxins convergently evolved as analogous domains with C-terminal A2 moieties that are able to

interact with different B subunits that has now conferred substantial versatility to the structure and functions of these toxins (241,265).

In summary, the evolutionary and molecular mechanisms underlying the disparity between Stxs and other AB₅ toxins despite these toxins adopting the conventional AB₅ architecture has mostly remained elusive. Our collective findings from this study provide some useful insights that may help explain the unique biology of these toxins. We identify and characterize two novel putative AB₅ toxins with RIP-mediated cytotoxicity in *Salmonella* that likely evolved from horizontal gene transfer and transposition events. Utilization of bioinformatic tools provided an avenue to retrace the possible evolutionary pathway that may have resulted in the unique biology and activity of Stxs. It is likely that STEC strains acquired the *rip* gene from an ancestor common to both RIP-HLT and RIP-TT a very long time ago, and overtime, substantial modification of this gene and its protein product occurred that ultimately allowed it to associate with a B subunit in a highly potent AB₅ complex that has caused immeasurable damage to several healthcare industries worldwide. The nature and diversity of Stx phages may have further contributed to the functional variations that are now observed in the Stx family. (76,266).

While no direct evidence thus far indicates that the RIP-TT and RIP-HLT toxins are associated with severe forms of disease in the *Salmonella* serovars in which they were identified, the level of cytotoxicity induced by these toxins suggests that they have the tendency to impact the virulence properties of not only *Salmonella* serovars but other Gram-negative organisms that may eventually acquire the genetic elements that encode these toxins. Considering the frequency at which novel AB₅ toxins are identified and the continuous emergence of highly virulent pathogens that harbour such toxins, it is crucial that studies aimed

at characterizing the assortment of AB-type toxins encoded by different bacterial species continue as it may have useful functional and therapeutic implications. Elucidating the importance of the structural and functional diversity of bacterial AB₅ toxins both in terms of benefits to the organisms harboring these genetic elements and the potential impact of these toxins on human health could hold important implications in human health and disease.

Chapter 4: General discussion and relevance of both studies

All identified and characterized AB₅ toxins share a common architecture and intoxicate cells using a similar mechanism of action initiated by the binding of the B oligomer to specific cell receptors, allowing toxin entry, intracellular trafficking and alteration of host cell biology by the enzymatic A subunit (66,125,182,204,267). Despite this, several studies including those presented here show that there is a lot of functional diversity both within and amongst distinct AB₅ toxin families. The prominent roles that AB₅ toxins play in human health and their potential application in cell biology and medicine necessitate the need to gain a thorough understanding of how these diverse and potent molecules evolved as well as the importance of this diversity as these could hold important meanings both within and beyond the scope of infectious disease control.

Bacteriophages or phages are among the most abundant organisms on earth. Evidence suggests that bacterial chromosomes and their associated prophages are coevolving. A major consequence of this is the emergence of novel virulence traits driven by genetic recombination events which promote the acquisition of other genetic elements that may alter the composition and architecture of bacterial genomes in a manner that benefits these organisms (268,269). Many Gram-negative bacterial species are known to harbour a variety of prophage-related genetic elements that appear to enhance bacterial survival and competition in hosts (218). The impact of phages on bacterial pathogenicity is further supported by their immense diversity and ecological distribution (266). A wealth of literature highlight the prominent role that phages play in the evolution of AB₅ toxins. The distribution of phage-encoded AB₅ genetic elements in diverse bacterial strains and species may also be influenced by phage host specificity which

may in turn account for some of the observed differences in host reservoir in the bacterial strains that encode similar AB₅ toxins (151). However, deciphering the extent to which these phage-related AB₅ genetic elements shape the pathogenic properties of the bacterial species that encode them has been hindered by their sporadic distribution in a diverse range of bacterial strains and serovars which also limits our understanding of their potential role in disease. Phage-encoded AB₅ genetic elements are widespread in *Salmonella* and based on the findings presented in both chapters of this thesis, are abundantly distributed in several NTS strains and serovars, some of which are increasingly being linked to severe human infections in many parts of the world.

The Stx family of toxins represent one of the most well studied AB₅ toxin families and despite this, there is a lack of proper understanding of the evolutionary link between members of the Stx family of toxins and other characterised AB₅ toxins. Deciphering such possible evolutionary relationship is also complicated by the relatively rapid evolution of *stx* genes, which is highly driven by the nature of Stx-phages (181). So far, members of the Stx family toxins have been identified in over 500 serogroups of *E. coli* as well as other bacterial species (266). Production of these toxins in some serogroups, constitutes central virulence factors making them attractive targets in the development of control strategies to curb STEC infections. Hence, clarifying the underlying genetic and molecular factors that drive the emergence and distribution of these potent toxins could provide insights into alternative prevention and treatment options for STEC infections. There are numerous other examples of how the spread of phage-encoded AB₅ genetic elements has contributed to the emergence of highly virulent bacterial strains and novel hybrid toxins like the RIP-TT toxin, which have the capacity to kill cells and possibly elicit harmful biological effects in hosts. The spread of phage-encoded AB₅

genetic elements may also equip otherwise non-pathogenic or environmental bacterial strains with the capacity to become highly pathogenic (270). The ways in which phages significantly shape the evolution of AB₅ toxins while quite remarkable, could have serious biological implications and needs to be further explored.

With advancements in structural tools and the availability of comprehensive genomic databases, it is becoming more apparent that the AB₅ scaffold is highly amenable to structural manipulation such that some parts of the toxin complex may be interchanged in a LEGO-like system, allowing subunit switching and functional diversification (269). In this thesis, we uncover a substantial amount of sequence diversity and flexibility in the B subunits of *Salmonella* AB₅ toxins like ArtAB and newly discovered toxins like RIP-TT and RIP-HLT. Phylogenetic and comparative genomic studies indicate that despite predicted evolutionary relationships between the B subunits of AB₅ toxins from the same family, the series of genetic changes such as gene deletions, duplications and exchanges that have occurred over time has yielded an array of toxins with varying binding properties, intracellular trafficking mechanisms and host specificity, factors which may impact toxin potency and activity (271).

The C-terminal A2 α -helical structure which links the enzymatic A1 subunit to its B pentamer is one of the main structural features that stabilizes the AB₅ complex and as such is an integral part of the AB₅ scaffold. Modifications in the length or composition of the A2 C-terminal structure has been shown to impact complex formation which may in turn disrupt toxin entry and cytotoxicity (181,198). Among members of the different AB₅ toxin families, significant differences in the length and orientation of the A2 C-terminal structures relative to their B pentamers can be observed (198) and such differences may limit the extent of flexibility attributed to the AB₅ scaffold. It is thought that the amino acid residues that line the pentameric

pore vary in different B subunits, however, comparable molecular interactions between the A2 C-terminal structure and B pentamers have been observed between AB₅ toxins in the same family, allowing subunit switching (198). From an evolutionary standpoint, this suggests that the A2 C-terminal structures of individual AB₅ toxins have evolved to adapt to the biology and structural architecture of a range of B subunits while retaining a relatively conserved enzymatic activity. This is likely driven by modifications in the amino acid residues that make up the C-terminal α -helix and/or line the central pore of the pentameric B subunit, allowing similar A subunits to form stable interactions with different B subunits while preserving the integrity of the AB₅ complex (156). This evolutionary highlight may account for the limited number of established enzymatic A subunit classes, and by association, the limited number of AB₅ toxin families characterized thus far.

The flexibility of the AB₅ scaffold which allows a range of A and B subunit combinations, can be exploited in the assembly of protein carriers to safely deliver therapeutic compounds to specific sites in the human body. This structural feature makes AB₅ toxins attractive candidates for manipulation in the development of therapeutics for the treatment of a number of non-infectious diseases such as those associated with neoplasia (272). Importantly, studies such as those presented here that aim to characterize the diverse arsenal of AB₅ toxins are vital to their potential therapeutic applications as it provides a large suite of toxins that may be used as protein carriers to target a variety of cell and tissue types. For example, accumulation of well-characterized diverse B subunit proteins means that we can in theory, assemble different combinations of protein complexes via fusion of non-toxic B subunits to therapeutic molecules and select desired candidates based on factors such as the strength and stability of interactions and the receptor-binding specificity of the B subunits. Effective targeting and delivery of

therapeutic molecules to specific diseased cells and tissues in the human body is a major requirement for the successful development and administration of novel therapeutic agents (273) and the remarkable binding specificities and trafficking properties of AB₅ toxins make them useful vehicles for direct targeting and delivery of therapeutic compounds to biochemically relevant sites in the human body (63,272). Members of the Ctx family of toxins including type I and II heat-labile toxins have gained popularity for their favourable application as protein carriers in therapeutic drug delivery and as mucosal adjuvants in vaccine development due to their binding properties. The strong binding avidity displayed by the B subunits of the Ctx family toxins and their cognate ganglioside receptors greatly supports efficient binding and subsequent drug delivery (269). Additionally, the abundance and distribution of ganglioside receptors like GM1 in a variety of cell types including intestinal epithelial and immune system cells, allows targeting to many relevant cell types and their immunostimulatory effects to be realized at various biological sites (265). The B subunits from members of the Ctx family of toxins have also been implicated in the development of prevention strategies against the Japanese encephalitis virus (JEV), a viral pathogen known to cause inflammation of the brain (encephalitis) predominantly in Southeast Asia and the Western Pacific (265,274). This involves manipulation of the pentameric scaffold of the Ctx family B subunits to allow association with a JEV-protective antigen which is then delivered to specific cells via oral and intraperitoneal routes (265).

Other than their use in therapeutics, AB₅ toxins also serve as important tools in several cell biology studies (63). Toxins like Ptx have proven to be valuable tools for investigating certain cell signalling pathways like the G protein-coupled receptor pathway (181). Hence, uncovering and characterizing toxins with similar biology to Ptx whether in terms of the ADP-ribosylating

activity of the toxin or the binding and trafficking properties, would likely have promising implications in other similar cell biology studies.

AB₅ toxins are also being investigated as potential targets in the prevention and treatment of AB₅ toxin-mediated diseases. One promising strategy that is currently underway involves the use of structural inhibitors to obstruct B subunit binding to cell surface receptors, thus preventing toxin uptake and subsequent cytotoxicity (275). The availability of structural data on AB₅ toxin complexes bound to various small molecules and ligands has so far supported the ongoing design of inhibitory molecules against a range of existing AB₅ toxins (275). Alternatively, disrupting intracellular trafficking of the AB₅ holotoxin from the early endosome through the trans-Golgi network to the ER and host cytosol by targeting the toxins to the late endosomes and ensuring lysosomal degradation also constitutes a promising control strategy (276). A third strategy involves inhibiting the interaction between the A1 subunit and its target molecule or protein, for example blocking the association of the Stx A1 subunit with ribosomal P-stalk proteins (277). As more studies investigate the biology and activity of diverse AB₅ toxins, we can piece together a framework for understanding the biological relevance of the flexibility of AB₅ toxins and may ultimately be able to translate such knowledge into effective defence mechanisms to combat these toxins and the diseases associated with the bacterial strains that produce and utilize them.

Lastly, based on the results obtained from our analyses of the RIP-TT and RIP-HLT toxins, we can hypothesize to an extent some of the possible biological effects that may ensue assuming these toxins contribute in some way to the survival, fitness or disease properties of the *Salmonella* strains that encode them. For both RIP-TT and RIP-HLT, the almost exclusive distribution of the toxins in NTS serovars suggests that these toxins may function to support the

biology and disease properties associated with NTS serovars. For example, the predicted binding of the toxins to cell surface glycans- Neu5Ac/Gc for RIP-TT and GD1 for RIP-HLT suggests that both toxins may be able to target both human and animal cell types that express the glycan receptors. With the continuous rise in invasive NTS disease, these toxins may also equip certain NTS serovars with the potential to cause more severe disease types in humans. *S. Stanleyville*, the representative serovar used in our analysis of the *rip-tt* genomic locus is mainly considered an environmental organism, however, this serovar has recently been linked to a series of minor outbreaks of systemic infections in humans and has now been isolated from a variety of clinical samples including urine, blood and stool (278). In combination with the RIP-mediated cytotoxicity displayed by the RIP-TT toxin in our cell viability assays, it is evident that this toxin has the capacity to play a role in bacterial pathogenesis and disease. Like ArtAB and LT-II, both the RIP-TT and RIP-HLT toxins may also play a role in enhancing bacterial survival within hosts, perhaps by inducing a strong proinflammatory response during infection to promote the influx of macrophages and other inflammatory mediators which may result in intestinal damage, competitive killing of other gut microbes, and bacterial dissemination to the bloodstream. Further investigations into the nature of cell surface receptors, intracellular trafficking mechanisms and the RIP-mediated biological effects of both RIP-TT and RIP-HLT may eventually prove useful not only in the control of salmonellosis but as useful immunostimulatory, therapeutic and cell biology tools.

In summary, increasing evidence suggests that AB₅ toxins likely enhance the virulence properties of several bacterial strains associated with severe human infections. Based on our collective results, the importance and extent of AB₅ toxin diversity is likely underappreciated and more in-depth analyses into the evolution, distribution and diversity of these remarkable

toxins could potentially guide the development of strategies aimed at preventing and treating the assortment of AB₅ toxin-mediated diseases we see today and hold important therapeutic implications beyond the scope of bacterial pathogenesis and disease.

References

1. Kirk MD, Pires SM, Black RE, Caipo M, Crump JA, Devleeschauwer B, et al. World Health Organization Estimates of the Global and Regional Disease Burden of 22 Foodborne Bacterial, Protozoal, and Viral Diseases, 2010: A Data Synthesis. Von Seidlein L, editor. PLOS Med. 2015 Dec 3;12(12):e1001921.
2. PAD Grimont FW, FX Weill. Antigenic Formulae of the *Salmonella* Serovars.
3. Brenner FW, Villar RG, Angulo FJ, Tauxe R, Swaminathan B. *Salmonella* Nomenclature. J Clin Microbiol. 2000 Jul;38(7):2465–7.
4. Le Minor L, Véron M, Popoff M. [The taxonomy of *Salmonella*]. Ann Microbiol (Paris). 1982;133(2):223–43.
5. Crosa JH, Brenner DJ, Ewing WH, Falkow S. Molecular Relationships Among the Salmonelleae. J Bacteriol. 1973 Jul;115(1):307–15.
6. Alikhan NF, Zhou Z, Sergeant MJ, Achtman M. A genomic overview of the population structure of *Salmonella*. Casadesús J, editor. PLOS Genet. 2018 Apr 5;14(4):e1007261.
7. Acheson D, Hohmann EL. Nontyphoidal Salmonellosis. Clin Infect Dis. 2001 Jan 15;32(2):263–9.
8. Gong B, Li H, Feng Y, Zeng S, Zhuo Z, Luo J, et al. Prevalence, Serotype Distribution and Antimicrobial Resistance of Non-Typhoidal *Salmonella* in Hospitalized Patients in Conghua District of Guangzhou, China. Front Cell Infect Microbiol. 2022;12:805384.

9. Monack DM, Mueller A, Falkow S. Persistent bacterial infections: the interface of the pathogen and the host immune system. *Nat Rev Microbiol.* 2004 Sep;2(9):747–65.
10. Jones TF, Ingram LA, Fullerton KE, Marcus R, Anderson BJ, McCarthy PV, et al. A Case-Control Study of the Epidemiology of Sporadic *Salmonella* Infection in Infants. *Pediatrics.* 2006 Dec 1;118(6):2380–7.
11. Majowicz SE, Musto J, Scallan E, Angulo FJ, Kirk M, O'Brien SJ, et al. The Global Burden of Nontyphoidal *Salmonella* Gastroenteritis. *Clin Infect Dis.* 2010 Mar 15;50(6):882–9.
12. Kariuki S, Revathi G, Kariuki N, Kiiru J, Mwituria J, Hart CA. Characterisation of community acquired non-typhoidal *Salmonella* from bacteraemia and diarrhoeal infections in children admitted to hospital in Nairobi, Kenya. *BMC Microbiol.* 2006;6(1):101.
13. Fàbrega A, Vila J. *Salmonella enterica* Serovar Typhimurium Skills To Succeed in the Host: Virulence and Regulation. *Clin Microbiol Rev.* 2013 Apr;26(2):308–41.
14. Kozak GK, MacDonald D, Landry L, Farber JM. Foodborne Outbreaks in Canada Linked to Produce: 2001 through 2009. *J Food Prot.* 2013 Jan;76(1):173–83.
15. Centers for Disease Control and Prevention. Foodborne outbreak online database (FOOD). Prevention, CfDCa (Ed.). 2013.
16. Andino A, Hanning I. *Salmonella enterica*: Survival, Colonization, and Virulence Differences among Serovars. *Sci World J.* 2015;2015:1–16.

17. Braden CR. *Salmonella enterica* Serotype Enteritidis and Eggs: A National Epidemic in the United States. *Clin Infect Dis*. 2006 Aug 15;43(4):512–7.
18. Gal-Mor O, Boyle EC, Grassl GA. Same species, different diseases: how and why typhoidal and non-typhoidal *Salmonella enterica* serovars differ. *Front Microbiol*. 2014;5:391.
19. Won G, Lee JH. *Salmonella* Typhimurium, the major causative agent of foodborne illness inactivated by a phage lysis system provides effective protection against lethal challenge by induction of robust cell-mediated immune responses and activation of dendritic cells. *Vet Res*. 2017 Dec;48(1):66.
20. Ao TT, Feasey NA, Gordon MA, Keddy KH, Angulo FJ, Crump JA. Global burden of invasive nontyphoidal *Salmonella* disease, 2010(1). *Emerg Infect Dis*. 2015 Jun;21(6):941–9.
21. Berkley JA, Lowe BS, Mwangi I, Williams T, Bauni E, Mwarumba S, et al. Bacteremia among Children Admitted to a Rural Hospital in Kenya. *N Engl J Med*. 2005 Jan 6;352(1):39–47.
22. Mandomando I, Bassat Q, Sigauque B, Massora S, Quintó L, Ácacio S, et al. Invasive *Salmonella* Infections Among Children From Rural Mozambique, 2001–2014. *Clin Infect Dis*. 2015 Nov 1;61(suppl 4):S339–45.
23. Feasey NA, Dougan G, Kingsley RA, Heyderman RS, Gordon MA. Invasive non-typhoidal *Salmonella* disease: an emerging and neglected tropical disease in Africa. *Lancet Lond Engl*. 2012 Jun 30;379(9835):2489–99.

24. Millen SH, Lewallen DM, Herr AB, Iyer SS, Weiss AA. Identification and characterization of the carbohydrate ligands recognized by pertussis toxin via a glycan microarray and surface plasmon resonance. *Biochemistry*. 2010 Jul 20;49(28):5954–67.
25. Dhanoa A, Fatt QK. Non-typhoidal *Salmonella* bacteraemia: Epidemiology, clinical characteristics and its' association with severe immunosuppression. *Ann Clin Microbiol Antimicrob*. 2009;8(1):15.
26. Kariuki S, Gordon MA, Feasey N, Parry CM. Antimicrobial resistance and management of invasive *Salmonella* disease. *Vaccine*. 2015 Jun 19;33 Suppl 3(0 3):C21-29.
27. Jacob JJ, Anandan S, Venkatesan M, Neeravi A, Vasudevan K, Pragasam AK, et al. Genomic analysis of human invasive *Salmonella enterica* serovar Typhimurium ST313 isolate B3589 from India. *Infect Genet Evol*. 2019 Sep;73:416–24.
28. Martinez-Sanguiné AY, D'Alessandro B, Langleib M, Traglia GM, Mónaco A, Durán R, et al. *Salmonella enterica* Serovars Dublin and Enteritidis Comparative Proteomics Reveals Differential Expression of Proteins Involved in Stress Resistance, Virulence, and Anaerobic Metabolism. *Infect Immun*. 2021 Feb 16;89(3):e00606-20.
29. Sudhaharan S, Kanne P, Vemu L, Bhaskara A. Extraintestinal infections caused by nontyphoidal *Salmonella* from a tertiary care center in India. *J Lab Physicians*. 2018;10(4):401–5.
30. Li CW, Chen PL, Lee NY, Lee HC, Chang CM, Lee CC, et al. Non-typhoidal *Salmonella* bacteremia among adults: An adverse prognosis in patients with malignancy. *J Microbiol Immunol Infect*. 2012 Oct;45(5):343–9.

31. Buckle GC, Walker CLF, Black RE. Typhoid fever and paratyphoid fever: Systematic review to estimate global morbidity and mortality for 2010. *J Glob Health*. 2012 Jun;2(1):010401.
32. Hancuh M, Walldorf J, Minta AA, Tevi-Benissan C, Christian KA, Nedelec Y, et al. Typhoid Fever Surveillance, Incidence Estimates, and Progress Toward Typhoid Conjugate Vaccine Introduction - Worldwide, 2018-2022. *MMWR Morb Mortal Wkly Rep*. 2023 Feb 17;72(7):171–6.
33. Parry CM, Hien TT, Dougan G, White NJ, Farrar JJ. Typhoid Fever. *N Engl J Med*. 2002 Nov 28;347(22):1770–82.
34. Wain J, Hendriksen RS, Mikoleit ML, Keddy KH, Ochiai RL. Typhoid fever. *The Lancet*. 2015 Mar;385(9973):1136–45.
35. Crump JA, Luby SP, Mintz ED. The global burden of typhoid fever. *Bull World Health Organ*. 2004 May;82(5):346–53.
36. Crump JA, Mintz ED. Global trends in typhoid and paratyphoid Fever. *Clin Infect Dis Off Publ Infect Dis Soc Am*. 2010 Jan 15;50(2):241–6.
37. Levantesi C, Bonadonna L, Briancesco R, Grohmann E, Toze S, Tandoi V. *Salmonella* in surface and drinking water: Occurrence and water-mediated transmission. *Food Res Int*. 2012 Mar;45(2):587–602.
38. Karkey A, Jombart T, Walker AW, Thompson CN, Torres A, Dongol S, et al. The Ecological Dynamics of Fecal Contamination and *Salmonella* Typhi and *Salmonella*

- Paratyphi A in Municipal Kathmandu Drinking Water. Crump JA, editor. PLoS Negl Trop Dis. 2016 Jan 6;10(1):e0004346.
39. Gonzalez-Escobedo G, Marshall JM, Gunn JS. Chronic and acute infection of the gall bladder by *Salmonella* Typhi: understanding the carrier state. Nat Rev Microbiol. 2011 Jan;9(1):9–14.
 40. Bhunia AK. *Salmonella enterica*. In: Foodborne Microbial Pathogens [Internet]. New York, NY: Springer New York; 2018 [cited 2023 Jun 12]. p. 271–87. (Food Science Text Series). Available from: http://link.springer.com/10.1007/978-1-4939-7349-1_15
 41. Mogasale V, Maskery B, Ochiai RL, Lee JS, Mogasale VV, Ramani E, et al. Burden of typhoid fever in low-income and middle-income countries: a systematic, literature-based update with risk-factor adjustment. Lancet Glob Health. 2014 Oct;2(10):e570–80.
 42. J. Barton A, Hill J, J. Blohmke C, J. Pollard A. Host restriction, pathogenesis and chronic carriage of typhoidal *Salmonella*. FEMS Microbiol Rev. 2021 Mar 5;fuab014.
 43. Cheng RA, Eade CR, Wiedmann M. Embracing Diversity: Differences in Virulence Mechanisms, Disease Severity, and Host Adaptations Contribute to the Success of Nontyphoidal *Salmonella* as a Foodborne Pathogen. Front Microbiol. 2019 Jun 26;10:1368.
 44. Marcus SL, Brumell JH, Pfeifer CG, Finlay BB. *Salmonella* pathogenicity islands: big virulence in small packages. Microbes Infect. 2000 Feb;2(2):145–56.

45. Wotzka SY, Nguyen BD, Hardt WD. *Salmonella* Typhimurium Diarrhea Reveals Basic Principles of Enteropathogen Infection and Disease-Promoted DNA Exchange. *Cell Host Microbe*. 2017 Apr;21(4):443–54.
46. Santos RL, Raffatellu M, Bevins CL, Adams LG, Tükel C, Tsolis RM, et al. Life in the inflamed intestine, *Salmonella* style. *Trends Microbiol*. 2009 Nov;17(11):498–506.
47. Kurtz JR, Goggins JA, McLachlan JB. *Salmonella* infection: Interplay between the bacteria and host immune system. *Immunol Lett*. 2017 Oct;190:42–50.
48. De Jong HK, Parry CM, Van Der Poll T, Wiersinga WJ. Host–Pathogen Interaction in Invasive Salmonellosis. Chitnis CE, editor. *PLoS Pathog*. 2012 Oct 4;8(10):e1002933.
49. Nickerson KP, Senger S, Zhang Y, Lima R, Patel S, Ingano L, et al. *Salmonella* Typhi Colonization Provokes Extensive Transcriptional Changes Aimed at Evading Host Mucosal Immune Defense During Early Infection of Human Intestinal Tissue. *EBioMedicine*. 2018 May;31:92–109.
50. Hu X, Chen Z, Xiong K, Wang J, Rao X, Cong Y. Vi capsular polysaccharide: Synthesis, virulence, and application. *Crit Rev Microbiol*. 2017 Jul 4;43(4):440–52.
51. McClelland M, Sanderson KE, Clifton SW, Latreille P, Porwollik S, Sabo A, et al. Comparison of genome degradation in Paratyphi A and Typhi, human-restricted serovars of *Salmonella enterica* that cause typhoid. *Nat Genet*. 2004 Dec 1;36(12):1268–74.

52. Kubicek-Sutherland JZ, Xie G, Shakya M, Dighe PK, Jacobs LL, Daligault H, et al. Comparative genomic and phenotypic characterization of invasive non-typhoidal *Salmonella* isolates from Siaya, Kenya. *PLoS Negl Trop Dis*. 2021 Feb;15(2):e0008991.
53. Langridge GC, Fookes M, Connor TR, Feltwell T, Feasey N, Parsons BN, et al. Patterns of genome evolution that have accompanied host adaptation in *Salmonella*. *Proc Natl Acad Sci*. 2015 Jan 20;112(3):863–8.
54. Bäumlér AJ, Tsolis RM, Ficht TA, Adams LG. Evolution of Host Adaptation in *Salmonella enterica*. Orndorff PE, editor. *Infect Immun*. 1998 Oct;66(10):4579–87.
55. Jones GW, Rabert DK, Svinarich DM, Whitfield HJ. Association of adhesive, invasive, and virulent phenotypes of *Salmonella* Typhimurium with autonomous 60-megadalton plasmids. *Infect Immun*. 1982 Nov;38(2):476–86.
56. Borden Lacy D, Stevens RC. Unraveling the structures and modes of action of bacterial toxins. *Curr Opin Struct Biol*. 1998 Dec;8(6):778–84.
57. Song J. Bacterial AB toxins and host–microbe interactions. In: *Advances in Microbial Physiology* [Internet]. Elsevier; 2022 [cited 2023 Jun 12]. p. 67–109. Available from: <https://linkinghub.elsevier.com/retrieve/pii/S0065291122000170>
58. Odumosu O, Nicholas D, Yano H, Langridge W. AB toxins: a paradigm switch from deadly to desirable. *Toxins*. 2010 Jul;2(7):1612–45.
59. Lemichez E, Barbieri JT. General aspects and recent advances on bacterial protein toxins. *Cold Spring Harb Perspect Med*. 2013 Feb 1;3(2):a013573.

60. Johnson WM, Lior H. Response of Chinese hamster ovary cells to a cytolethal distending toxin (CDT) of *Escherichia coli* and possible misinterpretation as heat-labile (LT) enterotoxin. *FEMS Microbiol Lett.* 1987 Jul;43(1):19–23.
61. DiRienzo JM. Cytolethal Distending Toxin: A Unique Variation on the AB Toxin Paradigm. *New J Sci.* 2014 Sep 25;2014:1–26.
62. Biernbaum EN, Kudva IT. AB5 Enterotoxin-Mediated Pathogenesis: Perspectives Gleaned from Shiga Toxins. *Toxins.* 2022 Jan 16;14(1):62.
63. Beddoe T, Paton AW, Le Nours J, Rossjohn J, Paton JC. Structure, biological functions and applications of the AB5 toxins. *Trends Biochem Sci.* 2010 Jul;35(7):411–8.
64. Lencer WI, Saslowsky D. Raft trafficking of AB5 subunit bacterial toxins. *Biochim Biophys Acta.* 2005 Dec 30;1746(3):314–21.
65. Sixma TK, Kalk KH, van Zanten BA, Dauter Z, Kingma J, Witholt B, et al. Refined structure of *Escherichia coli* heat-labile enterotoxin, a close relative of cholera toxin. *J Mol Biol.* 1993 Apr 5;230(3):890–918.
66. Fraser ME, Chernaia MM, Kozlov YV, James MN. Crystal structure of the holotoxin from *Shigella dysenteriae* at 2.5 Å resolution. *Nat Struct Biol.* 1994 Jan;1(1):59–64.
67. Merritt EA, Hol WG. AB5 toxins. *Curr Opin Struct Biol.* 1995 Apr;5(2):165–71.
68. Lencer W. The intracellular voyage of cholera toxin: going retro. *Trends Biochem Sci.* 2003 Dec;28(12):639–45.

69. Nowakowska-Gołacka J, Sominka H, Sowa-Rogozińska N, Słomińska-Wojewódzka M. Toxins Utilize the Endoplasmic Reticulum-Associated Protein Degradation Pathway in Their Intoxication Process. *Int J Mol Sci*. 2019 Mar 15;20(6):1307.
70. Liu X, Chen Z, Jiao X, Jiang X, Qiu J, You F, et al. Molecular Insights into the Assembly and Functional Diversification of Typhoid Toxin. Brennan RG, editor. *mBio*. 2022 Feb 22;13(1):e01916-21.
71. Patry RT, Stahl M, Perez-Munoz ME, Nothaft H, Wenzel CQ, Sacher JC, et al. Bacterial AB5 toxins inhibit the growth of gut bacteria by targeting ganglioside-like glycoconjugates. *Nat Commun*. 2019 Mar 27;10(1):1390.
72. Gyles CL. Shiga toxin-producing *Escherichia coli*: an overview. *J Anim Sci*. 2007 Mar;85(13 Suppl):E45-62.
73. Karmali MA, Steele BT, Petric M, Lim C. Sporadic cases of haemolytic-uraemic syndrome associated with faecal cytotoxin and cytotoxin-producing *Escherichia coli* in stools. *Lancet Lond Engl*. 1983 Mar 19;1(8325):619–20.
74. Pickering LK, Obrig TG, Stapleton FB. Hemolytic-uremic syndrome and enterohemorrhagic *Escherichia coli*. *Pediatr Infect Dis J*. 1994 Jun;13(6):459–75; quiz 476.
75. Tarr PI. *Escherichia coli* O157:H7: clinical, diagnostic, and epidemiological aspects of human infection. *Clin Infect Dis Off Publ Infect Dis Soc Am*. 1995 Jan;20(1):1–8; quiz 9–10.

76. Trachtman H, Austin C, Lewinski M, Stahl RAK. Renal and neurological involvement in typical Shiga toxin-associated HUS. *Nat Rev Nephrol.* 2012 Nov;8(11):658–69.
77. Fraser ME, Fujinaga M, Cherney MM, Melton-Celsa AR, Twiddy EM, O'Brien AD, et al. Structure of shiga toxin type 2 (Stx2) from *Escherichia coli* O157:H7. *J Biol Chem.* 2004 Jun 25;279(26):27511–7.
78. Tumer NE, Li XP. Interaction of ricin and Shiga toxins with ribosomes. *Curr Top Microbiol Immunol.* 2012;357:1–18.
79. Cherla RP, Lee SY, Mees PL, Tesh VL. Shiga toxin 1-induced cytokine production is mediated by MAP kinase pathways and translation initiation factor eIF4E in the macrophage-like THP-1 cell line. *J Leukoc Biol.* 2006 Feb;79(2):397–407.
80. Thorpe CM, Hurley BP, Lincicome LL, Jacewicz MS, Keusch GT, Acheson DWK. Shiga Toxins Stimulate Secretion of Interleukin-8 from Intestinal Epithelial Cells. McGhee JR, editor. *Infect Immun.* 1999 Nov;67(11):5985–93.
81. Waddell T, Head S, Petric M, Cohen A, Lingwood C. Globotriosyl ceramide is specifically recognized by the *Escherichia coli* verocytotoxin 2. *Biochem Biophys Res Commun.* 1988 Apr 29;152(2):674–9.
82. Lingwood CA, Law H, Richardson S, Petric M, Brunton JL, De Grandis S, et al. Glycolipid binding of purified and recombinant *Escherichia coli* produced verotoxin in vitro. *J Biol Chem.* 1987 Jun 25;262(18):8834–9.

83. Ling H, Boodhoo A, Hazes B, Cummings MD, Armstrong GD, Brunton JL, et al. Structure of the Shiga-like toxin I B-pentamer complexed with an analogue of its receptor Gb3. *Biochemistry*. 1998 Feb 17;37(7):1777–88.
84. Spooner RA, Lord JM. How ricin and Shiga toxin reach the cytosol of target cells: retrotranslocation from the endoplasmic reticulum. *Curr Top Microbiol Immunol*. 2012;357:19–40.
85. Sandvig K, Garred O, Prydz K, Kozlov JV, Hansen SH, van Deurs B. Retrograde transport of endocytosed Shiga toxin to the endoplasmic reticulum. *Nature*. 1992 Aug 6;358(6386):510–2.
86. Paton JC, Paton AW. Pathogenesis and diagnosis of Shiga toxin-producing *Escherichia coli* infections. *Clin Microbiol Rev*. 1998 Jul;11(3):450–79.
87. Cimolai N, Carter JE. Bacterial genotype and neurological complications of *Escherichia coli* O157:H7-associated haemolytic uraemic syndrome. *Acta Paediatr Oslo Nor* 1992. 1998 May;87(5):593–4.
88. Magnus T, Röther J, Simova O, Meier-Cillien M, Repenthin J, Möller F, et al. The neurological syndrome in adults during the 2011 northern German *E. coli* serotype O104:H4 outbreak. *Brain*. 2012 Jun;135(6):1850–9.
89. Scheutz F, Teel LD, Beutin L, Piérard D, Buvens G, Karch H, et al. Multicenter evaluation of a sequence-based protocol for subtyping Shiga toxins and standardizing Stx nomenclature. *J Clin Microbiol*. 2012 Sep;50(9):2951–63.

90. Melton-Celsa AR. Shiga Toxin (Stx) Classification, Structure, and Function. *Microbiol Spectr*. 2014 Aug;2(4):EHEC-0024-2013.
91. Caprioli A, Luzzi I, Gianviti A, Russmann H, Karch H. Pheno-genotyping of verotoxin 2 (VT2)-producing *Escherichia coli* causing haemorrhagic colitis and haemolytic uraemic syndrome by direct analysis of patients' stools. *J Med Microbiol*. 1995 Nov;43(5):348–53.
92. Piérard D, Muyldermans G, Moriau L, Stevens D, Lauwers S. Identification of new verocytotoxin type 2 variant B-subunit genes in human and animal *Escherichia coli* isolates. *J Clin Microbiol*. 1998 Nov;36(11):3317–22.
93. Fuller CA, Pellino CA, Flagler MJ, Strasser JE, Weiss AA. Shiga Toxin Subtypes Display Dramatic Differences in Potency. Blanke SR, editor. *Infect Immun*. 2011 Mar;79(3):1329–37.
94. Persson S, Olsen KEP, Ethelberg S, Scheutz F. Subtyping method for *Escherichia coli* shiga toxin (verocytotoxin) 2 variants and correlations to clinical manifestations. *J Clin Microbiol*. 2007 Jun;45(6):2020–4.
95. Head SC, Karmali MA, Lingwood CA. Preparation of VT1 and VT2 hybrid toxins from their purified dissociated subunits. Evidence for B subunit modulation of a subunit function. *J Biol Chem*. 1991 Feb 25;266(6):3617–21.
96. Russo LM, Melton-Celsa AR, Smith MJ, O'Brien AD. Comparisons of native Shiga toxins (Stxs) type 1 and 2 with chimeric toxins indicate that the source of the binding subunit dictates degree of toxicity. *PloS One*. 2014;9(3):e93463.

97. Unkmeir A, Schmidt H. Structural Analysis of Phage-Borne *stx* Genes and Their Flanking Sequences in Shiga Toxin-Producing *Escherichia coli* and *Shigella dysenteriae* Type 1 Strains. O'Brien AD, editor. *Infect Immun*. 2000 Sep;68(9):4856–64.
98. Mauro SA, Koudelka GB. Shiga toxin: expression, distribution, and its role in the environment. *Toxins*. 2011 Jun;3(6):608–25.
99. Haque QM, Sugiyama A, Iwade Y, Midorikawa Y, Yamauchi T. Diarrheal and environmental isolates of *Aeromonas spp.* produce a toxin similar to Shiga-like toxin 1. *Curr Microbiol*. 1996 May;32(5):239–45.
100. Hsueh BY, Waters CM. Combating Cholera. *F1000Research*. 2019;8:F1000 Faculty Rev-589.
101. Ali M, Nelson AR, Lopez AL, Sack DA. Updated global burden of cholera in endemic countries. *PLoS Negl Trop Dis*. 2015;9(6):e0003832.
102. Hsiao A, Hall AH, Mogasale V, Quentin W. The health economics of cholera: A systematic review. *Vaccine*. 2018 Jul;36(30):4404–24.
103. Zhang RG, Scott DL, Westbrook ML, Nance S, Spangler BD, Shipley GG, et al. The three-dimensional crystal structure of cholera toxin. *J Mol Biol*. 1995 Aug 25;251(4):563–73.
104. Cassel D, Pfeuffer T. Mechanism of cholera toxin action: covalent modification of the guanyl nucleotide-binding protein of the adenylate cyclase system. *Proc Natl Acad Sci U S A*. 1978 Jun;75(6):2669–73.

105. Svoboda M, Furnelle J, Christophe J. The differential detergent solubilization of adenylate cyclase and polypeptides ADP-ribosylated with cholera toxin suggests an excess of G/F protein relative to adenylate cyclase in rat pancreatic plasma membranes. *FEBS Lett.* 1981 Nov 30;135(1):207–11.
106. Sanchez J, Holmgren J. Cholera toxin - a foe & a friend. *Indian J Med Res.* 2011 Feb;133(2):153–63.
107. Nelson EJ, Harris JB, Morris JG, Calderwood SB, Camilli A. Cholera transmission: the host, pathogen and bacteriophage dynamic. *Nat Rev Microbiol.* 2009 Oct;7(10):693–702.
108. Heggelund JE, Burschowsky D, Bjørnestad VA, Hodnik V, Anderluh G, Krenzelok U. High-Resolution Crystal Structures Elucidate the Molecular Basis of Cholera Blood Group Dependence. *PLoS Pathog.* 2016 Apr;12(4):e1005567.
109. Van Heyningen WE. Gangliosides as membrane receptors for tetanus toxin, cholera toxin and serotonin. *Nature.* 1974 May;249(5456):415–7.
110. Holmgren J, Lönnroth I, Svennerholm L. Tissue receptor for cholera exotoxin: postulated structure from studies with GM1 ganglioside and related glycolipids. *Infect Immun.* 1973 Aug;8(2):208–14.
111. Merritt EA, Sarfaty S, Akker FVD, L'Hoir C, Martial JA, Hol WGJ. Crystal structure of cholera toxin B-pentamer bound to receptor G_{M1} pentasaccharide: Cholera toxin pentamer:G_{M1} pentasaccharide. *Protein Sci.* 1994 Feb;3(2):166–75.

112. Wands AM, Fujita A, McCombs JE, Cervin J, Dedic B, Rodriguez AC, et al. Fucosylation and protein glycosylation create functional receptors for cholera toxin. *eLife*. 2015 Oct 29;4:e09545.
113. Dubreuil JD, Isaacson RE, Schifferli DM. Animal Enterotoxigenic *Escherichia coli*. *EcoSal Plus*. 2016 Oct;7(1).
114. Jobling MG, Holmes RK. Type II Heat-Labile Enterotoxins from 50 Diverse *Escherichia coli* Isolates Belong Almost Exclusively to the LT-IIc Family and May Be Prophage Encoded. Otto M, editor. *PLoS ONE*. 2012 Jan 5;7(1):e29898.
115. Lasaro MA, Rodrigues JF, Mathias-Santos C, Guth BEC, Balan A, Sbrogio-Almeida ME, et al. Genetic diversity of heat-labile toxin expressed by enterotoxigenic *Escherichia coli* strains isolated from humans. *J Bacteriol*. 2008 Apr;190(7):2400–10.
116. Sixma TK, Pronk SE, Kalk KH, Wartna ES, Van Zanten BAM, Witholt B, et al. Crystal structure of a cholera toxin-related heat-labile enterotoxin from *E. coli*. *Nature*. 1991 May;351(6325):371–7.
117. Qadri F, Svennerholm AM, Faruque ASG, Sack RB. Enterotoxigenic *Escherichia coli* in developing countries: epidemiology, microbiology, clinical features, treatment, and prevention. *Clin Microbiol Rev*. 2005 Jul;18(3):465–83.
118. Moss J, Richardson SH. Activation of adenylate cyclase by heat-labile *Escherichia coli* enterotoxin. Evidence for ADP-ribosyltransferase activity similar to that of cholera toxin. *J Clin Invest*. 1978 Aug;62(2):281–5.

119. Spangler BD. Structure and function of cholera toxin and the related *Escherichia coli* heat-labile enterotoxin. *Microbiol Rev.* 1992 Dec;56(4):622–47.
120. Fukuta S, Magnani JL, Twiddy EM, Holmes RK, Ginsburg V. Comparison of the carbohydrate-binding specificities of cholera toxin and *Escherichia coli* heat-labile enterotoxins LT_h-I, LT-II_a, and LT-II_b. *Infect Immun.* 1988 Jul;56(7):1748–53.
121. Teneberg S, Hirst TR, Angström J, Karlsson KA. Comparison of the glycolipid-binding specificities of cholera toxin and porcine *Escherichia coli* heat-labile enterotoxin: identification of a receptor-active non-ganglioside glycolipid for the heat-labile toxin in infant rabbit small intestine. *Glycoconj J.* 1994 Dec;11(6):533–40.
122. Mudrak B, Kuehn MJ. Heat-labile enterotoxin: beyond G(m1) binding. *Toxins.* 2010 Jun;2(6):1445–70.
123. Nardi ARM, Salvadori MR, Coswig LT, Gatti MSV, Leite DS, Valadares GF, et al. Type 2 heat-labile enterotoxin (LT-II)-producing *Escherichia coli* isolated from ostriches with diarrhea. *Vet Microbiol.* 2005 Feb;105(3–4):245–9.
124. Guth BE, Pickett CL, Twiddy EM, Holmes RK, Gomes TA, Lima AA, et al. Production of type II heat-labile enterotoxin by *Escherichia coli* isolated from food and human feces. *Infect Immun.* 1986 Nov;54(2):587–9.
125. Den Akker FV, Sarfaty S, Twiddy EM, Connell TD, Holmes RK, Hol WG. Crystal structure of a new heat-labile enterotoxin, LT-II_b. *Structure.* 1996 Jun;4(6):665–78.

126. Pickett CL, Weinstein DL, Holmes RK. Genetics of type IIa heat-labile enterotoxin of *Escherichia coli*: operon fusions, nucleotide sequence, and hybridization studies. *J Bacteriol.* 1987 Nov;169(11):5180–7.
127. Pickett CL, Twiddy EM, Coker C, Holmes RK. Cloning, nucleotide sequence, and hybridization studies of the type IIb heat-labile enterotoxin gene of *Escherichia coli*. *J Bacteriol.* 1989 Sep;171(9):4945–52.
128. Berenson CS, Nawar HF, Kruzel RL, Mandell LM, Connell TD. Ganglioside-binding specificities of *E. coli* enterotoxin LT-IIc: Importance of long-chain fatty acyl ceramide. *Glycobiology.* 2013 Jan;23(1):23–31.
129. Yeung KHT, Duclos P, Nelson EAS, Hutubessy RCW. An update of the global burden of pertussis in children younger than 5 years: a modelling study. *Lancet Infect Dis.* 2017 Sep;17(9):974–80.
130. Carbonetti NH. Contribution of pertussis toxin to the pathogenesis of pertussis disease. *Pathog Dis.* 2015 Nov;73(8):ftv073.
131. Zhang L, Prietsch SO, Axelsson I, Halperin SA. Acellular vaccines for preventing whooping cough in children. In: The Cochrane Collaboration, editor. *Cochrane Database of Systematic Reviews* [Internet]. Chichester, UK: John Wiley & Sons, Ltd; 2011 [cited 2023 Jul 23]. p. CD001478.pub4. Available from: <https://doi.wiley.com/10.1002/14651858.CD001478.pub4>
132. Loch C, Coutte L, Mielcarek N. The ins and outs of pertussis toxin: Pertussis toxin. *FEBS J.* 2011 Dec;278(23):4668–82.

133. Katada T, Ui M. ADP ribosylation of the specific membrane protein of C6 cells by islet-activating protein associated with modification of adenylate cyclase activity. *J Biol Chem.* 1982 Jun 25;257(12):7210–6.
134. Jakway JP, DeFranco AL. Pertussis toxin inhibition of B cell and macrophage responses to bacterial lipopolysaccharide. *Science.* 1986 Nov 7;234(4777):743–6.
135. Spangrude GJ, Sacchi F, Hill HR, Van Epps DE, Daynes RA. Inhibition of lymphocyte and neutrophil chemotaxis by pertussis toxin. *J Immunol Baltim Md 1950.* 1985 Dec;135(6):4135–43.
136. Klimova N, Holubova J, Streparola G, Tomala J, Brazdilova L, Stanek O, et al. Pertussis toxin suppresses dendritic cell-mediated delivery of *B. pertussis* into lung-draining lymph nodes. *PLoS Pathog.* 2022 Jun;18(6):e1010577.
137. Fowler CC, Chang SJ, Gao X, Geiger T, Stack G, Galán JE. Emerging insights into the biology of typhoid toxin. *Curr Opin Microbiol.* 2017 Feb;35:70–7.
138. Galán JE. Typhoid toxin provides a window into typhoid fever and the biology of *Salmonella* Typhi. *Proc Natl Acad Sci.* 2016 Jun 7;113(23):6338–44.
139. Cheng, Wiedmann. The ADP-Ribosylating Toxins of *Salmonella*. *Toxins.* 2019 Jul 16;11(7):416.
140. Tamamura Y, Tanaka K, Uchida I. Characterization of pertussis-like toxin from *Salmonella* spp. that catalyzes ADP-ribosylation of G proteins. *Sci Rep.* 2017 Jun 1;7(1):2653.

141. Uchida I, Ishihara R, Tanaka K, Hata E, Makino S ichi, Kanno T, et al. Salmonella enterica serotype Typhimurium DT104 ArtA-dependent modification of pertussis toxin-sensitive G proteins in the presence of [³²P]NAD. *Microbiology*. 2009 Nov 1;155(11):3710–8.
142. Saitoh M, Tanaka K, Nishimori K, Makino S ichi, Kanno T, Ishihara R, et al. The artAB genes encode a putative ADP-ribosyltransferase toxin homologue associated with Salmonella enterica serovar Typhimurium DT104. *Microbiology*. 2005 Sep 1;151(9):3089–96.
143. Leekitcharoenphon P, Hendriksen RS, Le Hello S, Weill FX, Baggesen DL, Jun SR, et al. Global Genomic Epidemiology of Salmonella enterica Serovar Typhimurium DT104. Kivisaar M, editor. *Appl Environ Microbiol*. 2016 Apr 15;82(8):2516–26.
144. Poppe C, Smart N, Khakhria R, Johnson W, Spika J, Prescott J. Salmonella typhimurium DT104: a virulent and drug-resistant pathogen. *Can Vet J Rev Veterinaire Can*. 1998 Sep;39(9):559–65.
145. Lan R, Reeves PR, Octavia S. Population structure, origins and evolution of major Salmonella enterica clones. *Infect Genet Evol*. 2009 Sep;9(5):996–1005.
146. Helms M, Ethelberg S, Mølbak K, DT104 Study Group. International Salmonella Typhimurium DT104 infections, 1992-2001. *Emerg Infect Dis*. 2005 Jun;11(6):859–67.
147. Gao X, Deng L, Stack G, Yu H, Chen X, Naito-Matsui Y, et al. Evolution of host adaptation in the Salmonella typhoid toxin. *Nat Microbiol*. 2017 Dec;2(12):1592–9.

148. Cohen M, Varki A. The Sialome—Far More Than the Sum of Its Parts. *OMICS J Integr Biol*. 2010 Aug;14(4):455–64.
149. Byres E, Paton AW, Paton JC, Löfling JC, Smith DF, Wilce MCJ, et al. Incorporation of a non-human glycan mediates human susceptibility to a bacterial toxin. *Nature*. 2008 Dec 4;456(7222):648–52.
150. Deng L, Song J, Gao X, Wang J, Yu H, Chen X, et al. Host adaptation of a bacterial toxin from the human pathogen *Salmonella Typhi*. *Cell*. 2014 Dec 4;159(6):1290–9.
151. Khan N, Sasmal A, Khedri Z, Secrest P, Verhagen A, Srivastava S, et al. Sialoglycan-binding patterns of bacterial AB5 toxin B subunits correlate with host range and toxicity, indicating evolution independent of A subunits. *J Biol Chem*. 2022 May;298(5):101900.
152. Ghosh S. Sialic acid and biology of life: An introduction. In: *Sialic Acids and Sialoglycoconjugates in the Biology of Life, Health and Disease* [Internet]. Elsevier; 2020 [cited 2023 Jun 12]. p. 1–61. Available from: <https://linkinghub.elsevier.com/retrieve/pii/B9780128161265000019>
153. Carroll LM, Piacenza N, Cheng RA, Wiedmann M, Guldemann C. A multidrug-resistant *Salmonella enterica* Typhimurium DT104 complex lineage circulating among humans and cattle in the United States lost the ability to produce pertussis-like toxin ArtAB [Internet]. *Microbiology*; 2022 Apr [cited 2023 Jun 12]. Available from: <http://biorxiv.org/lookup/doi/10.1101/2022.04.06.487395>
154. Wang H, Paton JC, Herdman BP, Rogers TJ, Beddoe T, Paton AW. The B Subunit of an AB5 Toxin Produced by *Salmonella enterica* Serovar Typhi Up-Regulates Chemokines,

- Cytokines, and Adhesion Molecules in Human Macrophage, Colonic Epithelial, and Brain Microvascular Endothelial Cell Lines. Pirofski L, editor. *Infect Immun*. 2013 Mar;81(3):673–83.
155. Herdman BP, Paton JC, Wang H, Beddoe T, Paton AW. Vacuolation Activity and Intracellular Trafficking of ArtB, the Binding Subunit of an AB5 Toxin Produced by *Salmonella enterica* Serovar Typhi. *Infect Immun*. 2017 Aug;85(8):e00214-17.
156. Song J, Gao X, Galán JE. Structure and function of the *Salmonella* Typhi chimaeric A2B5 typhoid toxin. *Nature*. 2013 Jul;499(7458):350–4.
157. Yang YA, Lee S, Zhao J, Thompson AJ, McBride R, Tsogtbaatar B, et al. In vivo tropism of *Salmonella* Typhi toxin to cells expressing a multiantennal glycan receptor. *Nat Microbiol*. 2017 Dec 4;3(2):155–63.
158. Tamamura Y, Tanaka K, Uchida I. Characterization of pertussis-like toxin from *Salmonella* spp. that catalyzes ADP-ribosylation of G proteins. *Sci Rep*. 2017 Jun 1;7(1):2653.
159. Lara-Tejero M, Galán JE. A bacterial toxin that controls cell cycle progression as a deoxyribonuclease I-like protein. *Science*. 2000 Oct 13;290(5490):354–7.
160. Haghjoo E, Galán JE. *Salmonella typhi* **encodes a functional cytolethal distending toxin that is delivered into host cells by a bacterial-internalization pathway**. *Proc Natl Acad Sci*. 2004 Mar 30;101(13):4614–9.

161. Chou HH, Hayakawa T, Diaz S, Krings M, Indriati E, Leakey M, et al. Inactivation of CMP-N-acetylneuraminic acid hydroxylase occurred prior to brain expansion during human evolution. *Proc Natl Acad Sci U S A*. 2002 Sep 3;99(18):11736–41.
162. Del Bel Belluz L, Guidi R, Pateras IS, Levi L, Mihaljevic B, Rouf SF, et al. The Typhoid Toxin Promotes Host Survival and the Establishment of a Persistent Asymptomatic Infection. *PLoS Pathog*. 2016 Apr;12(4):e1005528.
163. Ge Z, Schauer DB, Fox JG. *In vivo* virulence properties of bacterial cytolethal-distending toxin. *Cell Microbiol*. 2008 Aug;10(8):1599–607.
164. Fowler CC, Galán JE. Decoding a Salmonella Typhi Regulatory Network that Controls Typhoid Toxin Expression within Human Cells. *Cell Host Microbe*. 2018 Jan;23(1):65-76.e6.
165. Chang SJ, Song J, Galán JE. Receptor-Mediated Sorting of Typhoid Toxin during Its Export from Salmonella Typhi-Infected Cells. *Cell Host Microbe*. 2016 Nov 9;20(5):682–9.
166. Spanò S, Ugalde JE, Galán JE. Delivery of a Salmonella Typhi Exotoxin from a Host Intracellular Compartment. *Cell Host Microbe*. 2008 Jan;3(1):30–8.
167. Groisman EA. The pleiotropic two-component regulatory system PhoP-PhoQ. *J Bacteriol*. 2001 Mar;183(6):1835–42.

168. Geiger T, Pazos M, Lara-Tejero M, Vollmer W, Galán JE. Peptidoglycan editing by a specific LD-transpeptidase controls the muramidase-dependent secretion of typhoid toxin. *Nat Microbiol.* 2018 Nov;3(11):1243–54.
169. Chong A, Lee S, Yang YA, Song J. The Role of Typhoid Toxin in Salmonella Typhi Virulence. *Yale J Biol Med.* 2017 Jun;90(2):283–90.
170. Fowler CC, Stack G, Jiao X, Lara-Tejero M, Galán JE. Alternate subunit assembly diversifies the function of a bacterial toxin. *Nat Commun.* 2019 Aug 15;10(1):3684.
171. Garmendia J, Beuzón CR, Ruiz-Albert J, Holden DW. The roles of SsrA–SsrB and OmpR–EnvZ in the regulation of genes encoding the Salmonella typhimurium SPI-2 type III secretion system. *Microbiology.* 2003 Sep 1;149(9):2385–96.
172. Walthers D, Carroll RK, Navarre WW, Libby SJ, Fang FC, Kenney LJ. The response regulator SsrB activates expression of diverse Salmonella pathogenicity island 2 promoters and counters silencing by the nucleoid-associated protein H-NS. *Mol Microbiol.* 2007 Jul;65(2):477–93.
173. Fass E, Groisman EA. Control of Salmonella pathogenicity island-2 gene expression. *Curr Opin Microbiol.* 2009 Apr;12(2):199–204.
174. Bijlsma JJE, Groisman EA. The PhoP/PhoQ system controls the intramacrophage type three secretion system of Salmonella enterica: SPI-2 regulation by the PhoP/PhoQ system. *Mol Microbiol.* 2005 Jul;57(1):85–96.

175. Miller R, Wiedmann M. Dynamic Duo—The Salmonella Cytolethal Distending Toxin Combines ADP-Ribosyltransferase and Nuclease Activities in a Novel Form of the Cytolethal Distending Toxin. *Toxins*. 2016 Apr 25;8(5):121.
176. Gaballa A, Cheng RA, Harrand AS, Cohn AR, Wiedmann M. The Majority of Typhoid Toxin-Positive *Salmonella* Serovars Encode ArtB, an Alternate Binding Subunit. D’Orazio SEF, editor. *mSphere*. 2021 Feb 24;6(1):e01255-20.
177. den Bakker HC, Moreno Switt AI, Govoni G, Cummings CA, Ranieri ML, Degoricija L, et al. Genome sequencing reveals diversification of virulence factor content and possible host adaptation in distinct subpopulations of *Salmonella enterica*. *BMC Genomics*. 2011 Aug 22;12:425.
178. Rodriguez-Rivera LD, Bowen BM, Den Bakker HC, Duhamel GE, Wiedmann M. Characterization of the cytolethal distending toxin (typhoid toxin) in non-typhoidal *Salmonella* serovars. *Gut Pathog*. 2015 Dec;7(1):19.
179. Miller RA, Betteken MI, Guo X, Altier C, Duhamel GE, Wiedmann M. The Typhoid Toxin Produced by the Nontyphoidal *Salmonella enterica* Serotype Javiana Is Required for Induction of a DNA Damage Response In Vitro and Systemic Spread In Vivo. *mBio*. 2018 Mar 27;9(2):e00467-18.
180. Lee S, Yang YA, Milano SK, Nguyen T, Ahn C, Sim JH, et al. *Salmonella* Typhoid Toxin PltB Subunit and Its Non-typhoidal *Salmonella* Ortholog Confer Differential Host Adaptation and Virulence. *Cell Host Microbe*. 2020 Jun 10;27(6):937-949.e6.

181. Littler DR, Ang SY, Moriel DG, Kocan M, Kleifeld O, Johnson MD, et al. Structure-function analyses of a pertussis-like toxin from pathogenic *Escherichia coli* reveal a distinct mechanism of inhibition of trimeric G-proteins. *J Biol Chem*. 2017 Sep 8;292(36):15143–58.
182. Beddoe T, Paton AW, Le Nours J, Rossjohn J, Paton JC. Structure, biological functions and applications of the AB5 toxins. *Trends Biochem Sci*. 2010 Jul;35(7):411–8.
183. Chatterjee S, Raval IH. Pathogenic Microbial Genetic Diversity with Reference to Health. In: *Microbial Diversity in the Genomic Era* [Internet]. Elsevier; 2019 [cited 2023 Jun 12]. p. 559–77. Available from: <https://linkinghub.elsevier.com/retrieve/pii/B9780128148495000320>
184. Karasawa T, Ito H, Tsukamoto T, Yamasaki S, Kurazono H, Faruque SM, et al. Cloning and characterization of genes encoding homologues of the B subunit of cholera toxin and the *Escherichia coli* heat-labile enterotoxin from clinical isolates of *Citrobacter freundii* and *E. coli*. *Infect Immun*. 2002 Dec;70(12):7153–5.
185. Bai L, Xia S, Lan R, Liu L, Ye C, Wang Y, et al. Isolation and characterization of cytotoxic, aggregative *Citrobacter freundii*. *PloS One*. 2012;7(3):e33054.
186. Paton AW, Woodrow MC, Doyle RM, Lanser JA, Paton JC. Molecular characterization of a Shiga toxigenic *Escherichia coli* O113:H21 strain lacking *eae* responsible for a cluster of cases of hemolytic-uremic syndrome. *J Clin Microbiol*. 1999 Oct;37(10):3357–61.
187. Paton AW, Paton JC. *Escherichia coli* Subtilase Cytotoxin. *Toxins*. 2010 Jan 28;2(2):215–28.

188. Dougan G, Baker S. *Salmonella enterica* Serovar Typhi and the Pathogenesis of Typhoid Fever. *Annu Rev Microbiol.* 2014 Sep 8;68(1):317–36.
189. Gilchrist JJ, MacLennan CA. Invasive Nontyphoidal *Salmonella* Disease in Africa. *EcoSal Plus.* 2019 Jan;8(2).
190. Mahon BE, Fields PI. Invasive Infections with Nontyphoidal *Salmonella* in Sub-Saharan Africa. Scheld WM, Hughes JM, Whitley RJ, editors. *Microbiol Spectr.* 2016 May 6;4(3):4.3.18.
191. [Centres for Disease Control and Prevention (CDC), 2013;
192. Perez-Sepulveda BM, Heavens D, Pulford CV, Predeus AV, Low R, Webster H, et al. An accessible, efficient and global approach for the large-scale sequencing of bacterial genomes. *Genome Biol.* 2021 Dec;22(1):349.
193. Jones TF, Ingram LA, Cieslak PR, Vugia DJ, Tobin-D'Angelo M, Hurd S, et al. Salmonellosis outcomes differ substantially by serotype. *J Infect Dis.* 2008 Jul 1;198(1):109–14.
194. Tamber S, Dougherty B, Nguy K. *Salmonella enterica* serovars associated with bacteremia in Canada, 2006–2019. *Can Commun Dis Rep.* 2021 Jun 9;47(56):259–68.
195. Fan E, Merritt EA, Verlinde CL, Hol WG. AB5 toxins: structures and inhibitor design. *Curr Opin Struct Biol.* 2000 Dec;10(6):680–6.
196. Vanden Broeck D, Horvath C, De Wolf MJS. *Vibrio cholerae*: Cholera toxin. *Int J Biochem Cell Biol.* 2007;39(10):1771–5.

197. Johannes L, Römer W. Shiga toxins — from cell biology to biomedical applications. *Nat Rev Microbiol*. 2010 Feb;8(2):105–16.
198. Ng NM, Littler DR, Paton AW, Le Nours J, Rossjohn J, Paton JC, et al. EcxAB is a founding member of a new family of metalloprotease AB5 toxins with a hybrid cholera-like B subunit. *Struct Lond Engl* 1993. 2013 Nov 5;21(11):2003–13.
199. van den Akker F, Sarfaty S, Twiddy EM, Connell TD, Holmes RK, Hol WG. Crystal structure of a new heat-labile enterotoxin, LT-IIb. *Struct Lond Engl* 1993. 1996 Jun 15;4(6):665–78.
200. Reidl J, Klose KE. *Vibrio cholerae* and cholera: out of the water and into the host. *FEMS Microbiol Rev*. 2002 Jun;26(2):125–39.
201. Tarr PI, Gordon CA, Chandler WL. Shiga-toxin-producing *Escherichia coli* and haemolytic uraemic syndrome. *The Lancet*. 2005 Mar;365(9464):1073–86.
202. Kilgore PE, Salim AM, Zervos MJ, Schmitt HJ. Pertussis: Microbiology, Disease, Treatment, and Prevention. *Clin Microbiol Rev*. 2016 Jul;29(3):449–86.
203. Song J, Willinger T, Rongvaux A, Eynon EE, Stevens S, Manz MG, et al. A Mouse Model for the Human Pathogen *Salmonella Typhi*. *Cell Host Microbe*. 2010 Oct;8(4):369–76.
204. Song J, Gao X, Galán JE. Structure and function of the *Salmonella Typhi* chimaeric A(2)B(5) typhoid toxin. *Nature*. 2013 Jul 18;499(7458):350–4.

205. Yang YA, Lee S, Zhao J, Thompson AJ, McBride R, Tsogtbaatar B, et al. In vivo tropism of *Salmonella* Typhi toxin to cells expressing a multiantennal glycan receptor. *Nat Microbiol.* 2018 Feb;3(2):155–63.
206. Rodriguez-Rivera LD, Bowen BM, den Bakker HC, Duhamel GE, Wiedmann M. Characterization of the cytolethal distending toxin (typhoid toxin) in non-typhoidal *Salmonella* serovars. *Gut Pathog.* 2015;7:19.
207. Gibani MM, Jones E, Barton A, Jin C, Meek J, Camara S, et al. Investigation of the role of typhoid toxin in acute typhoid fever in a human challenge model. *Nat Med.* 2019 Jul;25(7):1082–8.
208. Akinyemi KO, Coker AO, Olukoya DK, Oyefolu AO, Amorighoye EP, Omonigbehin EO. Prevalence of Multi-Drug Resistant *Salmonella* typhi among Clinically Diagnosed Typhoid Fever Patients in Lagos, Nigeria. *Z Für Naturforschung C.* 2000 Jun 1;55(5–6):489–93.
209. Pulford CV, Perez-Sepulveda BM, Rodwell EV, Weill FX, Baker KS, Hinton JCD. *Salmonella enterica* Serovar Panama, an Understudied Serovar Responsible for Extraintestinal Salmonellosis Worldwide. Andrews-Polymenis HL, editor. *Infect Immun.* 2019 Sep;87(9):e00273-19.
210. Rodrigues JF, Mathias-Santos C, Sbrogio-Almeida ME, Amorim JH, Cabrera-Crespo J, Balan A, et al. Functional Diversity of Heat-labile Toxins (LT) Produced by Enterotoxigenic *Escherichia coli*. *J Biol Chem.* 2011 Feb;286(7):5222–33.

211. Tehran D, Pirazzini M. Novel Botulinum Neurotoxins: Exploring Underneath the Iceberg Tip. *Toxins*. 2018 May 10;10(5):190.
212. Madeira F, Park YM, Lee J, Buso N, Gur T, Madhusoodanan N, et al. The EMBL-EBI search and sequence analysis tools APIs in 2019. *Nucleic Acids Res*. 2019 Jul 2;47(W1):W636–41.
213. Tamura K, Stecher G, Kumar S. MEGA11: Molecular Evolutionary Genetics Analysis Version 11. Battistuzzi FU, editor. *Mol Biol Evol*. 2021 Jun 25;38(7):3022–7.
214. Murrell B, Weaver S, Smith MD, Wertheim JO, Murrell S, Aylward A, et al. Gene-Wide Identification of Episodic Selection. *Mol Biol Evol*. 2015 May;32(5):1365–71.
215. Zhou Y, Liang Y, Lynch KH, Dennis JJ, Wishart DS. PHAST: A Fast Phage Search Tool. *Nucleic Acids Res*. 2011 Jul 1;39(suppl):W347–52.
216. Arndt D, Grant JR, Marcu A, Sajed T, Pon A, Liang Y, et al. PHASTER: a better, faster version of the PHAST phage search tool. *Nucleic Acids Res*. 2016 Jul 8;44(W1):W16–21.
217. Sullivan MJ, Petty NK, Beatson SA. Easyfig: a genome comparison visualizer. *Bioinformatics*. 2011 Apr 1;27(7):1009–10.
218. Hiley L, Fang NX, Micalizzi GR, Bates J. Distribution of Gifsy-3 and of Variants of ST64B and Gifsy-1 Prophages amongst *Salmonella enterica* Serovar Typhimurium Isolates: Evidence that Combinations of Prophages Promote Clonality. Hensel M, editor. *PLoS ONE*. 2014 Jan 24;9(1):e86203.

219. Dion MB, Oechslin F, Moineau S. Phage diversity, genomics and phylogeny. *Nat Rev Microbiol.* 2020 Mar;18(3):125–38.
220. Wagner PL, Livny J, Neely MN, Acheson DWK, Friedman DI, Waldor MK. Bacteriophage control of Shiga toxin 1 production and release by *Escherichia coli*: Phage control of Stx1 production and release. *Mol Microbiol.* 2002 May 9;44(4):957–70.
221. Jobling MG. The chromosomal nature of LT-II enterotoxins solved: a lambdoid prophage encodes both LT-II and one of two novel pertussis-toxin-like toxin family members in type II enterotoxigenic *Escherichia coli*. Frisan T, editor. *Pathog Dis.* 2016 Apr;74(3):ftw001.
222. Friedman DI, Court DL. Transcription antitermination: the λ paradigm updated. *Mol Microbiol.* 1995 Oct;18(02):191–200.
223. Miura S, Tamamura Y, Takayasu M, Sasaki M, Nishimura N, Tokugawa K, et al. Influence of SOS-inducing agents on the expression of ArtAB toxin gene in *Salmonella enterica* and *Salmonella bongori*. *Microbiol Read Engl.* 2020 Aug;166(8):785–93.
224. Li WH, Gojobori T, Nei M. Pseudogenes as a paradigm of neutral evolution. *Nature.* 1981 Jul 16;292(5820):237–9.
225. Wolfe KH, Li WH. Molecular evolution meets the genomics revolution. *Nat Genet.* 2003 Mar;33(S3):255–65.
226. Angata T, Varki A. Chemical Diversity in the Sialic Acids and Related α -Keto Acids: An Evolutionary Perspective. *Chem Rev.* 2002 Feb 1;102(2):439–70.

227. Lamas A, Miranda JM, Regal P, Vázquez B, Franco CM, Cepeda A. A comprehensive review of non-enterica subspecies of *Salmonella enterica*. *Microbiol Res*. 2018 Jan;206:60–73.
228. Stevens MP, Kingsley RA. *Salmonella* pathogenesis and host-adaptation in farmed animals. *Curr Opin Microbiol*. 2021 Oct;63:52–8.
229. Nguyen T, Lee S, Yang YA, Ahn C, Sim JH, Kei TG, et al. The role of 9-O-acetylated glycan receptor moieties in the typhoid toxin binding and intoxication. Kubori T, editor. *PLOS Pathog*. 2020 Feb 21;16(2):e1008336.
230. Deng Q, Barbieri JT. Molecular Mechanisms of the Cytotoxicity of ADP-Ribosylating Toxins. *Annu Rev Microbiol*. 2008 Oct 1;62(1):271–88.
231. De St. Groth SF, Webster RG, Datyner A. Two new staining procedures for quantitative estimation of proteins on electrophoretic strips. *Biochim Biophys Acta*. 1963;71:377–91.
232. Wittig I, Braun HP, Schägger H. Blue native PAGE. *Nat Protoc*. 2006 Jun;1(1):418–28.
233. Mosmann T. Rapid colorimetric assay for cellular growth and survival: Application to proliferation and cytotoxicity assays. *J Immunol Methods*. 1983 Dec;65(1–2):55–63.
234. Kamruzzaman M, Wu AY, Iredell JR. Biological Functions of Type II Toxin-Antitoxin Systems in Bacteria. *Microorganisms*. 2021 Jun 11;9(6):1276.
235. Nicolas E, Oger CA, Nguyen N, Lambin M, Draime A, Leterme SC, et al. Unlocking Tn3-family transposase activity in vitro unveils an asymmetric pathway for transposome

- assembly. Proc Natl Acad Sci [Internet]. 2017 Jan 31 [cited 2023 Jul 26];114(5). Available from: <https://pnas.org/doi/full/10.1073/pnas.1611701114>
236. Reith ME, Singh RK, Curtis B, Boyd JM, Bouevitch A, Kimball J, et al. The genome of *Aeromonas salmonicida* subsp. *salmonicida* A449: insights into the evolution of a fish pathogen. BMC Genomics. 2008;9(1):427.
 237. Di R, Kyu E, Shete V, Saidasan H, Kahn PC, Tumer NE. Identification of amino acids critical for the cytotoxicity of Shiga toxin 1 and 2 in *Saccharomyces Cerevisiae*. Toxicon. 2011 Mar;57(4):525–39.
 238. Aletrari MO, McKibbin C, Williams H, Pawar V, Pietroni P, Lord JM, et al. Eeyarestatin 1 Interferes with Both Retrograde and Anterograde Intracellular Trafficking Pathways. Holowka D, editor. PLoS ONE. 2011 Jul 25;6(7):e22713.
 239. Deresiewicz RL, Calderwood SB, Robertus JD, Collier RJ. Mutations affecting the activity of the Shiga-like toxin I A-chain. Biochemistry. 1992 Mar 31;31(12):3272–80.
 240. Hovde CJ, Calderwood SB, Mekalanos JJ, Collier RJ. Evidence that glutamic acid 167 is an active-site residue of Shiga-like toxin I. Proc Natl Acad Sci. 1988 Apr;85(8):2568–72.
 241. Kymre L, Simm R, Skotland T, Sandvig K. Different roles of the C-terminal end of Stx1A and Stx2A for AB₅ complex integrity and retrograde transport of Stx in HeLa cells. Sebo P, editor. Pathog Dis. 2015 Dec;73(9):ftv083.
 242. Melton-Celsa AR, Darnell SC, O'Brien AD. Activation of Shiga-like toxins by mouse and human intestinal mucus correlates with virulence of enterohemorrhagic *Escherichia coli*

- O91:H21 isolates in orally infected, streptomycin-treated mice. *Infect Immun.* 1996 May;64(5):1569–76.
243. Connell TD, Holmes RK. Molecular genetic analysis of ganglioside GD1b-binding activity of *Escherichia coli* type IIa heat-labile enterotoxin by use of random and site-directed mutagenesis. *Infect Immun.* 1992 Jan;60(1):63–70.
244. Connell TD, Holmes RK. Mutational analysis of the ganglioside-binding activity of the type II *Escherichia coli* heat-labile enterotoxin LT-IIb. *Mol Microbiol.* 1995 Apr;16(1):21–31.
245. Jobling MG, Holmes RK. Analysis of structure and function of the B subunit of cholera toxin by the use of site-directed mutagenesis. *Mol Microbiol.* 1991 Jul;5(7):1755–67.
246. Tsuji T, Honda T, Miwatani T, Wakabayashi S, Matsubara H. Analysis of receptor-binding site in *Escherichia coli* enterotoxin. *J Biol Chem.* 1985 Jul;260(14):8552–8.
247. Hajishengallis G, Tapping RI, Martin MH, Nawar H, Lyle EA, Russell MW, et al. Toll-like receptor 2 mediates cellular activation by the B subunits of type II heat-labile enterotoxins. *Infect Immun.* 2005 Mar;73(3):1343–9.
248. Cao C, Kurazono H, Yamasaki S, Kashiwagi K, Igarashi K, Takeda Y. Construction of Mutant Genes for a Non-Toxic Verotoxin 2 Variant (VT2vp1) of *Escherichia coli* and Characterization of Purified Mutant Toxins. *Microbiol Immunol.* 1994 Jun;38(6):441–7.
249. Fujii J, Matsui T, Heatherly DP, Schlegel KH, Lobo PI, Yutsudo T, et al. Rapid apoptosis induced by Shiga toxin in HeLa cells. *Infect Immun.* 2003 May;71(5):2724–35.

250. Fujii J, Wood K, Matsuda F, Carneiro-Filho BA, Schlegel KH, Yutsudo T, et al. Shiga Toxin 2 Causes Apoptosis in Human Brain Microvascular Endothelial Cells via C/EBP Homologous Protein. *Infect Immun*. 2008 Aug;76(8):3679–89.
251. Inward CD, Williams J, Chant I, Crocker J, Milford DV, Rose PE, et al. Verocytotoxin-1 induces apoptosis in vero cells. *J Infect*. 1995 May;30(3):213–8.
252. Tesh VL. Induction of apoptosis by Shiga toxins. *Future Microbiol*. 2010 Mar;5(3):431–53.
253. Van Tonder A, Joubert AM, Cromarty AD. Limitations of the 3-(4,5-dimethylthiazol-2-yl)-2,5-diphenyl-2H-tetrazolium bromide (MTT) assay when compared to three commonly used cell enumeration assays. *BMC Res Notes*. 2015 Dec;8(1):47.
254. Lee MS, Cherla RP, Tesh VL. Shiga Toxins: Intracellular Trafficking to the ER Leading to Activation of Host Cell Stress Responses. *Toxins*. 2010 Jun 17;2(6):1515–35.
255. Overgaard E, Morris B, Mohammad Mousa O, Price E, Rodriguez A, Cufurovic L, et al. Cellular Activity of Salmonella Typhimurium ArtAB Toxin and Its Receptor-Binding Subunit. *Toxins*. 2021 Aug 27;13(9):599.
256. Johansson K, Willysson A, Kristoffersson AC, Tontanahal A, Gillet D, Ståhl A lie, et al. Shiga Toxin-Bearing Microvesicles Exert a Cytotoxic Effect on Recipient Cells Only When the Cells Express the Toxin Receptor. *Front Cell Infect Microbiol*. 2020 May 25;10:212.

257. Rodríguez-Angeles MG, Giono-Cerezo S, Valdespino-Gómez JL. [Cytotoxic and cytotoxic effect of cholera toxin on Vero cells and its relation to PCR]. *Rev Latinoam Microbiol.* 1994;36(4):263–71.
258. Giugliano LG, Mann GF, Drasar BS. Response of Mammalian Cell Lines to the Toxins of *Escherichia Coli*. *J Med Microbiol.* 1982 Nov 1;15(4):531–9.
259. Donta ST, Poindexter NJ, Ginsberg BH. Comparison of the binding of cholera and *E. coli* enterotoxins to Y1 adrenal cells. *Biochemistry.* 1982 Feb 16;21(4):660–4.
260. Melton-Celsa AR, Kokai-Kun JF, O’Brien AD. Activation of Shiga toxin type 2d (Stx2d) by elastase involves cleavage of the C-terminal two amino acids of the A2 peptide in the context of the appropriate B pentamer. *Mol Microbiol.* 2002 Jan;43(1):207–15.
261. Basso P, Ragno M, Elsen S, Reboud E, Golovkine G, Bouillot S, et al. *Pseudomonas aeruginosa* Pore-Forming Exolysin and Type IV Pili Cooperate To Induce Host Cell Lysis. Miller SI, editor. *mBio.* 2017 Mar 8;8(1):e02250-16.
262. Rodighiero C, Aman AT, Kenny MJ, Moss J, Lencer WI, Hirst TR. Structural Basis for the Differential Toxicity of Cholera Toxin and *Escherichia coli* Heat-labile Enterotoxin. *J Biol Chem.* 1999 Feb;274(7):3962–9.
263. Serrano A, Guyette JL, Heim JB, Taylor M, Cherubin P, Kregel U, et al. Holotoxin disassembly by protein disulfide isomerase is less efficient for *Escherichia coli* heat-labile enterotoxin than cholera toxin. *Sci Rep.* 2022 Jan 7;12(1):34.

264. Cherubin P, Quiñones B, Teter K. Cellular recovery from exposure to sub-optimal concentrations of AB toxins that inhibit protein synthesis. *Sci Rep*. 2018 Feb 6;8(1):2494.
265. Ahn J, Yu JE, Kim H, Sung J, Han G, Sohn MH, et al. AB5-Type Toxin as a Pentameric Scaffold in Recombinant Vaccines against the Japanese Encephalitis Virus. *Toxins*. 2023 Jun 29;15(7):425.
266. Allison HE. Stx-phages: drivers and mediators of the evolution of STEC and STEC-like pathogens. *Future Microbiol*. 2007 Apr;2(2):165–74.
267. Fan E, Merritt EA, Verlinde CL, Hol WG. AB(5) toxins: structures and inhibitor design. *Curr Opin Struct Biol*. 2000 Dec;10(6):680–6.
268. Brüssow H, Canchaya C, Hardt WD. Phages and the Evolution of Bacterial Pathogens: from Genomic Rearrangements to Lysogenic Conversion. *Microbiol Mol Biol Rev*. 2004 Sep;68(3):560–602.
269. The Comprehensive Sourcebook of Bacterial Protein Toxins [Internet]. Elsevier; 2006 [cited 2023 Jul 24]. Available from: <https://linkinghub.elsevier.com/retrieve/pii/B9780120884452X50008>
270. Faruque SM, Mekalanos JJ. Phage-bacterial interactions in the evolution of toxigenic *Vibrio cholerae*. *Virulence*. 2012 Nov 15;3(7):556–65.
271. Yamamoto T, Nakazawa T, Miyata T, Kaji A, Yokota T. Evolution and structure of two ADP-ribosylation enterotoxins, *Escherichia coli* heat-labile toxin and cholera toxin. *FEBS Lett*. 1984 Apr 24;169(2):241–6.

272. Lingwood C. Therapeutic Uses of Bacterial Subunit Toxins. *Toxins*. 2021 May 26;13(6):378.
273. Lichtenstein BR, Höcker B. Engineering an AB5 Protein Carrier. *Sci Rep*. 2018 Aug 23;8(1):12643.
274. Mulvey P, Duong V, Boyer S, Burgess G, Williams DT, Dussart P, et al. The Ecology and Evolution of Japanese Encephalitis Virus. *Pathogens*. 2021 Nov 24;10(12):1534.
275. Yamini G, Nestorovich EM. Multivalent Inhibitors of Channel-Forming Bacterial Toxins. In: Barth H, editor. *Uptake and Trafficking of Protein Toxins* [Internet]. Cham: Springer International Publishing; 2016 [cited 2023 Jul 24]. p. 199–227. (Current Topics in Microbiology and Immunology; vol. 406). Available from: http://link.springer.com/10.1007/82_2016_20
276. Mukhopadhyay S, Linstedt AD. Retrograde trafficking of AB5 toxins: mechanisms to therapeutics. *J Mol Med*. 2013 Oct;91(10):1131–41.
277. Kulczyk AW, Sorzano COS, Grela P, Tchórzewski M, Tumer NE, Li XP. Cryo-EM structure of Shiga toxin 2 in complex with the native ribosomal P-stalk reveals residues involved in the binding interaction. *J Biol Chem*. 2023 Jan;299(1):102795.
278. Ngandjio A, Tchendjou P, Koki Ndombo P, Gonsu Kamga H, Fonkoua MC. Emergence of multi-drug resistant *Salmonella enterica* serotype Stanleyville infections among children in Yaounde, Cameroon. *J Trop Pediatr*. 2012 Apr 1;58(2):161–3.

Appendices

Table S3.1. Summary of *Salmonella* strains and serovars encoding the RIP-TT toxin, compiled in September 2021.

Strain name	Serovar	Accession Number	% identity of A subunit to Stanleyville	Source	Notes
<i>Salmonella enterica</i> subsp. Enterica RSE39	Stanleyville	AZT32170	100%	Pennsylvania State University, December 2018, USA.	Isolation source- meat retail from Rulindo district, Rwanda. Collection date- 13 th March, 2018.
<i>Salmonella enterica</i> subsp. Enterica 286688	Stanleyville	EAA7189132	100%	Public Health England, July 2018, UK.	Host = “homo sapiens” Collection date- June 2016.
<i>Salmonella enterica</i> FDA105212 2-C001-019	Not given	EAM3050518	100%	Center for Food Safety and Applied Nutrition, US Food and Drug Administration, May 2018, USA.	Isolation source- sorghum flour from Rwanda. Collection date- 1 ST May 2018.
<i>Salmonella enterica</i> subsp. Enterica RSE30	Stanleyville	AZT63258	100%	Pennsylvania State University, December 2018, USA.	Isolation source- meat retail from Rulindo district, Rwanda. Collection date- 5 th December 2017.
<i>Salmonella enterica</i> subsp. Enterica RSE01	Stanleyville	AZT67415	100%	Pennsylvania State University, December 2018, USA.	Isolation source- Bos taurus (cows) from a Farm in Rulindo district of Rwanda. Collection date- 21 st November 2017.
<i>Salmonella enterica</i> subsp. Enterica S-1643	Macclesfield	ASG16308	97%	Public Health Agency of Canada, National Microbiology Laboratory at Guelph, June 2017, Canada.	No information.
<i>Salmonella enterica</i> subsp. Enterica 172397	Kouka	EAA5488834	97%	Public Health England, June 2018, UK.	Host- Homo sapiens Collection date- October 2015.

<i>Salmonella enterica</i> subsp. Enterica 20899	Kambole	EAC1133949	97%	Public Health England, September 2018, UK.	Host- Homo sapiens Collection date- June 2014.
<i>Salmonella enterica</i> subsp. Enterica 748770		EBG0729883	97%	Public Health England, June 2019, UK.	Host- Homo sapiens Collection date- May 2019.
<i>Salmonella enterica</i> subsp. Enterica 741688	Everleigh	EBG2396662	97%	Public Health England, June 2019, UK.	Host- Homo sapiens Collection date- May 2019.
<i>Salmonella enterica</i> subsp. Enterica 388798	Eingedi	EBS1110190	97%	Public Health England, September 2018, UK.	Host- Homo sapiens Collection date- July 2017.
<i>Salmonella enterica</i> subsp. Enterica 401598	Kambole	EBS2656125	97%	Public Health England, July 2018, UK.	Host- Homo sapiens Collection date- August 2017.
<i>Salmonella enterica</i> subsp. Enterica 387141	Afula	EBV2195112	97%	Public Health England, June 2018, UK.	Host- Homo sapiens Collection date- June 2017.
<i>Salmonella enterica</i> subsp. Enterica 598044	Kambole	EBY4018594	97%	Public Health England, September 2018, UK.	Host- Homo sapiens Collection date- August 2018.
<i>Salmonella enterica</i> subsp. Enterica 267726	Everleigh	ECD5051645	97%	Public Health England, March 2019, UK.	Host- Homo sapiens Collection date- June 2016.
<i>Salmonella enterica</i> subsp. Enterica 416187	Kambole	ECG3342228	97%	Public Health England, February 2019, UK.	Host- Homo sapiens Collection date- August 2017.

<i>Salmonella enterica</i> subsp. Enterica 311154	Kambole	ECG4918173	97%	Public Health England, March 2019, UK.	Isolation source- food Collection date- October 2016.
<i>Salmonella enterica</i> subsp. Enterica 27033	Kambole	ECH9427285	97%	Public Health England, July 2018, UK.	Host- Homo sapiens Collection date- July 2014.
<i>Salmonella enterica</i> subsp. Enterica 790434	Kambole	ECO3184117	97%	Public Health England, August 2019, UK.	Host- Homo sapiens Collection date- August 2019.
<i>Salmonella enterica</i> subsp. Enterica 56959	Kambole	ECY5576887	97%	Public Health England, July 2018, UK.	Host- Homo sapiens
<i>Salmonella enterica</i> subsp. Enterica 823462	Kambole	EDN3629895	97%	Public Health England, October 2019, UK.	Host- Homo sapiens Collection date- October 2019.
<i>Salmonella enterica</i> subsp. Enterica 32461	Kambole	EDV4151838	97%	Public Health England, July 2018, UK.	Host- Homo sapiens Collection date- July 2014.
<i>Salmonella enterica</i> subsp. Enterica 130392	Bovismorbificans	EED9734958	97%	Public Health England, July 2018, UK.	Host- Homo sapiens
<i>Salmonella enterica</i> subsp. Enterica 965552	Kambole	EFT4465106	97%	Public Health England, July 2020, UK.	Host- Homo sapiens Collection date- July 2020.
<i>Salmonella enterica</i> subsp. Enterica 280692	Kambole	MKD05605	97%	Public Health England, July 2018, UK.	Host- Homo sapiens Collection date- July 2016.

<i>Salmonella enterica</i> subsp. Enterica 172397	Kouka	EAA5488834	97%	Public Health England, June 2018, UK.	Host- Homo sapiens Collection date- October 2015.
<i>Salmonella enterica</i> subsp. Enterica 388798	Eingedi	EBS1110190	97%	Public Health England, September 2018, UK.	Host- Homo sapiens Collection date- July 2017.
<i>Salmonella enterica</i> subsp. Enterica 387141	Afula	EBV2195112	97%	Public Health England, June 2018, UK.	Host- Homo sapiens Collection date- June 2017.
<i>Salmonella enterica</i> subsp. Enterica 267726	Everleigh	ECD5051645	97%	Public Health England, March 2019, UK.	Host- Homo sapiens Collection date- June 2016.
<i>Salmonella enterica</i> subsp. Enterica 130392	Bovismorbificans	EED9734958	97%	Public Health England, July 2018, UK.	Host- Homo sapiens
<i>Salmonella enterica</i> subsp. Enterica 741657	Nagoya	EBF8347858	97%	Public Health England, May 2019, UK.	Host- Homo sapiens Collection date- May 2019.
<i>Salmonella enterica</i> PNUSAS08 0567	Not given	EBH2656625	97%	Centers for Disease Control and Prevention, June 2019, USA.	No information
<i>Salmonella enterica</i> subsp. Enterica 293157	Nagoya	EBQ9562182	97%	Public Health England, June 2018, UK.	Host- Homo sapiens Collection date- August 2016
<i>Salmonella enterica</i> subsp. Enterica FDA945362 2-11	Solt	EED8302343	97%	Center for Food Safety and Applied Nutrition, US Food and Drug Administration, July 2018, USA.	Isolation source- Taco seasoning, Mexico. Collection date- 8 th February 2016.

<i>Salmonella enterica</i> subsp. Enterica 171279	Nagoya	EBQ9721637	97%	Public Health England, June 2018, UK.	Host- Homo sapiens Collection date- October 2015.
<i>Salmonella enterica</i> FDA086830 1-C002-022	Not given	EAM8730334	97%	Center for Food Safety and Applied Nutrition, US Food and Drug Administration, July 2018, USA.	Isolation source- Mango, Mexico. Collection date- 2014.
<i>Salmonella enterica</i> FDA086830 1-C001-002	Not given	EAY0054317	97%	Center for Food Safety and Applied Nutrition, US Food and Drug Administration, July 2018, USA.	Isolation source- Mango, Mexico. Collection date- 2014.
<i>Salmonella enterica</i> PNUSAS15 6889	Not given	EHF1888225	97%	Centers for Disease Control and Prevention, March 2021, USA.	No information.
<i>Salmonella enterica</i> FDA957244 -1	Not given	EAX4763605	97%	Center for Food Safety and Applied Nutrition, US Food and Drug Administration, July 2018, USA.	Isolation source- red pepper Spice, Ethiopia. Collection date- 21 st April 2016.
<i>Salmonella enterica</i> PNUSAS18 4341	Not given	EGT0617087	97%	Centers for Disease Control and Prevention, December 2020, USA.	No information.
<i>Salmonella enterica</i> isolate="PN USAS02418 4"	Not given	EBH5437088	96%	Centers for Disease Control and Prevention, July 2018, USA.	No information.
<i>Salmonella enterica</i> PNUSAS03 3323	serovar="Se rotype pending"	ECU0147888	96%	Centers for Disease Control and Prevention, July 2018, USA.	Isolation source- Urine Collection date- December 2017.
<i>Salmonella enterica</i> PNUSAS18 7687	Not given	EGY5172908	96%	Centers for Disease Control and Prevention, January 2021, USA.	No information.

<i>Salmonella enterica</i> subsp. Enterica PNUSAS00 1234	Isangi	EDW5000242	96%	Centers for Disease Control and Prevention, July 2018, USA.	Isolation source- stool Collection date- June 2014.
<i>Salmonella enterica</i> CFSAN057 231	Not given	EAA8874937	96%	Center for Food Safety and Applied Nutrition, US Food and Drug Administration, July 2018, USA.	Isolation source- soil Collection date- 8 th August 2016.
<i>Salmonella enterica</i> FDA466546 C1 1-1	Not given	EAW0645016	96%	Center for Food Safety and Applied Nutrition, US Food and Drug Administration, August 2018, USA.	Isolation source- Jalapeno peppers Collection date- 21 st July 2008.
<i>Salmonella enterica</i> FSIS118088 72	Not given	EBF0113973	96%	Center for Food Safety and Applied Nutrition, US Food and Drug Administration, July 2018, USA. Collected by USDA-FSIS.	Isolation source- Comminuted beef, Texas Collection date- 2018.
<i>Salmonella enterica</i> FSIS118088 71	Not given	EBN1736479	96%	Center for Food Safety and Applied Nutrition, US Food and Drug Administration, July 2018, USA. Collected by USDA-FSIS.	Isolation source- Comminuted beef, Texas Collection date- 2018.
<i>Salmonella enterica</i> CFSAN057 232	Not given	EBT1347883 (Record removed as of August 23 rd , 2021).	96%	Center for Food Safety and Applied Nutrition, US Food and Drug Administration, July 2018, USA.	Isolation source- soil Collection date- 8 th August 2016.
<i>Salmonella enterica</i> subsp. Enterica PNCS00431 1	Oranienburg	EHB3562303	96%	Pulse Net Canada, Public Health Agency of Canada, February 2021, Canada.	Host- Homo sapiens Isolation source- blood Collection date- 2017
<i>Salmonella enterica</i>	Mississippi	ECW0821157	96%	Center for Food Safety and Applied	Host- Homo sapiens, Australia

subsp. Enterica AUSMDU0 0004671					Nutrition, US Food and Drug Administration, September 2019, USA.	Collection date- 2008
<i>Salmonella</i> <i>enterica</i> PNUSAS07 2842	Not given	EAQ5055013	96%		Centers for Disease Control and Prevention, April 2019, USA.	No information.
<i>Salmonella</i> <i>enterica</i> FDA579870 1-1	Not given	EAW0685415	96%		Center for Food Safety and Applied Nutrition, US Food and Drug Administration, August 2018.	Isolation source- Chile arbol Collection date- 2010.
<i>Salmonella</i> <i>enterica</i> PNUSAS07 9674	Not given	EBH2386173	96%		Centers for Disease Control and Prevention, June 2019, USA.	No information.
<i>Salmonella</i> <i>enterica</i> subsp. <i>arizonae</i> FDA552679 1-10	Not given	EBP3213232	96%		Centers for Disease Control and Prevention, July 2018, USA.	Isolation source- chilli powder, India. Collection date- 24 TH June 2009.
<i>Salmonella</i> <i>enterica</i> subsp. <i>enterica</i> 299847	Rubislaw	EBX4722656	96%		Public Health England, July 2018, UK.	Host- Homo sapiens Collection date- September 2016.
<i>Salmonella</i> <i>enterica</i> subsp. Enterica 586808	Bovismorbif icans	EBY8985610	96%		Public Health England, September 2018, UK.	Host- Homo sapiens Collection date- August 2018.
<i>Salmonella</i> <i>enterica</i> subsp. Enterica FSW0196	II O-4:a:-	ECC2864268	96%		Center for Food Safety and Applied Nutrition, US Food and Drug Administration, July 2018, USA.	Isolation source- frozen silver fish, China. Collection date- 26 TH July 2011.
<i>Salmonella</i> <i>enterica</i> subsp.	<i>Salmonella</i> Ferlac	ECC3876550	96%		Public Health England, July 2018, UK.	Collection date- June 2016.

Indica
267048

<i>Salmonella enterica</i> subsp. Indica 461997	<i>Salmonella</i> Ferlac	ECF5886331	96%	Public Health England, July 2019, UK.	Isolation source- other Collection date- October 2012.
<i>Salmonella enterica</i> subsp. Enterica FDA245223	Banjul	ECI8271031	96%	Center for Food Safety and Applied Nutrition, US Food and Drug Administration, April 2019, USA.	Isolation source- frozen shrimp, Sri Lanka. Collection date- 26 TH August 2003.
<i>Salmonella enterica</i> subsp. Enterica PNUSAS00 2180	Rubislaw	EDB4750223	96%	Centers for Disease Control and Prevention, July 2018, USA.	Isolation source- blood. Collection date- February 2010.
<i>Salmonella enterica</i> subsp. Enterica FNE0147	6,14,24,25:a :e,n,z15	EDN7232658	96%	Center for Food Safety and Applied Nutrition, US Food and Drug Administration, July 2018, USA.	Isolation source- sambar powder, India. Collection date- 26 TH April 2013.
<i>Salmonella enterica</i> subsp. Enterica FSW0080	Oslo	EDR2770354	96%	Center for Food Safety and Applied Nutrition, US Food and Drug Administration, July 2018, USA.	Isolation source- frozen cut crab, Sri Lanka. Collection date- 23 RD October 2010.
<i>Salmonella enterica</i> subsp. Indica FDA829401	VI 1,6,14,25:a: e,n,z15	EDT9220671	96%	Center for Food Safety and Applied Nutrition, US Food and Drug Administration, July 2018, USA.	Isolation source- Shrimp, frozen, Sri Lanka. Collection date- 6 TH September 2013.
<i>Salmonella enterica</i> subsp. Diarizonae FDA217018	Not given	EEC4247149	96%	Center for Food Safety and Applied Nutrition, US Food and Drug Administration, July 2018, USA.	Isolation source- roasted chili powder, Sri Lanka. Collection date- 19 TH February 2003.

<i>Salmonella enterica</i> subsp. Enterica FDA145417	Banjul	EEJ0018485	96%	Center for Food Safety and Applied Nutrition, US Food and Drug Administration, July 2018, USA.	Isolation source- shrimp, Sri Lanka. Collection date- 23 RD AUGUST, 2001.
<i>Salmonella enterica</i> PNUSAS20 0223	Not given	EHM4932080	96%	Centers for Disease Control and Prevention, May 2021, USA.	No information.
<i>Salmonella enterica</i> FSE0116	Not given	EHN2303847	96%	Center for Food Safety and Applied Nutrition, US Food and Drug Administration, July 2018, USA.	Isolation source- deggi mirch, India. Collection date- 20 TH September 2013.
<i>Salmonella enterica</i> 1411-60	1,6,14,25:a:e,n,x	HAE2752109	96%	National Center for Biotechnology Information, National Library of Medicine, National Institutes of Health, July 2018, USA.	Isolation source- coconut, UK. Collection date- 1960.
<i>Salmonella enterica</i> 03-0384	No given	MBA3102202	96%	Centers for Disease Control and Prevention, July 2018, USA.	No information.
<i>Salmonella enterica</i> subsp. Indica NCTC12420	not available: to be reported later	SUI02336	96%	Wellcome Trust Sanger Institute, June 2018, UK.	No information.
<i>Salmonella enterica</i> subsp. Arizonae FDA552679 1-10	Not given	EBP3213232	96%	Center for Food Safety and Applied Nutrition, US Food and Drug Administration, July 2018, USA.	Isolation source- chilli powder, India Collection date- 24 th June 2009.
<i>Salmonella enterica</i> subsp. Enterica 299847	Rubislaw	EBX4722656	96%	Public Health England, July 2018, UK.	Host- Homo sapiens Collection date- September 2016.

<i>Salmonella enterica</i> subsp. Enterica 586808	Bovismorbificans	EBY8985610	96%	Public Health England, September 2018, UK.	Host- Homo sapiens Collection date- August 2018.
<i>Salmonella enterica</i> subsp. Enterica FSW0196	II O-4:a:-	ECC2864268	96%	Center for Food Safety and Applied Nutrition, US Food and Drug Administration, July 2018, USA.	Isolation source- frozen silver fish, China. Collection date- 26 th July 2011.
<i>Salmonella enterica</i> subsp. Indica 267048	<i>Salmonella</i> Ferlac	ECC3876550	96%	Public Health England, July 2018, UK.	Collection date- June 2016.
<i>Salmonella enterica</i> subsp. Enterica FSW0080	Oslo	EDR2770354	96%	Center for Food Safety and Applied Nutrition, US Food and Drug Administration, July 2018, USA.	Isolation source- Frozen cut crab, Sri Lanka Collection date- 23 rd October 2010. Collected by FSW.
<i>Salmonella enterica</i> subsp. Diarizonae FDA217018	Not given	EEC4247149	96%	Center for Food Safety and Applied Nutrition, US Food and Drug Administration, July 2018, USA.	Isolation source- roasted chilli powder, Sri Lanka Collection date- 19 th February 2003.
<i>Salmonella enterica</i> subsp. Enterica PNCS009595	Newport	EHF9575227	96%	Pulse Net Canada, Public Health Agency of Canada, March 2021, Canada.	Host- Homo sapiens Isolation source- stool Collection date- 8 th May 2017.
<i>Salmonella enterica</i> PNUSAS179534	Not given	EGO3302392	96%	Centers for Disease Control and Prevention, November 2020, USA.	No information.
<i>Salmonella enterica</i> subsp. Enterica 117265	Wagenia	EBY1391404	96%	Public Health England, July 2018, UK.	Host- Homo sapiens Collection date- May 2015.

<i>Salmonella enterica</i> subsp. Enterica 886624	Waycross	EEC4861019	96%	Public Health England, February 2020, UK.	Host- Homo sapiens Collection date- February 2020.
<i>Salmonella enterica</i> subsp. Enterica 1166972	Wagenia	EHM3262975	96%	Public Health England, May 2021, UK.	Host- Homo sapiens Collection date- April 2021.
<i>Salmonella enterica</i> subsp. Enterica 1182238	Wagenia	EHO3261736	96%	Public Health England, May 2021, UK.	Host- Homo sapiens Collection date- May 2021.
<i>Salmonella enterica</i> subsp. Enterica FDA132581-2	Warragul	EDT7240905	95%	Center for Food Safety and Applied Nutrition, US Food and Drug Administration, July 2018, USA.	Isolation source- frozen opossum, Australia Collection date- 6 th December 2001.
<i>Salmonella enterica</i> subsp. Enterica FDA132581-1	Warragul	MIG53652	95%	Center for Food Safety and Applied Nutrition, US Food and Drug Administration, July 2018, USA.	Isolation source- frozen opossum, Australia Collection date- 6 th December 2001.
<i>Salmonella enterica</i> FDA934049-C002-001	Not given	EGG1584408	96%	Center for Food Safety and Applied Nutrition, US Food and Drug Administration, September 2020, USA.	Isolation source- pepper, Cameroon Collection date- 17 th November 2015.
<i>Salmonella enterica</i> subsp. Enterica 873465	Brandenburg	EEG1607795	95%	Public Health England, January 2020, UK.	Host- Homo sapiens Collection date- January 2020.
<i>Salmonella enterica</i> subsp. Enterica 834312	Stourbridge	EEH5524392	95%	Public Health England, November 2019, UK.	Host- Homo sapiens Collection date- October 2019.

<i>Salmonella bongori</i> PNUSAS08 8562	Not given	EDP8669591	95%	Centers for Disease Control and Prevention, August 2019, USA.	No information.
<i>Salmonella enterica</i> FDA305581	Not given	EAA7605794	96%	Center for Food Safety and Applied Nutrition, US Food and Drug Administration, August 2018, USA.	Isolation source- frozen shrimp, Bangladesh Collection date- 3 rd November 2004.
<i>Salmonella enterica</i> subsp. Enterica 995824	<i>Salmonella enterica</i>	EGM1788472	95%	Public Health England, October 2020, UK.	Isolation source- food Collection date- September 2020.
<i>Salmonella enterica</i> subsp. Enterica 1040790	<i>Salmonella enterica</i>	EGR9489761	95%	Public Health England, December 2020, UK.	Isolation source- food Collection date- November 2020.
<i>Salmonella enterica</i> subsp. Enterica 730964	India	EBG5097139	95%	Public Health England, June 2019, UK.	Host- Homo sapiens Collection date- April 2019.
<i>Salmonella enterica</i> PNUSAS05 7633	Not given	MEN95089	95%	Centers for Disease Control and Prevention, October 2018, USA.	No information.
<i>Salmonella enterica</i> subsp. Enterica 130428	Typhimurium	EDM2310710	98%	Public Health England, July 2018, UK.	Host- Homo sapiens Collection date- June 2015.
<i>Salmonella enterica</i> PNUSAS05 7633	Not given	MEN96131	96%	Centers for Disease Control and Prevention, October 2018, USA.	No information.

```

RSE1 RIP-TT -----ATTATTTAGTCTTTTCTCTGGTTATGCAAGTGCCGTAAT 42
DT104 ArtAB ATGATAAAAAAGTAATATTTTTAGCATTTTTTCTGGTTATGCAAGTGCTGTGAT 60
          *          *          *          *          *          *          *          *
RSE1 RIP-TT TTTTATATCGTGGGATCGAGACCTCCGGATGTGATTTTCGGAATGGTTTAGTTCT 102
DT104 ArtAB TTTGATATCGTGGTGAATCGAGACCTCCGGATGTGATTTTCGGAATGGTTTAGTTCT 120
          *          *          *          *          *          *          *          *
RSE1 RIP-TT CACGGTAATAACAGAAATCTTCAGAACCTCAGAGGTGACTCTGTGCCGCCGGTAGT 162
DT104 ArtAB CATGGTAATAACAGGAATCTTCAGCAACATATTAGAGGTGACTCGTGTCCGCCGGTAGT 180
          *          *          *          *          *          *          *          *
RSE1 RIP-TT CGGGACAGTAACATATATGCGACTACCTCAGATATTAATGAGACTATAACATAGCACGG 205
DT104 ArtAB CGGGACAGTAACATATGCGACTACCTCAGATATTAATGAGACTATAACATAGCACGG 240
          *          *          *          *          *          *          *          *
RSE1 RIP-TT -----ATACAGAATGCGTGCAGAC 224
DT104 ArtAB GTATATTACTCCAGAACACATTTAGCGGCAGGTTGTATAGATACAGAAATCGTGCAGAC 300
          *          *          *          *          *          *          *          *
RSE1 RIP-TT AATAGTTTCTACAGCTTCCACCGTCTGTCGCTTATATTGTATCTCGTGGCCTCCAGTTT 284
DT104 ArtAB AATAGTTTCTACAGCTTCCACCGTCTGTCGCTTATATTGAGTACGTTGGTATCCAGTTT 360
          *          *          *          *          *          *          *          *
RSE1 RIP-TT AGTAATTTTAGCGAGTTATGATCGGTTACAAAGTGTGTATGTAGCCGTAATTTCTATC 344
DT104 ArtAB AGTCAATTTGAGCGAGTATGATCGGTTGCAAAAGTGTGTATGTAGCCGTAATTTCTATC 420
          *          *          *          *          *          *          *          *
RSE1 RIP-TT CCAACTGAAAATATTCAGAAAGCAGTTGCGCTTGTTTACGACAGAAATCAAGTCAGGTA 404
DT104 ArtAB CCAATTGAAAATATCCAGGAAGCAGTTGAGCTTGTTTACGACAGAAATCAAGTCAGGTA 480
          *          *          *          *          *          *          *          *
RSE1 RIP-TT AGAGGTGGACCTGGAAATCAAATCCCGTTATTTACGAGTGAATACAGGATTAATCTCT 464
DT104 ArtAB AGAGACGGATCTGGAAATCAAATCCCGTTATTTACGAGTGAATACAGGATTAATCTCT 540
          *          *          *          *          *          *          *          *
RSE1 RIP-TT GG-GTAATACCACTTACCAGTACACAGTAAATACCCGGGAAAGGATTAGTGCATTT 523
DT104 ArtAB GGGTAATACCACTTACCAGTACACAGTAAATACCCGGGAAAGGATTAGTGCATTT 600
          *          *          *          *          *          *          *          *
RSE1 RIP-TT GGIACCTTAATCAGTGTAGTTTTCAATGAGAGGAGTACGAGGGATGATGCACGTAGT 583
DT104 ArtAB GGTACCTTAATCAGTGTAGTTTTCAATGAGAGGAGTACGAGGGATGATGCACGTAGT 660
          *          *          *          *          *          *          *          *
RSE1 RIP-TT AAATATAACTACTATGAAATGGATTTTACGATCGCGGGAGTCTTACCAGAAGTATFG 643
DT104 ArtAB AATTATAACTACTATGAAATGGATTTTACGATCGCGGGAGTCTTACCAGAAGTATFG 720
          *          *          *          *          *          *          *          *
RSE1 RIP-TT AACTGATGATGGCATATAAAAAATATTTATTTTTTGTGTGAGTATCGTTGACAGTAA 703
DT104 ArtAB GACTGATGATAGCATAAAAACATTTCTTTTTTGTGTGAGTATCGTTGACAGTAA 780
          *          *          *          *          *          *          *          *
RSE1 RIP-TT AAATGAGTGTAGTATAATATTACATCCAGTTTCCCTATGTTTTTAATGTTATGGTAA 763
DT104 ArtAB AAAGGAGTGTAGTATAATATTACATCCAGTTTCCCTATGTTTTTAATGTTATGGTAA 840
          *          *          *          *          *          *          *          *
RSE1 RIP-TT ATATTGTTGGAGTGGATTATGAAAAATAAATAAGGTTTTGACGCTTGCTCTTGCGTCG 823
DT104 ArtAB ATATTGTTGGAGTGGATTATGAAAAATAAATAAGGTTTTGACGCTTGCTCTTGCGTCG 900
          *          *          *          *          *          *          *          *
RSE1 RIP-TT TTATCCAGTGTGTCATGCGAGTATGGCTGATTATAATAATATACGAGTGAAGTTTCAT 883
DT104 ArtAB TTATCCAGTGTGTTGTTATGCAACATGGCTGATTATAATAATACGAGTGAAGTTTCAG 960
          *          *          *          *          *          *          *          *
RSE1 RIP-TT ATTAAGAATCTGTCTATGGCGGTATAAATCAGGGGAGAAGGAGACTCAGTTTTTTTGT 943
DT104 ArtAB ATTAACAATCTGTCTATGGCGGTATAAATCAGGGGATAAGGAAAGTCAAGTTTTTTTGT 1020
          *          *          *          *          *          *          *          *
RSE1 RIP-TT ATCGAAGTGAAGCGGGGAGTGAAGTTCTTACTGTCGATACCATGTGTAATAATAGATGTG 1003
DT104 ArtAB GTCGGACTGAAGAGGGGGAGTCAAGTTCTAATGTCATACCATATGTAATAATAGATGTG 1080
          *          *          *          *          *          *          *          *
RSE1 RIP-TT TACGGGAATCATAAACAGGGGTTTATAAATGCTTACGACAGCAAGGTATCAATATGCA 1063
DT104 ArtAB TTCGGGACTCATAAACAGGGGTTTATAAATGCTTACGACAGCAAGGTATCAATATGCA 1140
          *          *          *          *          *          *          *          *
RSE1 RIP-TT ACAGGGCAGTCGGTAAGGTATATTATAAACCGGATGTTGGTCCGACCCGATTTCAA 1123
DT104 ArtAB ACAGGGAGGATGTAAGATATATTATAAAGGAAATGCTGGACTGACAGAAATTTACA 1200
          *          *          *          *          *          *          *          *
RSE1 RIP-TT TGTGGATTCCTCGTAATGAATTAATTCGATAACTACTGTGACTCATCAGTCAATTT 1183
DT104 ArtAB GCAGCATTCCTGGTAATGAATTAATTCGATAACTACTGTGACTCATCAGTCAATTT 1260
          *          *          *          *          *          *          *          *
RSE1 RIP-TT ATGGGCTCAGAGACAAATTA 1207
DT104 ArtAB ATGGGACTCAGTTGCCAACTAA 1284
          *          *          *          *          *          *          *          *

```

Figure S3.1. DNA sequence alignment of the *S. Stanleyville* RSE1 *rip-tt* locus and the *S. Typhimurium* DT104 *artAB* locus. The ArtA sequences are shown in purple, and the ArtB sequences are highlighted in blue. Red dashes indicate the 58 bp missing region of the RIP-TT ArtA sequence. Alignments were performed using the ClustalW Omega alignment program (EMBL, EBI, UK).

```

ArtB-1A      1-  --MKNKLVLTALTLASLSSVCYA-----NMADYNTYQSNVQINNLSYGVYRSGDKESQFFCVGLKRGSQVNVHTTICKIDVFG-----
ArtB-1B      1-  --MKNKLVLTALTLASLSSVCYA-----NMADYNTYQSNVQINNLSHGVIKSGGKDSQFFCIGLNNEQIPNANTMCKMDVFG-----
ArtB-1C      1-  --MKNKLVLTALTLASLSSVCYA-----DMAGYNKYVSNVQINNLSYGVIYSGGKQTPFFCVGLKRGSQTPDVNTMCKIDVFG-----
ArtB-1D      1-  --MKNKLVLTALTLASLSSVCYA-----NMAGYNKYVSNVQINNLSYGVIYSGAGKQTPFLCVGLKRGSQVDPVNTMCKIDVFG-----
ArtB-2A      1-  --MKKIFFAFALVLAGASNVIYATVNSWYLKDTTKY-ENVRITNVFYAPYLHSPRICAFYFTAS-----SGGSNVTGCAVADNGYYQKNA
ArtB-2B      1-  --MKKIFFAFVLMVAGASNVIYATVNNWYLKDTTKY-ENVKITNIFYAPYLHSPRICAFYFTAS-----SGGSNITGCSVADNGYYLKNE
ArtB-2C      1-  --MKRFFWVFTLVMMVAGASNVIYASVNRWYLKDTVKY-ENVKVTNVFYAPYLHSPRICAFYFTAS-----PGGSNVAGCAVADNDYYQKNT
PltC-Sap     1-  --MKKLVLTALALASLSSVCYA-----AMADYDITYSNVQINNLSYGVIYSGGKETQFFCIGLKHGSEAI SINAMCKVDVYG-----
PltC-Phage1  1-  --MKKLVLTALALASLSSVCYA-----GMADYDITYSNVQINNLSYGVYKSDDKETQFFCIGLKRGSSSI SINNICVDVYG-----
PltC-Phage2  1-  --MKKLVLTALALASLSSVCYA-----GMADYDKYISNAQINNLSYGVIYSGGKETQFFCIGLKRGSQVPAVNNICKIDVFG-----
PltC-Phage3  1-  --MKKLVLTALALASLSSVCYA-----GMADYDKYISNAQINNLSYGVIYSGGKETQFFCIGVKRGSVHVPDVNAICKFDVFG-----
RIP-TT      1-  --MKNKLVLTALALASLSSVCHA-----SMADYNNYTSVHIIKNSYGVYKSGEKETQFFCIELKRGSSEVLTVDTMCKIDVYG-----
PltB-S. Typhi 1-  MYMSKVPVYVYTLILLIYSPNASE--EWTGDNTNAYYSDEVISELVGQ---IDTSPYFCIRTKANGSGTPVAVCAVSKQS-----
          *.. . . : : : * . * . : : : . : : * . .

ArtB-1A      77-  THKQGFDNMLATARYYYATGEDVRIYKENVVWTDNRNFTAAPSGNELIAITTTCTSSDYCMGPTLPN
ArtB-1B      77-  THKQGFDNMLATARYYYTTGKRVRIYKENVWADNRNFTAGFSGNELIAITTCSSIDYCMGPTLPN
ArtB-1C      77-  THKQGFDNMLATARYYYATGESVVRVYMDSVWTDNRDFANAFSNKELISITTCSSASNYCMGPT---
ArtB-1D      77-  NHKQGFDNMLATARYYYATGEEVRLYIDNVWSDSDPTGAFSNKELISITTCSSASDYCMGPTVFN
ArtB-2A      82-  VQTSPEFMEIFDITVKYFYTTGEEKISVYIRINAF--SHEFSSVSQNEIVAIGTCN--QWCFGEIILK-
ArtB-2B      82-  AQTSPFMEIFDITVKYFYTTGEEKISVYIRINAF--PNFSSLSKNEIVAIGTCN--GWCFFGETIK-
ArtB-2C      82-  AQTSPFMEIFDITVKYFYTTGENISVYIKLNAF--PEFDTTVSKHEIVAIGTCN--GWCFFGETIK-
PltC-Sap     77-  NHKQGFDNMLATARYYYTTGGDVRVYKENVVWRDPDFKSAFSSRELIATTCSSSSYCMGPTVTN
PltC-Phage1  77-  SHKQGFDNMLATARYYYTTGEDVRIYKENVWSDTDFKSAFSSRELIATTCSSSSYCMGPTKKN
PltC-Phage2  77-  THKQGFDNMLATARYYYTTGADVVRVYKENVWGDREFTAAPFANELIALTSCSSPTYCMGPMNPQ
PltC-Phage3  77-  NHKQGFDNMLATARYYYATGEDVVRVYKENVWSDTNFTAAPFSGNELIALTTCSSSTYCMGPVNPV
RIP-TT      77-  NHKQGFDNMLATARYHYATGQSVRVYKPDVWSDPDFKCGFSRNELIAITTCSSGHCMPKPTN
PltB-S. Typhi 77-  IWAPSFKELLDQARYFYSTGQSVRIHVQKNITWYPLFVNTFSANALVGLSSCSA-TQCFGPK---
          * : : . : * : * : * : : : . : * . * . : : : * * : *

```

Figure S3.2. Complete amino acid sequence alignment of the B subunits of RIP-TT, *S. Typhi* PltB and the different ArtAB toxin subtypes and PltC groups. Asterisks (*) indicate positions of complete conservation of amino acid residues among all sequences and colons (:) or periods (.) indicate positions of partial conservation of amino acid residues. Alignments were performed using the ClustalW Omega alignment program (EMBL-EBI, UK).

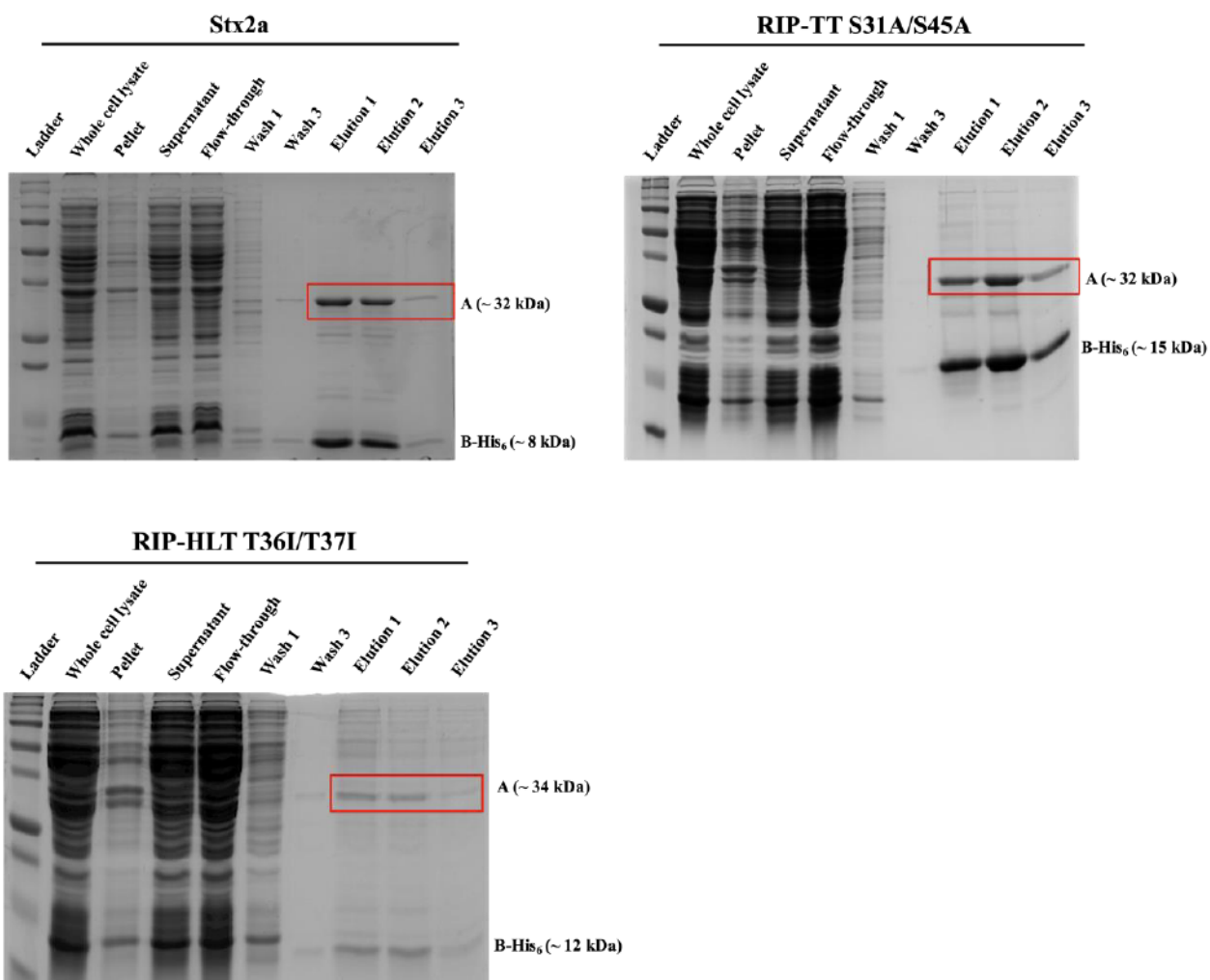


Figure S3.3. SDS-PAGE analysis of several fractions from the successful copurification of Stx2a, RIP-TT S31A/S35A binding mutant and RIP-HLT T36I/T37I binding mutant. Purification was done using Nickel Ni resin gravity columns and A-B interactions were confirmed by successful copurification (pull-down) of the A subunits with their respective His₆-tagged B subunits (red boxes).